Aus dem Institut für Humangenetik der Universitätsmedizin der
Johannes Gutenberg-Universität Mainz

The Role of MID1, MID2, and PAX6 during Neuronal Differentiation and Migration in the Embryonic Mouse Neocortex

Inauguraldissertation
zur Erlangung des Doktorgrades der Medizin

der Universitätsmedizin
der Johannes Gutenberg-Universität Mainz

vorgelegt von

Katharina Anna Ruppert
aus Neustadt a. d. Aisch

Mainz, 2024

Wissenschaftlicher Vorstand:	Univ.- Prof. Dr. H. Schild
Erstgutachter:	
Zweitgutachter:	
Tag der Promotion:	05.06.2024

To my family

List of Abbreviations

°C	degree Celsius
APs	Apical progenitor cells
bp	base pair
BPs	Basal progenitor cells
C. callosum	corpus callosum
Chap.	Chapter
DPBS	Dulbecco's phosphate-buffered saline
E	embryonic day
e.g.	example given
EMT	epithelial-mesenchymal transition
FACS	automated fluorescence-activated cell sorting
Fig.	Figure
FMRP	fragile X mental retardation 1 protein
h	hours
HS	high sensitivity
i.a.	inter alia
ICD	International Classification of Disease
ICF	International Classification of Function
ID	Intellectual disability
IUE	*In utero* electroporation
KD	Knock-down
kD	kilodalton
KO	knock-out
MAPK	mitogen-activated protein kinase
MIDAS	MID1 association sequence
min	minutes
ml	milliliter
mTOR	mechanistic target of rapamycin
MZ	marginal zone

NaCl	sodium chloride
NaOH	sodium hydroxide
ng	nanogram
nm	nanometer
NMD	nonsense mediated decay
nt	nucleotide
OE	overexpression
OS	Opitz syndrome
PAR	pseudoautosomal region
PFA	paraformaldehyde
pg	picogram
RGC	radial glia cells
rpm	rounds per minute
RT	room temperature
RT-qPCR	reverse transcriptase quantitative polymerase chain reaction
SD	Standard deviation
shh	sonic hedgehog
Tab.	table
Tbr1	T-box brain protein 1
Tbr2	T-box brain protein 2
U	unit
µg	microgram
µl	microliter

List of Figures

List of Tables

1 Introduction

1.1 Intellectual Disability in Context of MID1 and MID2

Intellectual disability (ID) is defined by the World Health Organization as ‘‘a condition of arrested or incomplete development of the mind, which is especially characterized by impairment of skills manifested during the developmental period, skills which contribute to the overall level of intelligence, i.e. cognitive, language, motor, and social abilities. Retardation can occur with or without any other mental or physical condition.” (1). The prevalence of ID around the globe is estimated to be around 1%, although this number varies according to income group. Additionally, males have a higher risk for suffering from ID than females (2).

Pathomechanisms of ID can be divided into endogenous and exogenous causes. Exogenous or acquired forms can be induced by a wide spectrum of events. During the intrauterine period, hypoxia, infections or toxic substances e.g. alcohol or exposure to radiation are a threat to development. Postnatally, ID and developmental delay can be triggered by complications after birth such as cerebral hemorrhage or parenteral nutrition (3). Endogenously determined forms ordinarily are driven by genetic causes. ID may occur as part of an underlying syndromal condition or as an isolated symptom. In 2014, the German guidelines on ID published that about 2780 genetic syndromes were known to be associated with ID. Mutations in 450 genes were cited to be involved in the development of ID, but the established number of involved genes to be expected in the future will be three times higher (3, 4). A review from the same year stated there may be 2500 autosomal genes causing ID, most of them with a recessive inheritance (5). Supporting this former assumption, in 2023 the Genomics England’s PanelApp provides a Panel for neurodevelopmental disorders with over 1300 target genes (6, 7).

Clinically recognizable and well known to society is the chromosomal numeral aberration trisomy 21. It is associated with heart defects, endocrinological, oncological, gastrointestinal and neurological disorders with a great variance in the severity of clinical features and represent a classical example of syndromal ID (8).

X-linked ID is an intellectual impairment that primarily affects boys and men. 5% of the human genome are included of the X-chromosome, astonishingly 10 – 12% of X-chromosome genes have been associated with ID (9). A well-known syndrome is fragile X syndrome. The syndrome is caused by a trinucleotide repeat mutation, in which >200 repeats of the CGG motif in the underlying gene causing fragile X syndrome *FMR1* leads to silencing of the gene. The protein expressed by *FMR1* is called fragile X mental retardation 1 protein (FMRP). FMRP regulates expression of multiple mRNAs involved in neuronal synaptic functions (10).

ID is with a prevalence of 1% a common symptom, variety of genetic causes makes it hard to find underlying mutations as disease-causing mutations are still a rare event. But even if the causative mutations are known, a conclusion to the underlying molecular or cellular mechanism is difficult.

Mutations in the *Midline-1(MID1)* gene can cause a syndromic form of ID, the Opitz BBB/G syndrome whereas mutations in its sister gene *Midline-2 (MID2)* have been associated with nonsyndromic ID (11, 12).

In the following, these genes and their related proteins will be described, the corresponding diseases will be addressed and the basics of neurogenesis will be introduced.

1.2 Opitz BBB/G Syndrome

Opitz BBB/G syndrome (OS) is a monogenic disorder first described by John Opitz in 1969 (13, 14). By then it was divided into two different clinical pictures. On the one hand the BBB syndrome, which was named after members of the examined family, was characterized by cleft lip and palate as well as developmental disorder. On the other hand, patients diagnosed with the G syndrome showed gastrointestinal malformations. In 1978 Cordero and Holmes described that both syndromes showed overlapping symptoms and conflated both into the Opitz BBB/G syndrome (15).

OS belongs to the neurocristopathies, a group of diseases characterized by malformations in the tissues and organs that originate from the neural crest (16, 17). The neural crest is formed after closure of the neural tube. Cells undergo a epithelial-mesenchymal transition (EMT) and migrate from the neural ridge to

specific destinations in the embryo where they differentiate into distinct cell types or regain their epithelial properties (18). Consequently, neurocristopathies may result from deficient neural crest cell migration, proliferation or differentiation.

Patients with OS show defects of the ventral midline as an overarching characteristic feature, which is considered to be a consequence of disturbed neural crest development during embryogenesis. However, patients with this syndrome show a great heterogeneity in the expression of clinical features, not all of them may be caused by neural crest abnormalities (19). Clinically, even siblings with the same mutation can present with different manifestations of OS (12).

The most common symptom of OS is hypertelorism which is found in 90% of patients. Further clinical characteristics are hypospadias, laryngo-tracheo-esophageal defects, cleft lip and palate, heart defects or hypoplasia and agenesis of the cerebellum or corpus callosum (C. callosum). About 30% of patients show motor and cognitive delays (12).

Genetically, OS can be caused by mutations in two different genes. The better studied x-chromosomal form affects *MID1* on locus Xp22.2 (See Midline-1 Gene) (20). Various mutations have already been investigated, including missense, nonsense, frameshift and splice site mutations. Also, exon deletions, duplications and even whole gene deletions have been identified (12). The mutations in MID1 lead to a loss-of-function, a decrease of enzyme activity, but also the opposite - a gain-of-function - was considered as the pathomechanism (21, 22). The gain-of-function hypothesis is supported by data of OS patients with C-terminal mutations that could lead to truncated MID1 proteins. In animal experiments terminal truncated Mid1 protein led to a neuronal migration defect in Mid1 knockout (KO) mice (22). Most mutations of patients are located in the C-terminal region, although mutations are also known to occur in all other regions, except for the RING finger domain (See Midline-1 Protein) hum. The loss-of-function hypothesis is strongly upheld by experiments with Mid1 KO mice. These animals show brain anomalies comparable to those of OS patients like hypoplasia of the cerebella vermis (12).

In addition to the X chromosomal form with mutations of the *MID1* gene, an autosomal dominant form of OS has been described. One study describes mutations in the *SPECC1L* gene, which is located on 22q11.2 in patients with

OS (23). Yet SPECC1L mutations have not been found in other patients with suspected autosomal inheritance of OS and mutations on chromosome 22q11.2 (24-26). These findings suggest that SPECC1L is not the only responsible gene in this chromosomal region. However, it remains unclear if other mutations are also responsible for the autosomal dominant inheritance.
It is not known why and to what extent both hereditary traits influence the development of the neural crest, even if the clinical picture suggests it (27-29).

1.3 Midline-1 Gene

The human *MID1* gene is located on the short arm of the X chromosome, on locus Xp22.2. It spans 400 kb of genomic sequence and consists of 9 coding exons and at least 14 alternative exons, so that a total of up to 63 splice variants can be generated (30). Most splice variants regulate the expression of the protein by introducing premature stop codons into the mRNA. It is thought that these transcripts are identified and degraded by nonsense-mediated mRNA decay (NMD) (30).
MID1 expression varies in different tissues. This tissue-specific transcription is ensured by at least five different promoter regions distributed over 250kb genomic sequence and leading to different 5'UTRs of *MID1* transcripts (31). Each promoter region has its own transcription initiation point and corresponding polyadenylation site, that regulate the expression of the *MID1* gene in the different tissues (30, 32, 33).
The murine homolog of *MID1* is located within the pseudoautosomal region (PAR). In mice this leads to a frequent unequal crossover. Interestingly, *Mid1* in mice is not a subject to X-inactivation, while in human it is (34).

1.4 Midline-1 Protein

The product of the *MID1* gene is the 667 amino-acid containing Midline-1 (MID1) protein. It belongs to the family of RING (Really Interesting New Gene) finger proteins which all show a very similar structure (35, 36).
The protein comprises of 72 kD and has six different domains (Figure 1). The first four domains belong to the RBCC (N-terminal RING finger/B-box/coiled coil) or TRIM (tripartite motif) protein family. MID1 is therefore also called TRIM 18.

The RBCC/TRIM family belongs to the largest group of E3 ubiquitin ligases. All proteins have a very homologous structure which can also be found in MID1. N-terminal is the RING finger domain, which is characterized by a Cys-His motif. This domain is important for protein interactions (37). The RING finger domain is followed by two B-Box domains. These also contain Cys-His motifs and play a role in protein interaction. The B-box1 of the MID1 protein binds to the α4 protein, the regulatory subunit of protein phosphatase 2A (PP2A) (38, 39). The following coiled coil domain is involved in the homodimerization of MID1 and heterodimerization with MID2 (37). It contains several alpha helices arranged in parallel and antiparallel (40).

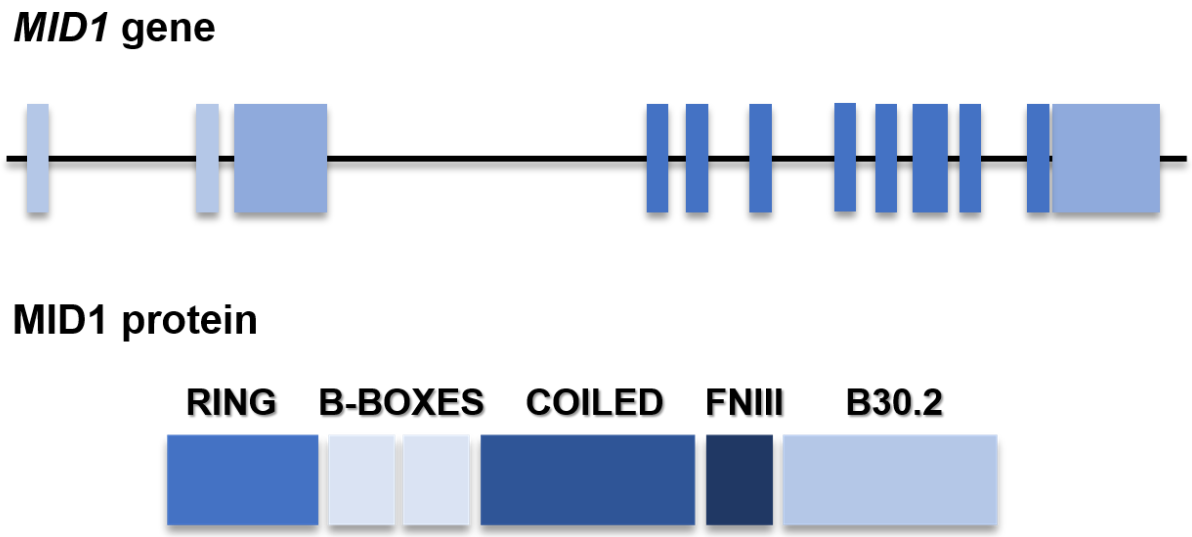

Figure 1 Scheme of the*MID1* gene and MID1 protein (adapted from Schweiger, Schneider 2003)

At the C-terminal side of the MID1 protein is a fibronectin type III domain, short known as FNIII, as well as a B30.2 domain. Both are involved in protein interactions (41, 42). Of particular note is the ability of the C-terminal end of MID1 to bind to microtubules (41).

As an E3 ubiquitin ligase, MID1 is essential for the specific cleavage of other proteins via proteasomal degradation. The process of ubiquitination begins with the activation of ubiquitin by an E1 enzyme and ATP at which ubiquitin binds covalently to E1 via a thioester bond. This activated ubiquitin is transferred to an E2 enzyme, the ubiquitin-conjugating enzyme. Finally, the E3 ubiquitin protein ligase couples the ubiquitin to the lysine residue of the target protein or an

already present ubiquitin. To ensure the specificity of degradation, there are approximately 10 E1-, 100 E2- and 1000 E3 ubiquitin ligases (43). By mono- or polyubiquitination, the target protein is labelled for degradation by the proteasome. Since MID1 is an E3 ubiquitin ligase, its activity is specific for a few target proteins. Best known is the ubiquitination of the catalytic subunit PP2Ac (Figure 2) (39). PP2A is an important serine/threonine phosphatase, which is ubiquitously expressed. It is evolutionarily highly conserved and a deletion in the catalytic subunit leads to a lethal phenotype in yeast and mice (44, 45). PP2Ac forms a heterotrimer with the two subunits A and B, which dephosphorylates different substrates with different B subunits regulating substrate specificity. The α4 subunit reduces its activity when bound to PP2Ac (46). Different subcellular pools of PP2A exist; one of them is microtubule-associated (39).

Ubiquitination and degradation of PP2Ac can occur, if non-mutant MID1 binds to α4. If MID1 is mutated, like in OS, it cannot associate with microtubules and aggregates in the cytosol. Hence, it can also not bind to α4 and the ubiquitination of PP2A is not possible (Figure 2) (39).

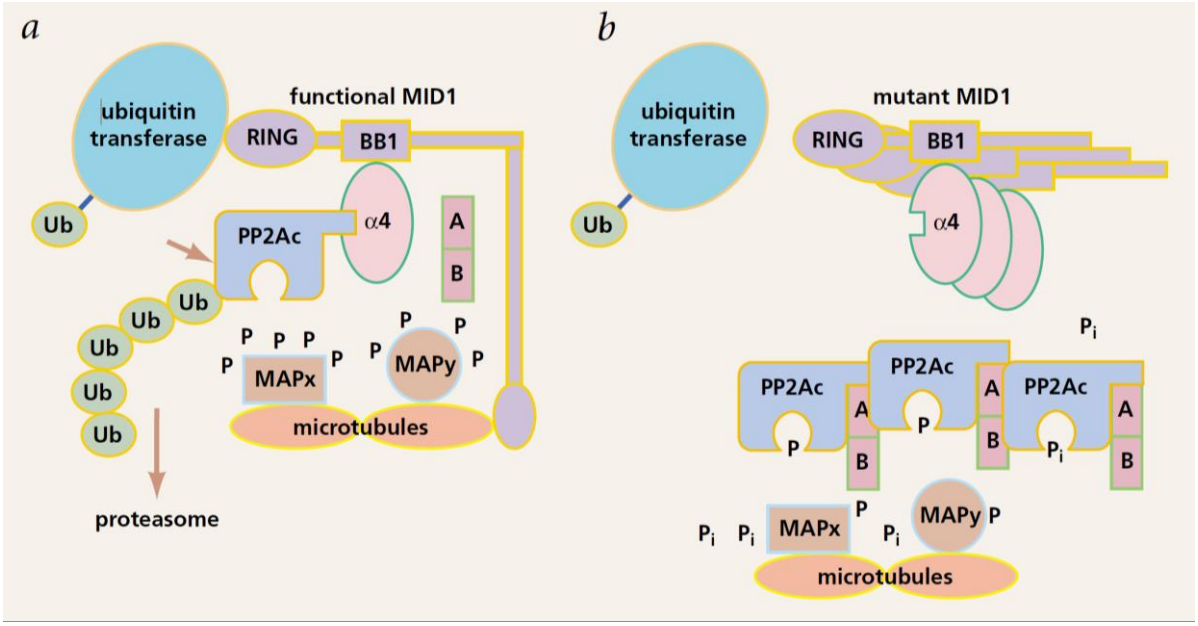

Figure 2 E3 ubiquitin ligase MID1 (a) Model of ubiquitination-dependent regulation of PP2Ac by MID1 (b) Mutated MID1 aggregates in the cells and cannot ubiquitinate PPAc; levels of PP2Ac in the cell increase (Trockenbacher et al. 2001)

MID1 thus regulates the breakdown of the catalytic subunit of PP2A, but also α4 is degraded via two different pathways mediated by MID1. On the one hand,

MID1 leads to polyubiquitination and proteasomal degradation, on the other hand it uses monoubiquitination to conduct degradation via the calpain pathway (47). The reduction of PP2A activity leads to an activation of its opposing kinase mechanistic target of rapamycin (mTOR). In particular, the formation of mTOR Complex 1 (mTORC1) is increased. This complex is involved in translation regulation and other central cellular processes by phosphorylating numerous substrates. Special attention is paid to eukaryotic initiation factor 4E-binding protein (4E-BP1) and 40s ribosomal S6 kinase (S6K), which are involved in the start of translation (16, 48).

If, as shown in Figure 2 (b), MID1 is not functional, this leads to an accumulation and increase in PP2A activity and thus to a decrease in mTORC1 (49).

Two other important targets of the E3-ubiquitin ligase function of MID1 are the Fused protein (Fu), which plays a role in the sonic hedgehog (shh) signaling cascade (50) and Paired box 6 protein (PAX6) (51).

Many roles of MID1 have been identified in cellular processes, including regulating the activity of the translational regulators PP2A and mTOR and assembling microtubule-associated protein complex involved in mRNA transport and translation (42). MID1 is also discussed to have a role in carcinogenesis and the pathogenesis of neurodegenerative diseases such as Alzheimer's and Huntington’s disease (16, 19, 50, 52-54). Challenging in studying MID1 is the lack of knowledge to what extent the function of MID1 is conserved in different organisms, especially between mouse and human. Experimental research shows differences in the functions between species (21, 28).

1.5 *Midline-2* Gene and Midline-2 Protein

The *MID2* gene, also called *FXY2*, is located on locus Xq22.3 and probably originated during evolution by an intrachromosomal gene duplication of the *MID1* gene (55). Accordingly, the structure of the two genes is quite similar. The murine *Mid2* gene is even more conserved between mouse and human than the *MID1* gene (56).

For the *MID2* gene, nine exons and two known transcripts have been described (57). The sites with the positions of splice junctions and the exon size are similar

in both genes. The exception is exon 6 of *MID2* which encodes for 30 additional amino acids (55).

Like its sister protein, MID2 is an E3 ubiquitin ligase and is called TRIM1 in the TRIM/RBCC protein family (33).

The amino acid sequence is 77% identical to that of MID1, with 30 additional amino acids. The functional structure between MID1 and MID2 is even more conserved. In the literature, the numbers for similarity vary between 83% and up to 92%. The individual domains show varying degrees of similarity, but never less than 68% (55).

While mutations in MID1 can lead to OS, as association of MID2 with genetic disorders is not so clear. During the analysis of an extended family, a mutation in the *MID2* gene was found to segregate with non-syndromic ID and developmental delay in the affected male members of the family (OMIM 300928). *In vitro* experiments could show that the mutation which is located in the C-terminal end leads to an accumulation of the protein in the cytosol (11).

The protein MID2 is often only investigated in the context of MID1. Therefore, its functions will be discussed in detail in the next chapter and compared to those of its sister protein.

1.6 Comparison of MID1 and MID2 Functions

As already mentioned, MID1 and MID2 proteins share 77% of the same amino acid sequence and the two genes are 70% identical in their nucleotide sequence (37). But although MID1 and MID2 have very similar functions, it is unclear to what extent defects of one protein can be compensated by the other (22). This could also play a role in the pathogenesis of OS. Since OS patients show a great variability in the expression of clinical symptoms, one assumption expressed in literature is that MID2 can partially take over functions of MID1 (58). This speculation exists for the *Mid1* KO mice described by Lancioni (21). The strain shows no signs of neurocristopathy. Therefore, the authors speculate that Mid2 can compensate for the function of the missing Mid1. First concrete evidence for the theory however, comes from chicken, where functional redundancy between MID1 and MID2 was detected during left-right determination (59). Similar redundancy was found in humans in cytotoxic T cells (CTL) in which MID1,

among other things, regulates exocytosis. In *Mid1* KO mice the exocytosis of lytic vesicles from CTL is reduced by 25%, while Mid2 is upregulated. By overexpressing Mid2, the phenotype could be rescued. This proves that Mid2 has partially the same functions in CTL and can replace them in the absence of Mid1 (60).

Due to the outstanding similarity some binding partners are identical. Identical functions are shown in the formation of homo- and heterodimers via the coiled coin domains. Also, the interaction partners of both proteins are partly identical. In *Xenopus laevis* it was shown that both proteins bind α4 via the B-Box domain and attach to microtubules, while Mid2 has a higher affinity to microtubules than Mid1 (37, 40). Both can regulate the homeostasis of this cytoskeletal component and are essential for neural tube closure (59).

One of the most important target proteins of MID1 is PP2Ac via the binding of α4 (22). Like MID1, MID2 interacts with α4 (37). Although there is no proof for the ubiquitination of PP2Ac, Cox et al. concludes that MID2 also has an ubiquitinating effect due to its high similarity to MID1 (33).

Still, differences can be found in various aspects. For example, the expression levels are inconsistent and cell- and stage-specific (11). In the cells of most tissues the MID2 concentration is lower that its sister protein. Exceptions are the heart, thymus and thyroid gland during embryonic development. It is particularly noticeable that MID2 is expressed in embryonic hearts unlike MID1 (56).

The target protein Astrin which has microtubule-organizing functions that are particularly important in mitosis, can be clearly assigned to MID2. Although it binds both MID1 and 2, it is only ubiquitinated by MID2. Through the degradation of Astrin, MID2 has a regulating effect on cell division (61).

For PAX6 which is also ubiquitinated by MID1, there is no information concerning ubiquitination by MID2 (51).

In conclusion further research is needed to understand the capacity and control for compensating the functions of the sister proteins. It should also be emphasized that the models for studying different proteins are not always fully transferable from one species to another.

1.7 Paired Box 6 Gene

PAX6 is the short form for *paired box 6* gene which belongs to a family of important paired type homeobox transcription factors (TF) (62, 63). The gene is located at locus 11p13 in humans, consists of 16 exons and spans about 30 000 bp (57). The murine representative is located on chromosome 2, a protein coding gene (63, 64).

Five relevant splice variants of the gene are known from literature. Of great relevance is the alternatively spliced *Pax6*(5a), which has an insertion of 14 amino acids in the protein. The expression of the two isoforms is tissue and development dependent (63). However, *Pax6*(5a) is not assigned specific functions in the cortex that cannot be taken over by *Pax6*, which is why it is of less importance in telencephalon than in other tissues (65).

The regulation of the Pax6 gene is very complex due to tissue specific regulators as well as upstream and downstream interactions. In the forebrain *Pax6* regulates itself by negative autoregulation (63, 66).

Mutations of the *Pax6* gene are mainly associated with eye diseases. The function of *Pax6* in the eye is maintained between vertebrates and invertebrates, so that a complete KO of the gene causes aniridia in different species (65). A heterozygous loss-of-function mutation also leads to severe developmental disorders of the eye and brain. These include midline anomalies (63).

In conclusion PAX6 is a highly conserved and central regulator in multiple cellular functions and especially in development of brain and eye. Its regulation and roles in different tissues is highly complex.

1.8 Paired Box Protein PAX6

Paired box protein PAX6 is also known as aniridia type 2 protein and consists of 422 amino acids. It has two DNA binding sites, the paired domain and the homeodomain (67).

PAX6 is a key TF involved in eye, brain and pancreas development. In the cortex it is expressed exclusively in dorsal telencephalon (62, 67). In the CNS it plays an important role in the regulation of the expression of numerous other proteins and genes. Specific KO analyses of the individual domains have shown that the

paired domain is of particular importance in the embryonic development of the cortex (65).

The role of PAX6 in regulation of the cell cycle is not consistent and depends highly on PAX6 expression levels. In neurogenesis it is known that PAX6 determinates neuronal fate and is highly expressed in the ventricular zone of the cortex in mice (63, 68).

In primate embryos PAX6 is expressed in tissues that are not yet evolutionary developed in rodents and expression patterns vary during development. Thus, it is important to analyze the roles of PAX6 in different species (63).

1.9 Embryonic Development of the Cortex

The overall brain structure in the embryo is similar in all mammals. Therefore, the basic principles will be described using humans as an example.

In all mammals the development of the cortex starts with the formation of the neural plate, which develops into the neural tube by closure. The neural tube is the origin of the spinal cord and brain, but also the neural cells of the head originate from the neural tube (69).

At the embryonic age of four weeks, three bilaterally symmetrical vesicles develop in the anterior part of the neural tube in the human embryo. The three vesicles form the first functional division into prosencephalon (forebrain), mesencephalon (midbrain) and rhombencephalon (hindbrain) (70).

The forebrain develops into the telencephalon with the two cerebral hemispheres and the unpaired diencephalon during the fifth week of embryonic development. Parts of the hindbrain develop into the cerebellum, which divides the rhombencephalon into the metencephalon and the myelencephalon. The mesencephalon lies between the rhombencephalon and the prosencephalon.

The telencephalon develops from the third to the seventh month of pregnancy. It is phylogenetically divided into neo- and allocortex. The forebrain development is characterized by rapid growth and concentric migration of cells from the ventricular matrix zone. These migrating cells later form the six cortical layers (I – VI) of the neocortex. The migrating cells find orientation mainly at the extensions of the radial glia cells (RGC) (71, 72). Figure 3 shows the layering in the fetal human cortex on the right side.

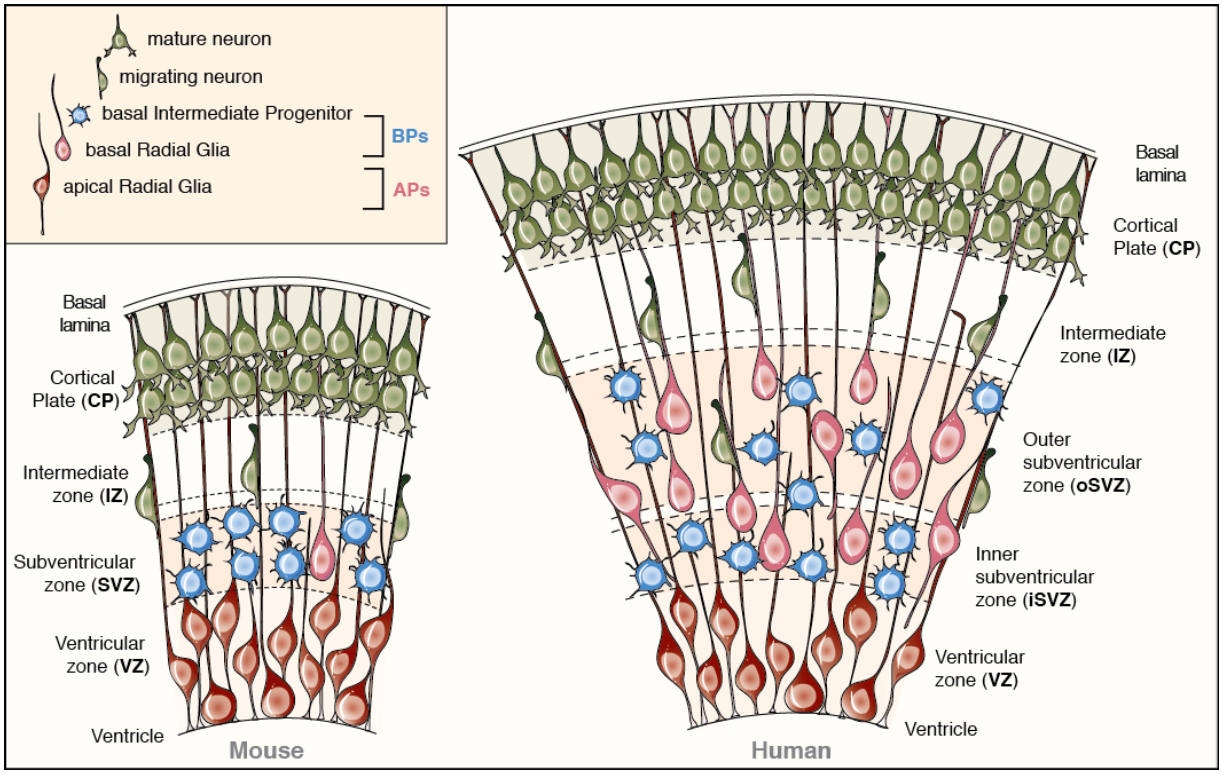

Figure 3 Scheme of embryonic cortex of mice and human. Figure illustrating APs and BPs in embryonic mouse (left) and fetal human (right) neocortex. Located near the ventricle is called apical, while the distant layers are referred as basal. The underlying structure is quite similar. Note the increase in BPs and the expansion of the SVZ in fetal human neocortex (Florio et al. 2016).

In the ventricular zone (VZ), also known as the mantle zone, RGCs can be found and are often referred to as apical progenitor cells (APs) (63). These cells have the ability to form neurons and precursor cells through asymmetrical division (73). In the early stages of brain development, only the subpial marginal zone can be differentiated from the VZ. Later, the subventricular zone (SVZ) forms basal to the VZ. In primates, the SVZ can be divided into an inner (iSVZ) and an outer subventricular zone (oSVZ). Comparing humans and non-human primates as gyrencephalic animals with lissencephalic animals like mice, the division into oSVZ and iSVZ is thought to be essential for the distinct developments of the cortex. In primates the SVZ starts to emerge at an earlier developmental stage and shows a greater expansion. The oSVZ then arises as a specialized layer with dense, radially orientated precursors (74-76).

In the mouse the SVZ contains intermediate progenitor cells (iPC), which undergo symmetric division and generate neurons. Together with basal radial glial cells, they are referred to as basal progenitors (BPs). Migration from the VZ forms the intermediate zone (IZ). The later the start of migration of the post-mitotic neurons from the VZ, the further they migrate outwards. This pattern is

called “inside-out”, neurons destined for the deep layers VI and V are born first, neurons that are generated late have to pass these neurons to settle more superficially in the layer IV, III and II (77, 78). Beneath the basal lamina, the cortical plate (CP) is formed at the end of embryonic development. The CP contains post-mitotic neurons, the precursor cells of the layers II–VI (79, 80). During neurogenesis the outmost layer the marginal zone (MZ) mainly contains Cajal-Retzius cells, which inhibit migration by expressing reelin (81, 82). It later forms layer 1 in the adult cortex, which is therefore distinct from its developmental origin (77).

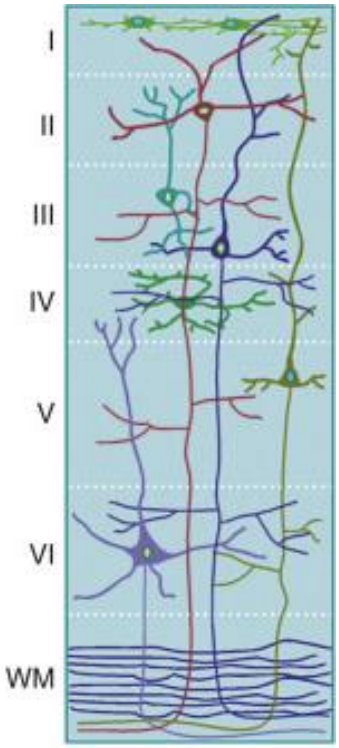

Figure 4 Layers of the adult mammalian brain. Layer I-VI are shown with the characteristically neurons and synapses. In the white matter axons follow the paths. (Bronner, Hatten, 2015)

During development the VZ loses its role as a proliferation zone, while the SVZ keeps a potential for neurogenesis until birth and even postnatally (83). Postpartum, neurons rarely proliferate. The plasticity of the brain even in adulthood is ensured by the ability of synapses to change by reorganization and altering their connectivity and strength (69). The cortex forms gray matter, which mainly consists of nerve cell bodies that surround the white matter, predominantly consisting of axons (Figure 4) (84).

Proliferation, differentiation and migration of neurons and progenitor cells are controlled by numerous proteins and translation factors. Of central importance are the nerve growth factor (NGF) and the brain-derived neurotrophic factor (BDNF), but during neurogenesis every zone has its own expression pattern. This is a result of an order of specific proteins being expressed and thus characterizing different cell types. These proteins can be used in stainings, protein analysis etc. to visualize the different zones in brain slices. In the VZ the RGCs express Pax6 (See Paired Box 6 Gene), a major TF in the brain. In iPCs, also called BPs, Pax6 is downregulated, while T-box brain protein 2 (Tbr2) is upregulated. iPCs can be found in the VZ and SVZ. After mitosis, these cells become postmitotic projection neurons and express T-box brain protein 1 (Tbr1). These cells can be found in the preplate,

the predecessor of the CP (68). This strict separation cannot be seen equally in all mammalian species. It is applicable on lissencephalic species like mice where corticogenesis occurs between embryonic day (E) 11.5 and E17.5. In gyrencephalic primates the developing cortex has a more complex expression pattern as shown in Figure 5. In these species Pax6 is expressed in the VZ, iSVZ and oSVZ and often co-expressed with Tbr2, illustrated on the right side of the figure, where some cells are striped in red and green (63).

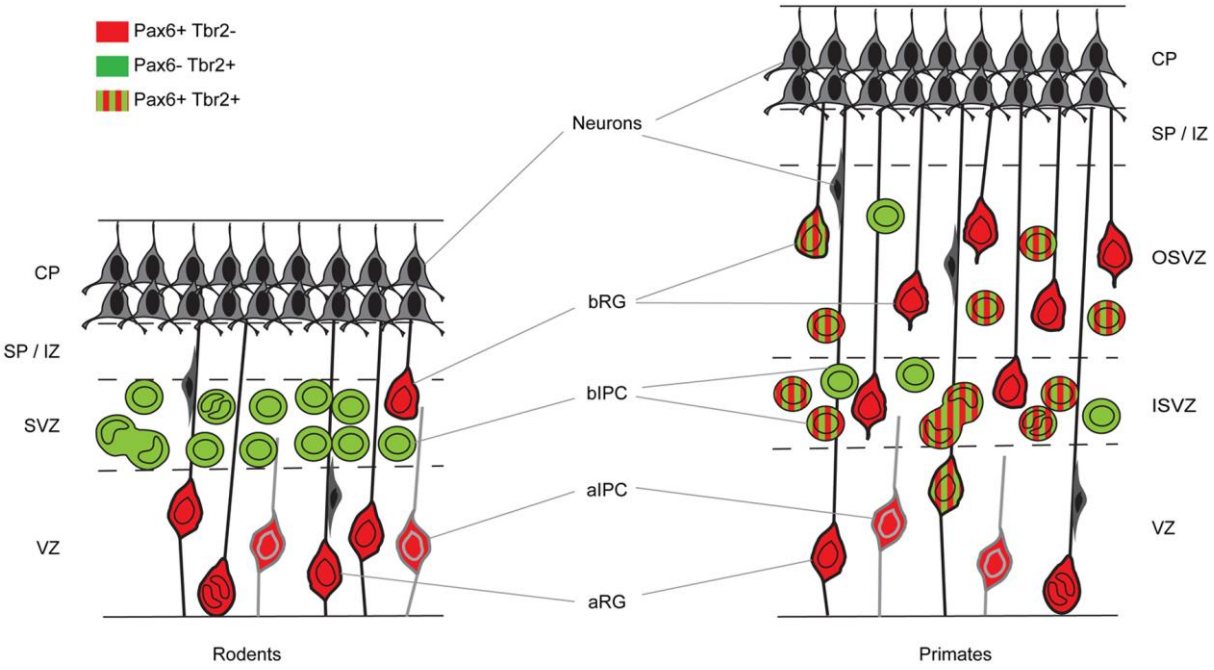

Figure 5 Expression pattern in embryonic cortex of rodents and primates. In primate cells in the iSVZ and oSVZ can coexpress Pax6 and Tbr2 (Manuel et al. 2015)

Also, other proteins can be used to mark specific cell types and layers. Satb2 (Special AT-rich sequence-binding protein 2) is a TF first expressed in immature, postmitotic neurons, when these neurons begin to migrate into the IZ and persists postnatally in the upper layer neurons (85, 86).

A functioning nerve system depends on the communication between neurons. Therefore, connections exist as axon paths between different cortical fields (association pathways), but also between the two cerebral hemispheres (commissure systems). One part of the commissure system affected in 30% of patients with OS is the Corpus Callosum (C. callosum) (See Opitz BBB/G-Syndrome) (87). The C. callosum is the commissure system of the two cerebral cortices consisting of 200–250 million axonal projections (88). Embryology of it is not well known, but the development is linked to the hemispheres. Due to the

massive increase of the hemisphere´s sizes, the C. callosum also increases in size, especially posteriorly, where it is bounded by the mesencephalon.

1.10 Embryonic Development of the Neural Crest

As OS belongs to the neurocristopathies affecting the development of the neural crest, it is important to understand the process behind it (See Opitz BBB/G-Syndrome). The formation and migration of neural crest cells (NCC) are two essential mechanisms in ventral midline development (40).

Apart from occurring during wound healing and in neoplastic cells, epithelial-mesenchymal transition (EMT) plays an important role in several steps of embryonic development. The principle of EMT is that epithelial cells that interact with a basal membrane can gain a mesenchymal phenotype. As mesenchymal cells, they have a higher migratory ability and invasiveness. For this process the cell adhesion protein E-cadherin need to be repressed, while N-cadherin is increase, the cytoskeleton is reorganized and expression of vimentin increases (40, 89).

During closure of the neural tube, neural crest cells arise from the border of the neuroectoderm and separate from the neural tube. The neural crest is then located next to the dorsal tube (Figure 6). The cells of the neural crest are multipotent stem cells. After undergoing EMT, these cells migrate throughout the embryo and differentiate into a large variety of cell types. For example cartilaginous and skeletal elements of the head, cardiac valves, melanocytes,

autonomic ganglion neurons and Schwann cells originate from NCCs after migration (90).

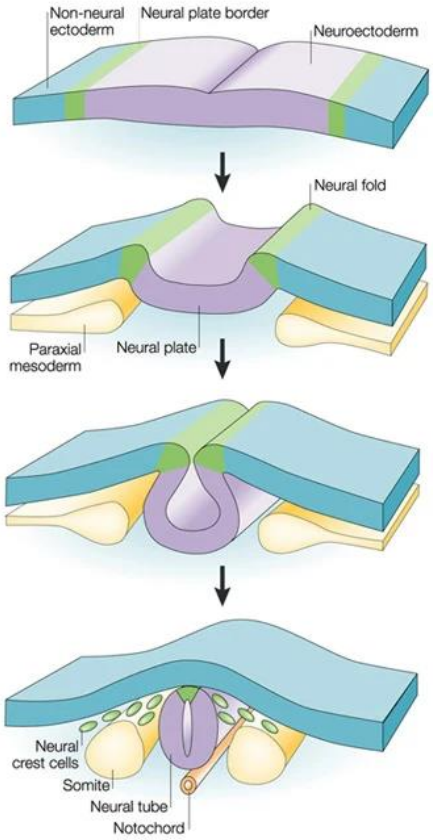

Figure 6 The neural plate border (green) elevate and become the neural folds and the neural tube forms. NCCs (green) delaminate from the neural folds and lie next to the dorsal neural tube (Gammil & Bronner-Fraser 2003)

It is poorly understood, how MID1 influences NCCs, their development and migration. Other neurocristopathies show hypoplasia of facial bones and cartilages, which is not present in OS. This may lead to the assumption that NCCs are formed, but migration, proliferation and/or differentiation may be affected in OS patients (16, 27, 28). Challenges to study the effect of MID1 on neural crest development is that *Mid1* KO mice do not show any neural-crest specific defects of the ventral midline (21).

1.11 MID1 in Neuronal Development

As described in Chapter 1.4 MID1 has multiple functions in development and pathogenesis, while it is mainly unknown how MID1 is involved in the developing brain. Murine *Mid1* is expressed throughout development, and in early

development (E9–E10.5) expression is ubiquitously (91). From E12.5 to E16.5 high levels of *Mid1* expression can be found in the CNS, especially in the proliferating neuroepithelium of the telencephalon, while its transcription is repressed in post-mitotic neurons. *Mid1* gene expression stays at a similar level from E14.5 to adult in the cerebral cortex of mice (22). In the neural retina *Mid1* is transcribed at E16.5. In human embryos *MID1* is expressed in early stages of development in the CNS (92).

To study the influence of *MID1* during development two different kind of experiments can be used. Studies on a cellular level provide information about the function of MID1 in neurons and other cell types, while research on organ level give broader insights to neurodevelopment. Hereafter findings from research on a cellular basis will be described first.

Depletion of Mid1 in growing neurons lead to an increased axon growth and branching. In *in utero* electroporated mice silencing Mid1 lead to a disruption in callosal axon projections to the contralateral hemisphere. No effect on neuronal-precursor cell proliferation and neuronal identity was observed. These effects published by Lu et al. and reproduced by Willam may be due to accumulation of PP2Ac (22, 93). As MID1 regulates degradation of PP2Ac, a loss-of-function of MID1 results in higher levels of PP2Ac (47). Subsequently, in fibroblasts from OS patients increased PP2Ac levels will result in changes of mTOR pathway that lead to reduced cell size (48, 94). In contrast, overexpression (OE) of Mid1 in HeLa cells lead to faster migration but had no significant effect on proliferation (93). Other findings showing effects of MID1 on cellular mechanisms, are that MID1 contributes to apoptosis mediated by p38 mitogen-activated protein kinase (MAPK) (12).

However, the function of MID1 in organogenesis is not fully understood. That MID1 has a role in neurodevelopment is clinically manifested in structural brain defects, which up to 36% of OS patients show (16). This effect is due to mutations in *MID1,* which is supported by the finding, that *Mid1* KO mice show similar structural brain defects (21). The most common malformation in these mice are cerebellar vermis agenesis or hypoplasia. Around 1/3 of OS patients show brain abnormalities with cerebellar vermis agenesis or hypoplasia the most common frequent one. These defects originate prenatally and may be due to disturbances

in dorsal midbrain and cerebellum cells. *Mid1* KO mice show motor coordination and motor learning impairment (21).

Literature states two different underlying mechanisms how *MID1* influences neurodevelopment and causes pathologies. On one hand Mid1 may regulate neural development by modulating the cytoskeleton via PP2A (22). On the other hand MID1 is linked to mRNAs via a purine-rich sequence motif called MIDAS (MID1 association sequence). This increases their stability and especially translational efficiency. Genes that carry MIDAS motifs play an important role during development, but there is only a small group of genes known to contain this sequence. Thus, MID1 protein regulates protein translation of these genes and mutations could lead to a loss of cytoskeleton-bound protein translation (94). Even if both theories have yet to be further analyzed, both concepts share the connection of MID1 to microtubule and therefore do not exclude each other.

Finally it is important to mention, that a major problem in studying the protein function of MID1 remains the largely unknown compensation capacity of MID2 (59).

1.12 PAX6 in Neuronal Development of the Forebrain

Pax6 is a major TF in the cortex and highly conserved between species (51). It influences development of the nervous system by regulating proneural genes (67). In the forebrain it impacts patterning, neurogenesis and proliferation through regulating stem and progenitor cell proliferation. Pax6 functions as a intracellular TF, but also extracellular Pax6 has an influence on cell migration, presenting cell autonomous and non-autonomous activities (95).

The expression of Pax6 follows a clear pattern in the developing mammalian cortex which is best studied in mice. *Pax6* is expressed by RGCs in the VZ of the forebrain in a high rostrolateral to low caudomedial gradient (Figure 7). The expression of *Pax6* is the first in a sequence of protein expression. Pax6 is followed by Ngn2, Tbr2 and finally Tbr1 is expressed. This order reflects the transition from RGCs to BPs to post-mitotic neurons in rodents (63). Contrary to rodents, in primates Pax6 is expressed not only in the VZ, but in the ISVZ and OSVZ (84) (See Embryonic Development of the Cortex).

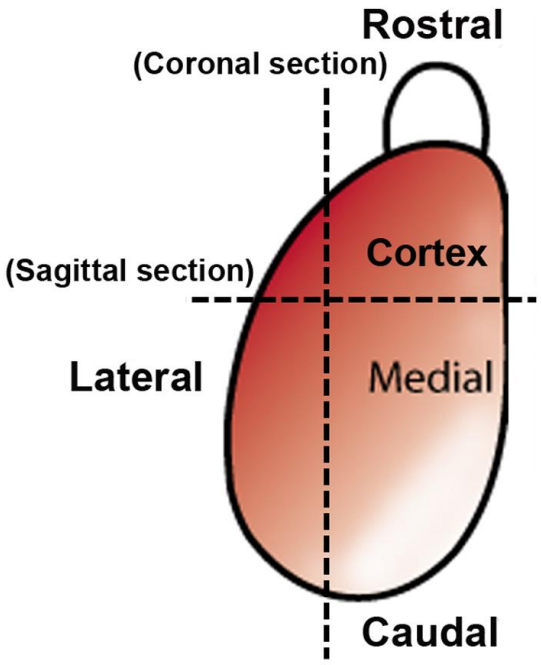

Figure 7 The gradient expression pattern of Pax6 protein in the embryonic mouse cortex. Pax6 protein expression is colored in red. It is expressed in a rostrolateral to caudomedial gradient. Rostral the expression is high, while in the caudal part of it is low. (Adapted from Manuel et al. 2015)

In the embryonic cortex *Pax6* can induce the RGCs of the VZ to generate neurons and glia cells and is therefore an intrinsic determinant of neuronal fate. Studies in *Pax6* KO mice showed that the number of neurons generated from RGCs is reduced by half (96). A KD experiment in human fetal RGCs also showed a decrease in the number of generated neurons, implying that the role of *Pax6* in neurogenesis is preserved throughout different species (97). In *PAX77* mice in which Pax6 protein levels are increased, the number of late cortical proliferating progenitor cells are reduced in the rostral, but not in the caudal cortex. The study showed that cell cycle length and exit was influenced by *Pax6* too (66). Interestingly neurogenesis which was reduced in *Pax6* KO was not affected by increased Pax6 expression at late stages of corticogenesis (96, 98). This might be affiliated to limited overexpression capacity of the *PAX77* mouse model due to autoregulation of protein expression (66, 99). To summarize, it should be noted that *Pax6* inhibits proliferation and promotes neurogenesis during forebrain development (62). As Pax6 is a central player in development and a component of many cellular processes, it is comprehensible that also its effects are complexly regulated, concluded. This was summarized by Manuel et al (63).

Humans with heterozygous loss-of-function mutations of *Pax6* gene suffer from severe defects of the eye as well as neurological and psychiatric disorders, for example autism and ID. But even in patients without ID, structural brain defects can be found. These include reduced size of C. callosum, abnormalities of the cortex and absence of the pineal gland (63).

1.13 Ubiquitination of PAX6 by MID1

As described in Chapter 1.4 Mid1 is an E3 ubiquitin ligase with several known target proteins. One of these interaction partners is Pax6. So far this has been investigated in eye development of *Xenopus laevis* (51).
Pax6 is an important TF in eye development and depends on defined expression levels (100). In the first step of eye development *Pax6* is expressed in the whole eye field. With the segregation of the eye field into the optic cup and the optic stalk, Pax6 expression is clearly restricted to the optic cup. It has not yet been investigated how this sharp boundary of gene expression is formed. Some authors argue that an upregulation of *Shh* lead to a downregulation of *Pax6* (101). Pfirrmann et al. found, that Mid1 ubiquitinates Pax6 in the eye stalk of *Xenopus* embryos. Across this path Mid1 regulates the proteasomal degradation of Pax6 protein. Moreover, they found that Shh controls *Mid1* expression in the eyestalk and thus regulates Pax6 activity (51).
It remains unclear if the findings apply to cortex development. In contrast to corticogenesis where *Pax6* inhibits proliferation and promotes neurogenesis, in the retina of the eye it promotes proliferation (62). However, as *Pax6* has a highly conserved sequence through species, while having different functions during cortex development, the question rises how the different effects of *Pax6* can be explained. This could be achieved by distinct upstream or downstream regulators (63). If *Mid1* has a function in these regulatory mechanisms is not yet known, although it should be noted that *Mid1* and *Pax6* are both associated with abnormal C. callosum (20, 63, 102).

1.14 Purpose of the Thesis

In this thesis the role of both, MID1 and MID2 protein during neurogenesis was investigated. Both are known to eventually cause ID if mutated. MID1 is well

investigated and responsible for the monogenic OS (16, 91). MID2 could only be linked to ID in family case studies and is not as well investigated (11). Nevertheless, it remains unclear how both of the proteins effect the phenotypes (11, 40). Therefore, *in vivo* studies in the embryonic mouse brain were conducted.

One aim of this thesis was to generate an OE of the gene *Mid1* via *in utero* electroporation (IUE) on embryonal day E13.5, which should reveal its influence on neuronal migration, differentiation and proliferation during neurogenesis. First, the OE efficacy was validated in cells, checking for expression of the plasmid and protein levels. Then, the electroporated embryonic mouse brains were frozen and cryosections were prepared. Afterwards, immunohistochemistry was conducted and analyzed.

Furthermore, a KO of *Mid1* and *Mid2* should give new insights into functions of both sister proteins and a possible compensation mechanism by *Mid2*. Using genetically modified $Mid1^{lox}$/$Mid2^{lox}$ mice, the IUE of a Cre recombinase plasmid should lead to a conditional KO of both genes. Again, immunofluorescent staining of cryosections was established. The impact of the KO of both proteins on neuronal migration, differentiation and proliferation during neurogenesis should be evaluated. The effect of the Cre recombinase plasmid *in vivo* should be verified by quantitative polymerase chain reaction (qPCR) analysis of electroporated cells.

Additionally, a KD construct for the Mid1 target Pax6 was developed and established for IUE.

2 Material and Methods

2.1 Material

2.1.1 Equipment

Table 1 Devices and Manufacturer

Devices	Manufacturer
ChemiDocsTM	Bio-Rad, Munich (DE)
Cryostat, Leica CM3050S	Leica, Nussloch (DE)
Gel Chamber PerfectBlue™ Gel System Mini L	VWR, Darmstadt (DE)
Gel Chamber PerfectBlue™ Gel System Mini M	VWR, Darmstadt (DE)
Gel Chamber PerfectBlue™ Gel System Mini S	VWR, Darmstadt (DE)
Incubator Certomat®H Heizen	B. Braun Biotech, Melsungen (DE)
Incubator Certomat®R Tischschüttler	B. Braun Biotech, Melsungen (DE)
Magnetic Stirrer MR3001	Heidolph Instruments, Schwabach (DE)
Microscope ECHO Revolve	Echo, San Diego (USA)
Microscope Leica DMRA2	Leica Mikrosysteme Vertrieb GmbH, Wetzlar (DE)
Microscope Leica SP5	Leica Mikrosysteme Vertrieb GmbH, Wetzlar (DE)
Mini-Inkubator INCU-Line	VWR, Darmstadt (DE)
Mini-PROTEAN® Tetra Cell	Bio-Rad, Munich (DE)
Mini Centrifuge neolab D-6015	neoLab Migge Laborbedarf-Vertriebs GmbH, Heidelberg (DE)
NanoDrop 1000 Spectrophotometer	ThermoScientific, Massachusetts (USA)
NanoDrop One^{c}	ThermoScientific, Massachusetts (USA)
Electrophoresis Power Supply peqlab EV215	VWR, Darmstadt (DE)

Slides SUPERFROST®PLUS	ThermoScientific, Massachusetts (USA)
Satorius pH Basic Meter PB-11	Satorius AG, Göttingen (DE)
Pipettors accu-jet®	Brand GmbH & CO KG, Wertheim (DE)
Qubit® 2.0 Fluorometer	ThermoScientific, Massachusetts (USA)
Tube Shaker REAX 2000	Heidolph Instruments, Schwabach (DE)
Roller Mixer SRT9D Stuart®	Bibby Scientific Limited, Staffordshire (UK)
Roller Trans-Blot® Turbo™ Transfer System	Bio-Rad, München (DE)
Stereo-Microscope Leica MZ12.5	Leica Microsystems, Wetzlar (DE)
StepOne Plus™ Real Time PCR System	ThermoScientific, Massachusetts (USA)
Thermocycler Peqstar	PEQLAB, Erlangen (DE)
Thermocycler Primus 96 Advanced	PEQLAB, Erlangen (DE)
ThermoMixer C	Eppendorf, Wesseling-Berzdorf (DE)
Tissue-Tek® Cryomold®	Sakura Finetek, Alphen aan den Rijn (NLD)
Thriller	PEQLAB, Erlangen (DE)
Trans-Blot® Turbo™ Transfer System	Bio-Rad, München (DE)
UV Transilluminator Intas Gel iX Imager	Intas-Science-Imaging Instruments GmbH, Göttingen (DE)
Scale Scout™ pro	Ohaus Europe GmbH, Nänikon (CHE)
Watherbath WNB 7	Memmert GmbH + Co. KG, Schwabach (DE)
Centrifuge 5415D	Eppendorf, Wesseling-Berzdorf (DE)
Centrifuge Biofuge fresco, Heraeus	ThermoScientific, Massachusetts (USA)
Centrifuge Megafuge, Heraeus, 16R Centrifuge	ThermoScientific, Massachusetts (USA)

Centrifuge Microfuge® 16	Beckman Coulter GmbH, Krefeld (DE)
Centrifuge Peqlab PerfectSpin 24R Refrigerated	PEQLAB, Erlangen (DE)
Centrifuge Peqlab PerfectSpinP	PEQLAB, Erlangen (DE)

2.1.2 **Reagents**

Table 2 Used Reagents, their Manufacturer and Order Number

Chemicals	**Manufacturer**	**Order Number**
10x Buffer for T4 DNA Ligase with 10mA ATP	New England Biolabs GmbH, Frankfurt am Main (DE)	B0202S
2-Mercaptoethanol	Roth, Karlsruhe (DE)	4227.3
2-Propanol	Roth, Karlsruhe (DE)	6752.1
6x DNA Loading Dye	ThermoScientific, Massachusetts (USA)	R0611
Agar-Agar	Roth, Karlsruhe (DE)	5210.2
Agarose	AppliChem, Darmstadt (DE)	A2114,0500
Ampicillin	AppliChem, Darmstadt (DE)	A0839,0010
APS (Ammonium Persulfate)	Sigma-Aldrich, München (DE)	A3678
Bromphenolblau	Roth, Karlsruhe (DE)	T116.1
BSA (Albumin Fraktion V)	Roth, Karlsruhe (DE)	T844.2
Buffer $MgCl_2$	New England Biolabs GmbH, Frankfurt am Main (DE)	B9021S
CutSmartTM Buffer	New England Biolabs GmbH, Frankfurt am Main (DE)	B7204S

DAPI (4′,6-Diamidino-2-phenylindole dihydrochloride)	Sigma-Aldrich, Missouri (USA)	D9542-5MG
DPBS (Dulbecco´s Phosphate Buffered Saline)	ThermoScientific, Massachusetts (USA)	14190-094
EDTA (Ethylenediaminetetra acetic Acid)	AppliChem, Darmstadt (DE)	A1104,1000
EGTA (Egtazic Acid)	Roth, Karlsruhe (DE)	3054.2
Ethanol 99%	AppliChem, Darmstadt (DE)	A2795,5000
Fluoromount™ Aqueous Mounting Medium	Sigma-Aldrich, München (DE)	F4680
Formamid	Roth, Karlsruhe (DE)	6749.1
Gel Loading Dye, Blue (6x)	New England Biolabs GmbH, Frankfurt am Main (DE)	B7021S
GeneRuler™ 1 kb DNA Ladder	ThermoScientific, Massachusetts (USA)	SM0313
GeneRuler™ 100 bp DNA Ladder	ThermoScientific, Massachusetts (USA)	SM0241
Glycerin	Roth, Karlsruhe (DE)	3783.1
Glycin	Roth, Karlsruhe (DE)	3790.2
Urea	Roth, Karlsruhe (DE)	2317.3
Tissue-Tek® O.C.T.™ Compound	Sakura Finetek, Alphen aan den Rijn (NLD)	4583

2.1.3 **Kits**

Table 3 Used Kits, Manufacturers and Order Numbers

Kit	**Manufacturer**	**Order Number**

Agarose GelExtract Mini Kit 50 Preps	5Prime, Hilden (D)	2300500
EndoFree® Plasmid Maxi Kit (10)	Qiagen, Venlo (NLD)	12362
Herculase II Fusion DNA Polymerase	Agilent	600675
MinElute® Extraction Kit	Qiagen, Venlo (NLD)	28604
QIAprep® Spin Miniprep Kit (250)	Qiagen, Venlo (NLD)	27106
QIAshredder (250)	Qiagen, Venlo (NLD)	27106
Qubit® Protein Assay Kit	ThermoScientific, Massachusetts (USA)	Q33211
Qubit® RNA HS Assay Kit	ThermoScientific, Massachusetts (USA)	Q32852
RevertedAid First Strand cDNA Synthesis Kit	ThermoScientific, Massachusetts (USA)	K1622
RNeasy® MicroKit (50)	Qiagen, Venlo (NLD)	74004

2.1.4 **Buffers and Solutions**

Table 4 Used Solutions and Buffers

Solution and Buffer	**Composition**
0,5 M Tris pH 6,8	30,275 g Tris ad 400 ml Millipore, adjust to pH 6,8 with HCl and fill up to 500 ml with Millipore
1,5 M Tris pH 8,8	90,825 g Tris ad 400 ml Millipore and adjust with HCl to pH 8,8, fill with Millipore ad 500 ml
10 % SDS	10 g SDS ad 90 ml Millipore and heat to 90 °C
10 % Seperating Gel	1,9 ml Millipore 1,3 ml 1,5 M Tris pH 8,8 1,7 ml 30 % Acrylamide 50 µl 10% SDS 50 µl 10 % APS 2 µl TEMED

10% Towbin Buffer	100 ml Towbin Buffer10x, 200 ml methanol and 700 ml deionized water
15 % Sucrose	7,5 g Sucrose ad 50 ml DPBS. Store at 4 °C
1x TAE Buffer	2 ml Millipore ad 100 ml 50x TAE
2x Magic Mix	48 % Urea 15 mM Tris pH 8 8,7 % Glycerin 1 % SDS 1 Tablette cOmplete ULTRA to 10 ml
30 % Sucrose	15 g Sucrose ad 50 ml DPBS. Store at 4°C.
4 % PFA	4 g PFA in 100 ml Millipore, heat to 60 °C, dissolve with 10 M NaOH. Store at -20 °C
5 % Stacking Gel	1,4 ml Millipore 250 µl 1,0 M Tris pH 6,8 330 µl 30% Acrylamide 20 µl 10 % SDS 20 µl 10 % APS 2 µl TEMED
50 % Tissue-Tek®	25 ml 30 % Sucrose ad 25 ml Tissue-Tek® Store at RT
50x TAE Puffer	242 g Tris 18,6 g EDTA 57,1 ml Acetic acid (100 %) ad 1 L Millipore
Agarose gel	8 g Agarose ad 400 ml 1x TAE Buffer heat. Per 100 ml 2 µl EtBr
Agar-Plates	10 g Tryptone 5 g Yeast extract 5 g NaCl 15 g Agar-Agar ad 1 l Millipore, autoclave and add 100 mg Ampicillin per Liter
Annealing Buffer	30 mM Hepes pH 7,4 100 mM Potassiumacetat 2 mM Magnesiumacetat ad 100 ml Millipore. Store at -20 °C
Blocking Buffer (Staining)	0,2 % Triton® X-100 2 % Sheep Serum in 1x PBS
Blocking Buffer (Western Blot)	2,5 g milk powder ad 50 ml PBS-T
Digestion Buffer	3 mL 1M Tris ph8, 400 µl 0,5 M EDTA, 6 mL 1M NaCl, 20,54 mL dH_20
LB-Medium	10 g Tryptone 5 g Yeast extract 5 g NaCl ad 1 l Millipore, autoclave, add 100 mg Ampicillin per liter
Natriumcitrate Buffer	10 mM NaCit ad 1 l Millipore
PBS-T	2 tablets PBS 0,1 % Tween® 20 ad 1 l Millipore
SDS Puffer	28,8 g Glycine 6 g Tris 2 g SDS ad 2 l Millipore

Washing Buffer (Staining)	0,2 % Triton® X-100 ad 50 ml DPBS

2.1.5 **Antibodies**

Table 5 Antibodies, Manufacturer and Order Numbers

Antibody	**Manufacturer**	**Order Number**
Anti-Actin rabbit	Sigma-Aldrich, München (DE)	A2066
Anti-Cleaved-Caspase3 Antibody	Cell Signaling, Massachusetts (USA)	#9661
Anti-GAPDH Antibody	Abcam, Cambridge (UK)	AB8245
Anti-GFP mouse IgG monoclonal antibody	Sigma-Aldrich, München (DE)	11814460001
Anti-GFP rabbit	ThermoScientific, Massachusetts (USA)	**#**MA5-15256
Anti-HA	Abcam, Cambridge (UK)	AB20084
Anti-Ki67 Antibody	ThermoScientific, Massachusetts (USA)	**#**14-5698-82
Anti-MID1	Selfmade	-
Anti-Pax6 Antibody	Millipore, Temecula (USA)	2237
Anti-Satb2 Antibody	Abcam, Cambridge (UK)	AB34735
Anti-TBR2 Antibody	Millipore, Temecula (USA)	AB15894
Fluoromount-G™ mit DAPI	ThermoScientific, Massachusetts (USA)	00-4959-52
Goat anti-Chicken igG (H+L) Secondary Antibody, Alexa Fluor® 594 conjugate	ThermoScientific, Massachusetts (USA)	A-11042
Goat anti-Mouse IgG (H+L) Secondary Antibody, Alexa Fluor® 488 conjugate	ThermoScientific, Massachusetts (USA)	A-11001

Goat anti-Mouse IgG (H+L) Secondary Antibody, Alexa Fluor® 594 conjugate	ThermoScientific, Massachusetts (USA)	A-11005
Goat anti-Rabbit IgG (H+L) Secondary Antibody, Alexa Fluor® 488 conjugate	ThermoScientific, Massachusetts (USA)	A-11008
Goat anti-Rabbit IgG (H+L) Secondary Antibody, Alexa Fluor® 594 conjugate	ThermoScientific, Massachusetts (USA)	A-11012
Goat Anti-Rat IgG H&L (Alexa Fluor® 594) preadsorbed	ThermoScientific, Massachusetts (USA)	AB150168

2.1.6 **Plasmids**

Table 6 Used Plasmids and Manufacturer

Plasmid	**Manufacturer**
pCAGGS-Cre-IRES-GFP	Verdon Taylor, Embryology and Stem Cell Biology Department of Biomedicine University of Basel (CHE)
pCAGGS-empty-IRES-GFP	
pSUPERIOR.puro	OligoEngine, Seattle (USA)
pCMV-tag 2A	
pCMV-tag 3A	
pCAG-IG	Jan Baumgart, TARC Mainz (D)

2.1.7 **Bacteria**

Table 7 Used Bacteria, Manufacturer and Order Number

Bacteria	**Manufacturer**	**Order Number**

One Shot Top10 Chemically Competent *E. coli*	ThermoScientific, Massachusetts (USA)	C404003

2.1.8 **Cells**

Table 8 Used Cells and their Origin

Cells	**Origin**
HeLa-cells	Sybille Krauss, Deutsches Zentrum für Neurodegenerative Erkrankungen in der Helmholtz-Gemeinschaft, Bonn (DE)

2.1.9 **Enzymes**

Table 9 Used Enzymes, their Manufacturer and Order Number

Enzyme	**Manufacturer**	**Order Number**
BglII	New England Biolabs GmbH, Frankfurt am Main (DE)	R0144S
EcoRI-HF®	New England Biolabs GmbH, Frankfurt am Main (DE)	R3101S
Expand long range, dNTPack	Roche Diagnostics GmbH, Indianapolis (USA)	04 829 034 001
FastStart Taq Polymerase	Roche Diagnostics, Mannheim (DE)	04 738 381 001
HindIII	New England Biolabs GmbH, Frankfurt am Main (DE)	R0104S
HindIII-HF®	New England Biolabs GmbH, Frankfurt am Main (DE)	R3104S

Proteinase K	New England Biolabs GmbH, Frankfurt am Main (DE)	P8107S
T4 DNA Ligase	New England Biolabs GmbH, Frankfurt am Main (DE)	M0202S
Takara TB Green™ Premisx Ex Taq™ II, ROX plus	Takara Bio, Göteborg (SWE)	RR82LR
Taq DNA Polymerase	Axon, Kaiserslautern (DE)	22466
XbaI	New England Biolabs GmbH, Frankfurt am Main (DE)	R0145S
XhoI	New England Biolabs GmbH, Frankfurt am Main (DE)	R0146S

2.1.10 **Primer**

Table 10 Used Primers

Primer	**Sequences (5´- 3´)**	Company
Bluescript	TCGAGGTCGACGGTATC	Sigma-Aldrich, München (DE)
CMV-F	CGCAAATGGGCGTAGGCGTG	Sigma-Aldrich, München (DE)
GAPDH For	TCCATGACAACTTTGGCATT	Sigma-Aldrich, München (DE)
GAPDH Rev	GTTGCTGTTGAAGTCGCAGG	Sigma-Aldrich, München (DE)
H1_Primer	TCGCTATGTGTTCTGGGAAA	Sigma-Aldrich, München (DE)
Mid1 Lf	CTGACCGTACACCAATTAGAGAAA TTCCG	PHENOMIN-ICS, Illkirch (FRA)

Mid1 Lf²	GGAATCCTGTCCTGCTATTGCCTATG	PHENOMIN-ICS, Illkirch (FRA)
Mid1 Lr	GCTCCAGACAAATAGGACAGGTCAGC	PHENOMIN-ICS, Illkirch (FRA)
***MID1* pCAG-IG F1**	CTGGTTGTTGTGCTGTCTCA	Sigma-Aldrich, München (DE)
***MID1* pCAG-IG F2**	ACGCTGTGAAGACCTGTGT	Sigma-Aldrich, München (DE)
***MID1* pCAG-IG F3**	ATGCATCACGTCAAGAAGCC	Sigma-Aldrich, München (DE)
***MID1* pCAG-IG F4**	CTCCCAACCCTCCCACAATT	Sigma-Aldrich, München (DE)
***MID1* pCAG-IG F5**	CCAGGGGAGCTATGGAGTAG	Sigma-Aldrich, München (DE)
***MID1* pCAG-IG R1**	AGGGCTTCTTATTCGGGTGA	Sigma-Aldrich, München (DE)
***MID1* pCAG-IG R2**	TCTGTCGTCTTTGCTGAATGA	Sigma-Aldrich, München (DE)
***MID1* pCAG-IG R3**	GGTCCAATGCACAGTGATGG	Sigma-Aldrich, München (DE)
***MID1* pCAG-IG R4**	CCACTTCCCAATAATGCCGG	Sigma-Aldrich, München (DE)
***MID1* pCAG-IG R5**	CACACCGGCCTTATTCCAAG	Sigma-Aldrich, München (DE)
MID1- Xhol R	ACTGCTCGAGTCACGGCAGCTGCTCTGTGCAGTCC	Sigma-Aldrich, München (DE)
Mid1_qPCR_P1_For	CAGCCATTCAGCTGATCCGA	Sigma-Aldrich, München (DE)
Mid1_qPCR_P1_Rev	TCAGCTATCGGCTTCCCCAT	Sigma-Aldrich, München (DE)
Mid1Er	CCTCTCTCCTCTCTTTGCAACAACTGC	PHENOMIN-ICS, Illkirch (FRA)

MID1-HA-Tag-EcoRi F	ACTGGAATTCGCCACCATGTACCCATACGATGTTCCAGATTACGCTGAAACACTGGAGTCAGAACT	Sigma-Aldrich, München (DE)
Mid2 Er	CATACATCCAGGCAAAACACCAATGG	Sigma-Aldrich, München (DE)
Mid2 Lf	GGAGGACAGGTTGATGGAGTACAGGG	Sigma-Aldrich, München (DE)
Mid2 Lf^2	GTGCCTTTGGAAGAGGCTCTTCTTTC	Sigma-Aldrich, München (DE)
Mid2 Lr	CCATACCTCCCTCGATAAGATCCACTC	Sigma-Aldrich, München (DE)
Mid2_qPCR_P2_For	GTCGTCACCGAGACCATCAG	Sigma-Aldrich, München (DE)
Mid2_qPCR_P2_Rev	GCAGTATTCACCTCAACTTGCT	Sigma-Aldrich, München (DE)

2.1.11 **Oligonucleotides**

Table 11 Used Oligonucleotides with Sequence

Oligonucleotide	**Sequence**
Pax6-shRNA1-f	GATCCCCAAGATTCTCCCGGCACAGATTCAAGAGATCTGTGCCGGGAGAATCTTTTTTTA
Pax6-shRNA1-r	ATTTTTTTCTAAGAGGGCCGTGTCTAGAGAACTTAGACACGGCCCTCTTAGAACCCCTAG
Pax6-shRNA2-f	GATCCCCCACAGAACTGCCCGCAGCATTCAAGAGATGCTGCGGGCAGTTCTGTGTTTTTA
Pax6-shRNA2-r	ATTTTTGTGTCTTGACGGGCGTCGTAGAGAACTTACGACGCCCGTCAAGACACCCCCTAG
Pax6-shRNA3-f	GATCCCCAGAACTGCCCGCAGCACTCTTCAAGAGAGAGTGCTGCGGGCAGTTCTTTTTTA
Pax6-shRNA3-r	ATTTTTTCTTGACGGGCGTCGTGAGAGAGAACTTCTCACGACGCCCGTCAAGACCCCTAG

Pax6-shRNA4-f	GATCCCCAGCTCTTGGCAGAAGACTTTTCAAGAGAAAGTCTTCTGCCAAGAGCTTTTTTA
Pax6-shRNA4-r	ATTTTTTCGAGAACCGTCTTCTGAAAGAGAACTTTTCAGAAGACGGTTCTCGACCCCTAG
Pax6-shRNA5-f	GATCCCCGAAGACTTTAACCAAGGGCTTCAAGAGAGCCCTTGGTTAAAGTCTTCTTTTTA
Pax6-shRNA5-r	ATTTTTCTTCTGAAATTGGTTCCCGAGAGAACTTCGGGAACCAATTTCAGAAGCCCCTAG

2.1.12 **Software and Online Tools**

Table 12 Used Software

Software	**Version**
BioEdit Sequence Alignment Editor	Version 7.1.3.0
Gel iX20 Imager	Windows Version
GraphPad Prism	Version 8.0
Image Lab v	Version 5.2.1
ImageJ 1.50i	Version 1.4.3.67
Intas Science Imaging GDS	Version 2013
Oligoengine Workstation 2	Version 12.0.1.122
StepOne	Version 2.3

Table 13 Used Online Tools

Name	**URL**
Addgene	http://www.addgene.org
Double Digest Finder	https://www.neb.com/tools-and-resources/interactive-tools/double-digest-finder
Ensembl Genome Browser	http://www.ensembl.org
Primer-BLAST	https://www.ncbi.nlm.nih.gov/tools/primer-blast/index.cgi

Reverse Complement	http://www.bioinformatics.org/sms/rev_comp.html
RefSeq	https://www.ncbi.nlm.nih.gov/refseq/

2.1.13 Mice

Table 14 Used Mice lines and their Origin

Mice	Origin
C57B6/J	Janvier, Marseille (FRA)
C57B6/N	Janvier, Marseille (FRA)
***Mid1*^{lox}/*Mid2*^{lox}**	Mouse Clinical Institute, Illkirch (FRA)

2.2 Methods

2.2.1 *Mid1*^{lox}/*Mid2*^{lox} mice

2.2.1.1 Establishment of *Mid1*^{lox}/*Mid2*^{lox} Mice

The mouse mutant line was established at the MCI (Mouse Clinical Institute; Illkirch, France) in the Genetic Engineering and Model Validation Department.

To generate the mouse line with two mutant genes, previously a *Mid1*^{lox} line was created. Therefore, a targeting vector was constructed as follows. A 1156 bps fragment encompassing exon 2 of *Mid1* (ENSMUSE00000436428) was amplified and subcloned in an MCI proprietary vector. This MCI vector contains a LoxP site as well as a floxed and flipped Neomycin resistance cassette. Two fragments were amplified by PCR and subcloned in the MCI proprietary plasmid to generate the final targeting construct.

The linearized construct was electroporated in C57BL/6N mouse embryonic stem (ES) cells. After selection, targeted clones were identified by PCR using external primers and further confirmed by Southern blot with a Neo probe (5' and 3' digests) as well as a 5' and 3' external probes.

Two positive ES clones were injected into BALB/cN blastocysts. Resulting male chimeras were bred with Flp deleter C57BL/6N females that show maternal contribution (103). Germline transmission of the conditional allele was obtained.

One of the *Mid1* positive ES cell clones was used for the second electroporation with the *Mid2* construct to generate the double floxed line.
A 540 bp fragment encompassing exon 4 of *Mid2* (ENSMUSE00000693854) was amplified by PCR and subcloned in an MCI proprietary vector. This MCI vector contains a Lox5171 site as well as a floxed and F3 surrounded Hygromycin resistance cassette. Two fragments were amplified by PCR and subcloned into the targeting plasmid.
A crRNA, targeting the sequence at the site of insertion of the HygroR selection cassette, was cloned into pX330 from Addgene a CRISPR/Cas9 plasmid. Both plasmids were electroporated circular in Mid1 targeted C57BL/6N mouse embryonic stem (ES) cells. After Hygromycin selection, targeted clones were identified by long-range PCR and further confirmed by Southern blot with an internal (Neo) probe and a 5' and 3' external probe.
One positive ES clone was validated by karyotype spreading and microinjected into BALB/cN blastocysts. Resulting male chimeras were bred with Flp deleter C57BL/6N females that show maternal contribution (103). Germline transmission of both conditional alleles was obtained.
Frozen sperm of the male offspring of *Mid1*^{lox}/*Mid2*^{lox} mice was shipped to the biotechnical laboratory at the TARC (Translational Animal Research Center) of the Johannes-Gutenberg-University Mainz. C57B6L/N WT females were fertilized via *in vitro* fertilization.

2.2.1.2 The Cre-Lox-System

The *Mid1*^{lox}/*Mid2*^{lox} mice contain a specific sequence called *loxP* sequence. This sequence is 34 bp long and can be used to flank specific exons. The *loxP* site serves as a recognition and binding site for the Cre recombinase, which leads to a deletion of the gene between the *loxP* sites. Thus, this mechanism can be used to create cell and stage specific KO of genes (conditional KO, cKO) (104). Physiologically bacteriophage P1 uses Cre as an intramolecular resolvase being important during cell division to convert P1 chromosome dimers to monomers (105). Only low concentrations are needed for an effect, which makes it a widespread tool for conditional mutagenesis (106).
Mid1^{lox}/*Mid2*^{lox} mice, which do not express a Cre recombinase are phenotypically wild types. Introducing a Cre recombinase can be carried out by e.g. mating with

specific Cre-expressing transgenic mice or by *in utero* electroporation of a vector containing an insert coding for Cre. The figure shows a scheme of the gene region of *Mid1* before and after recombination.

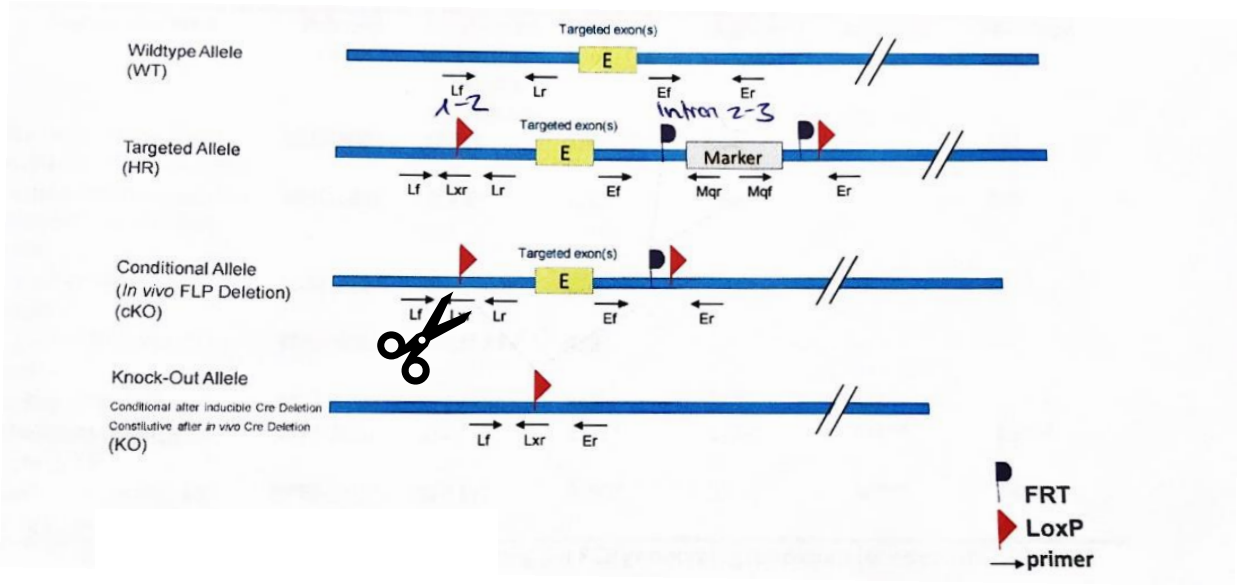

Figure 8 Scheme of cKO via Cre recombinase. The *loxP* sites marked in red mark the beginning an end of KO.

In the *Mid1* gene the second exon is flanked by the *loxP* sites, exceptional to that is the transcript Mid1-214 with the first exon being flanked. In *Mid2* gene the third or fourth exon is flanked by *loxP* sites depending on the transcript.

In this study IUE will be used to transfect neural stem cells of the neocortex with the Cre recombinase. This leads to a conditional KO of both genes in mouse embryos of *Mid1*^{lox}/*Mid2*^{lox} mice via Cre-Lox mediated gene excision. The plasmid pCAGGS-Cre-IRES-GFP, encoding for the Cre protein, will be electroporated into homo-/hemizygous floxed mice. Only in the electroporated neural stem cells, Cre will induce the recombination and cause a KO of the targeted alleles. Therefore, the effect of the KO of *Mid1* and *Mid2* on neuronal migration and proliferation can be studied. As the recombination affects only a few cells, the environment will not be influenced, and individual cells and their migration can be studied (107).

2.2.1.3 Breeding of *Mid1*^{lox}/*Mid2*^{lox} Mice

The breeding of all mouse lines was conducted in the TARC under the direction of Dr. Jan Baumgart. All animals were under care of the animal keepers of TARC. The offspring of the *in vitro* fertilization were checked for the right genotype. Then homozygous *Mid1*^{lox}/*Mid2*^{lox} females and hemizygote males were mated. For experiments only offspring of this breeding were used. *Mid1*^{lox}/*Mid2*^{lox} females were used for timed matings and *in utero* electroporation.

2.2.1.4 Breeding of *Mid1*^{lox} and *Mid2*^{lox} Mice

From the strain of *Mid1*^{lox}/*Mid2*^{lox} mice, two new mouse lines should be established by targeted mating. These mouse strains should inhabit only one of the floxed genes on the X-chromosome instead of both. Hence, with the following offspring a single conditional Knock-out line for *Mid1* or *Mid2* could be generated. Therefore *Mid1*^{lox}/*Mid2*^{lox} had to be backcrossed. The first maiting were *Mid1*^{lox}/*Mid2*^{lox} females with C57BL/6N males, the heterozygous female offspring were then mated again with C57BL/6N. The aim underlying this backcrossing was to create a crossing over. As both targeted genes lie on the X-chromosome, but on different arms, the distance between them is quite large. The farther apart two genes on a chromosome are, the more likely it is that these genes separate during meiosis (108). In homozygous females, this would have no effect, but in heterozygous females genetic recombination could lead to X-chromosomes only containing either the *Mid1*^{lox} or *Mid2*^{lox} gene.
The following figure shows the scheme of backcrossing.

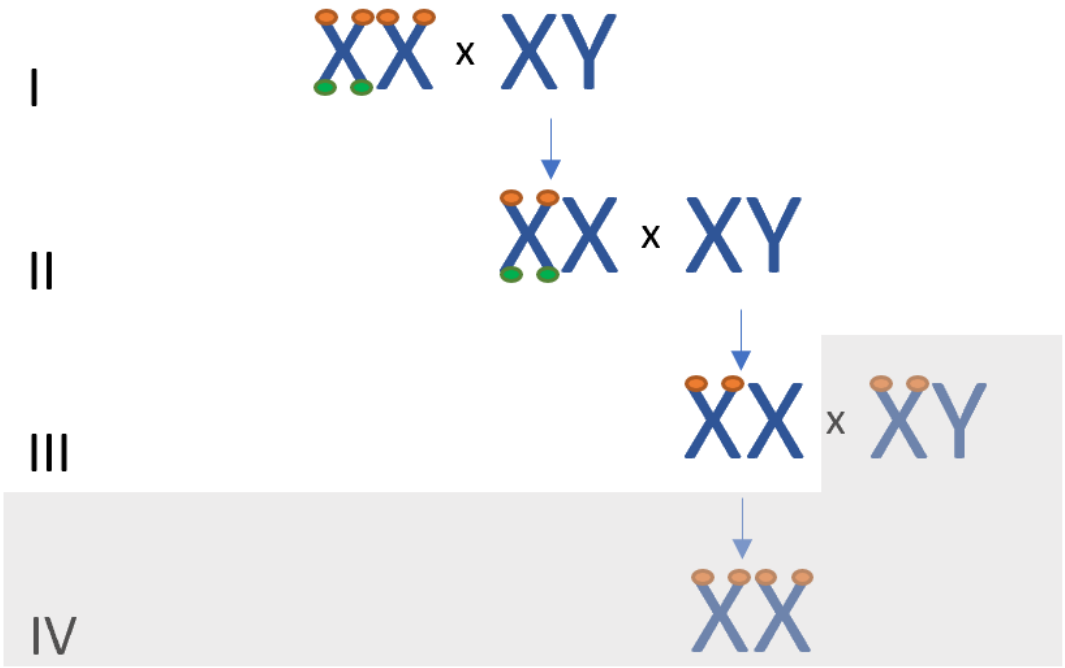

Figure 9 The backcrossing of Mid1lox/Mid2lox mice to single floxed mice. The orange marking on the X-chromosome symbolizes the floxed Mid1 gene, the green one the Mid2 gene. In the first (I) and second (II) generation the breeding was done with C57BL/6N males. In the litter of the 3rd (III) generation crossing over should occur, so that only one floxed gene would be preserved.

Each litter was genotyped and animals with the correct genotype were chosen for further breedings.

2.2.1.5 Breeding of Heterozygous *Mid1*^{lox}/*Mid2*^{lox} Mice

The second mouse line to be established was a heterozygous *Mid1*^{lox}/*Mid2*^{lox} mouse line. Females of this strain should contain one X-chromosome with both genes floxed and one wildtype X-chromosome, while males could only be hemizygous.

Homozygous Mid1^{lox}/Mid2^{lox} females were mated with C57BL/6N males, hence the female offspring were all heterozygous and the males hemizygous.

The following figure shows the mating scheme.

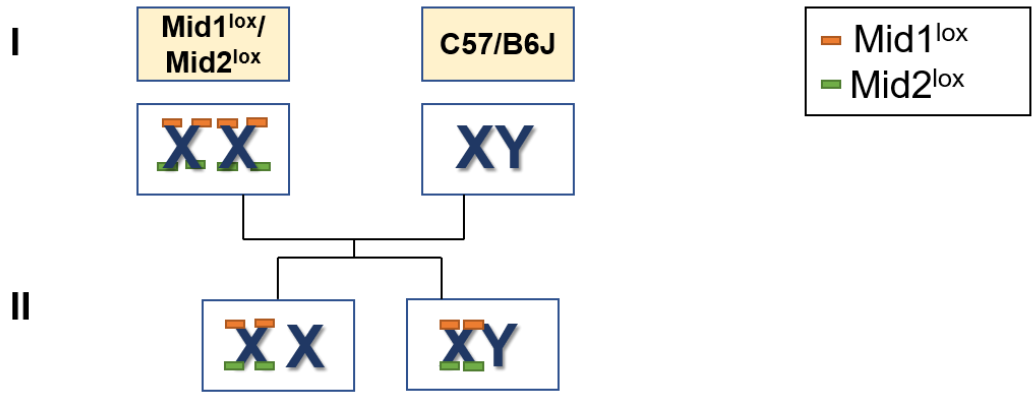

Figure 10 Breeding of heterozygous *Mid1*^{lox}/*Mid2*^{lox} mice. In the first generation a homozygous female was mated with a wildtype male. Female offspring were therefore heterozygous while males were hemizygous.

Genotyping checked for accuracy and homozygous females mated with C57Bl/6N males used for maintenance of the strain.

2.2.1.6 Genotyping and PCR

Genotyping is based on the detection of specific gene regions by Polymerase chain reaction (PCR) amplification. Regions are then distinguishable by size. In the following an exemplary genotyping of heterozygous *Mid1*^{lox}/*Mid2*^{lox} mice will be presented.

The required DNA was obtained from tail tips of ear punches of the animals, while weaning them at three weeks of age. The tissue samples were digested overnight at 56ºC in digestion buffer at 700 rpm. The next day the samples were centrifuged for 15 min at 13,000 rpm. From the supernatant 50 µl of the extracted DNA were pipetted into 100 µl H_20. For the genotyping PCR the following Master Mix was prepared. The quantities are given per sample and must be calculated individually for each run.

Table 15 Master Mix for Genotyping PCR

Component	**Quantity [µl]**
H_20	16,6
$MgCl_2$ Buffer	2,5
dNTPs	0,5
Primer Mid1 or Mid2 Lf	1

Primer Mid1 or Mid2 Lr	1
Fast Start Polymerase	0,4
DNA	1

The amplification program is shown in table 2. At the beginning of the PCR, the denaturation phase is initiated at 95 °C and serves to break the hydrogen bonds between the nucleotides of the double-stranded DNA to obtain single strands. The cycle starts again with a denaturation phase at 94ºC. The annealing phase serves to bind the forward and reverse primer to the target sequence. Subsequently, the primers are elongated at 72ºC by the Fast Start DNA Polymerase. The single strands are synthesized in 5'-3' direction to form complementary double strands. To obtain enough material, these three phases are repeated 34 times. After a final elongation for 7 min, the sample was stored at 4ºC.

Table 16 PCR program

Step		**Temperature [ºC]**	**Time**
1. Denaturation		95	4 min
2. Denaturation		94	30 sec
3. Annealing	**34x**	62	30 sec
4. Elongation		72	1 min
5. Elongation		72	7 min
6. Storage		4	forever

2.2.2 **Agarose Gel Electrophoresis**

After amplification by PCR, the DNA samples were separated in a 1.5% agarose gel using the method of agarose gel electrophoresis. The negative charge of the DNA leads to its movement in an electric field in the direction of the anode. Due to the constant charge-mass ratio, the fragments are separated depending on their size. Smaller fragments are therefore faster than larger ones.

After adding the DNA-intercalating ethidium bromide to the 1.5 % agarose solution it was poured into a gel chamber. After hardening of the agarose gel, the chamber was covered with 1x TAE buffer. 25 µl of the sample was mixed with 5

µl 10x Orange G loading buffer. As size standard the GeneRuler™ 1 kb or 100bp DNA Ladder was used. The separation in an electric field was performed at 170 V and a running time between 20 and 40 min. In the transilluminator the bands were visualized at a wavelength of 312 nm under UV light using the software Intas GDS Gel iX20 Imager.

2.2.3 Generation of a MID1 Overexpression Construct

2.2.3.1 Primer Design

To create an OE construct of MID1, the cDNA of *MID1* had to be amplified. The primers used for generating this construct were created using start (for) or end (rev) of the cDNA sequence of *MID1* (Transcript: MID1-201, ENST00000317552), including flanking restriction sites for either EcoRI (for) or XhoI (rev) and for forward primers also a Kozak sequence and a human influenza hemagglutinin (HA) tag. The Kozak sequence (5'-GCCACCATG-3') reinforces the initiation of the translation and thus increases efficiency. The HA tag (5'-TACCCATACGATGTTCCAGATTACGCT-3') is used for detection through immunofluorescent staining. After PCR the total length of the resulting construct is around 2000 bp.

Figure 11 Scheme of the MID1 Overexpression Construct flanked by the EcoRI, Kozak and HA sequence on 5'- site and XhoI sequence on 3'-site.

2.2.3.2 Amplification of *MID1*-cDNA

Through PCR, the target sequence of *MID1* was derived from the plasmid pCMV-tag 2A-MID1 and pCMV-tag 3A-MID1 by using the MID1-HA-tag-EcoRI Forward and MID1-XhoI Reverse Primer. The PCR was performed in a thermal cycler with Herculase II Fusion DNA Polymerase. The amount of used plasmid-DNA depends on its weight. For a target length of 1- 10 kb, 200 ng were recommended.

All components were pipetted into a PCR tube (Tab. 3). Additional to the samples, one control using H_20 instead of DNA was prepared.

Table 17 PCR protocol for amplification of *MID1*-cDNA

Component	**Quantity [µl] per sample**
5x Herculase II reaction buffer	10
$MgCl_2$	2
dNTP mix	0,5
DNA template (200 ng/µl)	1
Primer Forward	1,25
Primer Reverse	1,25
Herculase II fusion DNA polymerase	1,0
dH_20	41

The PCR is based on the principle described in Chapter 2.2.1.6 and was performed under the conditions shown in the table.

Table 18 PCR protocol for amplification of *MID1*-cDNA

Segment		**Temperature [ºC]**	**Duration**
Denaturation		95	2 min
Denaturation		95	30 sec
Annealing	**30x**	60	30 sec
Elongation		72	1 min
Elongation		72	10 min
Storage		4	forever

The amplified MID1 sequence was loaded on an agarose gel and separated via electrophoresis. The correct size of *MID1*-cDNA construct should be around 2000 bp.

2.2.3.3 Purification

The PCR products of *MID1*-cDNA were cut out of the agarose gel under UV light with a scalpel and transferred into one 2 ml reaction vessel. For the purification of the PCR products the Agarose MinElute® Gel Extraction Kit from Qiagen was

used. All subsequent centrifugation steps were performed in the Microfuge®16 benchtop centrifuge at 13.000 rpm.

The cut agarose gel was weighed and 3 volumes of Buffer QG were added. The QG buffer dissolves the agarose gel and provides the appropriate conditions for binding the DNA to the silica membrane in the column. The reaction vessel was placed in a 50°C heating block for 10 min and vortexed every two to three minutes until the agarose gel was completely dissolved. One volume of isopropanol was added and mixed by inverting. Then the MinElute spin column was placed in a 2 ml collection tube and the sample applied onto the silica membrane and centrifuged for 60 seconds. The flow-through was discarded, and 500µl of Buffer QG were added and again centrifuged for 60 sec. 750µl Buffer PE was pipetted onto the column and then centrifuged for 60 sec. After discarding the flow-through, an additional centrifugation step for 60 sec needs to be done in order to remove residual ethanol from the Buffer PE. The column was placed in a clean 1.5 ml collection tube. To elute DNA 10µl Buffer EB were pipetted onto the center of the membrane, incubated for one minute and centrifuged for 60 sec. This step was repeated a second time.

The concentration of the purified *MID1*-cDNA samples was then measured with the NanoDrop spectrophotometer.

2.2.3.4 Restriction Digestion

The restriction digestion was used to cut the double-stranded DNA of the PCR product of *MID1*-cDNA and the target plasmid pCAG-IG at enzyme-specific recognition sequences. The EcoRI and XhoI restriction enzymes used for both approaches are endonucleases that produce compatible 5' overhangs, which were essential for the subsequent ligation. For the restriction with two reaction enzymes, a buffer must be used that creates a suitable environment with optimal activity for both enzymes. This was determined using the Double Digest Finder from NEB.

Table 19 Recognition site of the restriction enzymes EcoRI and XhoI. Arrows mark the cutting point of the enzymes.

Restriction Enzyme	**Recognition Site**
EcoRI	5´ G ↓ A A T T C ´3 3´ C T T A A ↑ G ´5
XhoI	5´ C ↓ T C G A G ´3 3´ G A G C T ↑ C ´5

For the restriction digest the components shown in Table 6 were mixed. The restriction preparation was incubated for two hours at 37°C and underwent heat inactivation for 20 min at 65ºC.

Table 20 Restriction digestion for pCAG-IG and MID1 PCR product

Component	**Quantity [µl]**
10x BSA	3
NEB Buffer 3.1	3
EcoRI	1
XhoI	1
Plasmid pCAG-IG	0,5
PCR Product MID1	0,1
H_20	Add 30

After incubation, an agarose gel electrophoresis was performed to check the restriction on the one hand and to purify the cut and thus linearized plasmid pCAG-IG on the other hand.

2.2.3.5 Ligation

To connect the compatible 5'-overhangs of the linearized plasmid pCAG-IG and the digested target sequence of *MID1*-cDNA ligation was needed. Therefore, the T4 DNA ligase was used to connect both parts. Thereby, the plasmid converts back to its circular form. The reaction approach is summarized in Table 7.

Table 21 Ligation approach for pCAG-IG and MID1

Component	**Quantity [µl]**
H_20	8,4
Insert	6,3
Plasmid	2,3
10x Buffer T4	2,0
T4 DNA Ligase	1,0

The ligation mix was incubated at 16ºC overnight. In the morning of the next day, it was heated to 65ºC for 10 min for heat inactivation.

2.2.4 Generation of a Knock-down Construct for *Pax6*

2.2.4.1 Design of the Oligonucleotides

Silencing *Pax6* should be achieved by RNA interference using short hairpin RNAs (shRNAs). These shRNAs are incorporated into the RNA induced silencing complex (RISC) (109). Via the shRNA sequence the RISC recognizes the target mRNAs and suppress their expression (110).

Using the online software Oligoengine 2.0, the most effective hybridization sites in the corresponding gene were determined and output by the software as a sense strand. To produce a double strand, a forward and reverse strand must be designed. In order to obtain the hairpin structure, the resulting antisense strand was connected by nine nucleotides. The online tool Reverse Complement was used for this purpose.

For the forward oligonucleotide, the recognition sequence of the restriction enzyme BglII was added at the 5' end. The reverse oligonucleotide, which is complementary to the forward motif, was extended at the 5' end by the recognition sequence of the restriction enzyme HindIII. At the 3'-end the sequences thus behave complementary.

For incorporation into the plasmid, a 5' overhang is required, which is achieved by shortening the sequences at the 3' ends (Fig. 12).

Forward Oligonucleotide

BglII Sense Sequence Hairpin Antisense Sequence

5´- GATCCCCAAGATTCTCCCGGCACAGATTCAAGAGATCTGTGCCGGGAGAATCTTTTTTTA - 3´

Reverse Oligonucleotide

Sense Sequence Hairpin Antisense Sequence HindIII

3´- GGGTTCTAAGAGGGCGCGTGTCTAAGTTCTCTAGACACGGCCCTCTTAGAAAAAAATTCGA

Figure 12 Forward und reverse strand oligonucleotide shRNA1 Pax6. The forward strand consists of the target sequence (black), connected by the hairpin sequence (red). At the 5´-ends the recognition site of BglII and HindIII (blue) can be found. The reverse oligonucleotide is complementary tot he forward oligonucleotide.

2.2.4.2 Annealing

The designed oligonucleotides were commercially produced and delivered separately as foward and reverse strands. In order to obtain double-stranded DNA, 1 µl of each forward and reverse oligos was hybridized together.
The DNA was pipetted to 48 µl annealing buffer and placed in an incubator. The incubator was heated for 4 min at 95ºC for denaturation and then incubated for 10 min at 70ºC for annealing. The subsequent storage was at 4ºC.

2.2.4.3 Restriction Digestion

To clone the hybridized oligonucleotide into the vector, the vector had to be linearized and the appropriate interfaces, so-called sticky ends, had to be incorporated. For this purpose, a restriction digestion of the vector pSUPERIOR.puro with the restriction enzymes BglII and HindIII was performed. Restriction enzymes are endonucleases which were selected in a way that mutually compatible 5' or 3' overhangs were formed.
The following components were pipetted.

Table 22 Protocol for Restriction Digestion

Component	**Quantity [µl]**
Plasmid pSUPERIOR.puro	1
BglII	1
HindIII	1
10x BSA Buffer	3
NEB 3.1 Buffer	3
H_20	21

The preparation was incubated at 37ºC overnight in an incubator and then heat inactivated at 80ºC for 20 min. Storage was at 4ºC.

2.2.4.4 Purification and Ligation

After agarose gel electrophoresis was used to separate the digested plasmids as described in Chapter 2.2.2.3, the digested plasmid was cut out of the agarose gel under UV light and purified with the MinElute® Gel Extraction Kit.
Afterwards the shRNA construct *Pax6* and the plasmid pSUPERIOR.puro were ligated according to the approach in the table below.

Table 23 Protocol for Ligation of *Pax6* shRNA into pSUPERIOR.pure

Component	**Quantity [µl]**
Plasmid pSUPERIOR.puro	2
Pax6 shRNA 1-5	4
10x Buffer	2
T4 DNA Ligase	1
H_20	11

Incubation was overnight at 16ºC.

2.2.5 Amplification of the Constructs for Electroporation via *Escherichia coli*

High concentrations were required for the electroporation of the plasmids. Therefore, the ligated vectors had to be amplified by *Escherichia coli* (*E. coli*) bacteria and subsequently purified. One Shot Top 10 *E. coli* was used for this purpose.

The following protocol was used for the plasmids pCAG-IG-MID1, pCAG-IG-empty, pSUPERIOR.puro-Pax6, pSUPERIOR.puro-empty, pCAGGS-Cre-IRES-GFP and pCAGGS-empty-IRES-GFP.

2.2.5.1 Transformation

Thus, the *E.coli* strain was able to absorb free DNA in the form of plasmids, it had to undergo the process of transformation (111). For this purpose, 1 µl plasmid was pipetted into 50 µl *E. coli* and incubated for 30 min on ice. Then a heat shock for 90 sec at 42ºC in a water bath and an immediate incubation for 2 min on ice were performed. Afterwards 250 µl LB-medium were added and the sample was incubated at 37ºC for 30 min shaking.

200 µl of the preparation were spread out on agar plates containing 100mg/L ampicillin and stored overnight at 37ºC. All plasmids contain a gene, coding for ampicillin resistance. Thus, the growing colonies should contain the plasmid. The next day, about five of these grown colonies were picked and cultivated for another night in 3 ml LB medium containing 100 mg/L ampicillin on a shaker.

Storage was at 4ºC.

2.2.5.2 Plasmid Isolation via Minipreparation

The following Minipreparation was performed with the EndoFree® Plasmid Maxi Kit by Qiagen Quantities. The Miniprep method is based on the principle of alkaline lysis to break up the cells and release the DNA.

1.5 ml of the overnight culture were transferred into a reaction tube and centrifuged for five minutes at 6.000 rpm. This step and all further centrifugations were performed on the Microfuge®16 benchtop centrifuge. The supernatant was discarded, and the pellet was resuspended in 100 µl P1 lysis buffer. Then 100 µl P2 buffer was added, the sample inverted several times and incubated for five minutes at RT. The P2 buffer contains sodium dodecyl sulfate (SDS), which causes the cell membrane components to dissolve. After incubation, 100 µl P3 buffer, precooled at 4ºC, was added to the lysate and incubated for five minutes at RT. This buffer neutralizes the lysate. It was then centrifuged at 13.000 rpm for 10 min.

The supernatant was removed and pipetted together with 1 ml of 100% EtOH in a new reaction vessel. Centrifugation at 13.000 rpm for 10 min served to precipitate the plasmid DNA. The supernatant was discarded, and the DNA pellet was washed in 150 µl 70% EtOH for 5 min at 13.000 rpm. The supernatant was again discarded as carefully as possible and the remaining EtOH was removed by evaporation on the heating block at 50ºC.

The pellet was dissolved in 20-50 µl H_20 and stored at -20ºC.

2.2.5.3 Control Restriction Digestion

To check if the ligation into the target plasmid worked and thus pick samples for sequencing, the purified plasmids of pCAG-IG-MID1 were digested with the restriction enzymes EcoRI and XhoI. Therefore, the same protocol as in Chapter 2.2.3.4 was used.

After incubation an agarose gel electrophoresis was performed to check the restriction which samples show the *MID1*-HA-tag fragment.

2.2.5.4 Sequencing

The sequencing of the purified plasmids that were chosen after control restriction digestion, was checked for the presence of an insert in the plasmid and was

carried out by GATC Biotech. The concentrations of the individual samples were measured and diluted to a concentration of 100 ng/µl if necessary.
The sample preparation, which was requested by the company, was the following.

Table 24 Protocol for DNA Sequencing for GATC Biotech

Component	**Quantity [µl]**
Plasmid	5
Primer (1:20)	5

To sequence for *Pax6* the primers H1 and Bluescript were used. For pCAG-IG-MID1 the primers *MID1* pCAG-IG F1 and *MID1* pCAG-IG R1 were added to the sample.
The sequences were then checked using the BioEdit program for possible errors within the insert compared to the reference sequence.

2.2.5.5 Plasmid Isolation via Maxipreparation

Like the Minipreparation, the Maxipreparation is based on the principle of alkaline lysis and was performed with the EndoFree® Plasmid Maxi Kit from Qiagen. The buffers P1, P2 and P3 used are therefore described in detail in Chapter 2.2.5.2.
The samples determined as correct were prepared for Maxiprep by retransformation. For this purpose, 0.5µl of the sample was transformed into 50µl *E. coli*. 50µl of this preparation were plated out on agar-ampicillin plates. These were stored overnight at 37ºC and the next day colonies were picked and incubated again at 37ºC in 3 ml LB-Medium overnight while shaking. The culture was then added to 200 ml LB medium with ampicillin and incubated again overnight at 37º shaking.
The 200 ml overnight culture was centrifuged at 4ºC and 6.000 rpm for 15 minutes. The Avanti J-26XP device was used for this purpose. The supernatant was discarded, and the resulting bacterial pellet was resuspended in 10 ml lysis buffer P1. Subsequently, 10 ml buffer P2 was pipetted in and inverted several times. The suspension was then incubated for five minutes at RT. Then 10 ml buffer P3 was added and the solution was incubated in a filter column for 10 min.

To filter the viscous liquid, it was pressed through the filter column into a 50 ml tube using a stamp. 2.5 ml buffer ER was added, and the lysate was incubated on ice for 30 min. The second filter column was equilibrated with buffer QBT before use, then the lysate was placed on it. Buffer QC was added twice to the filter column for washing. Through the buffer QN 15 ml of DNA was eluted into a fresh tube. To precipitate the plasmid DNA, isopropanol was added with a factor of 0.7 of the eluate amount and centrifuged at 5.000 rpm and 4ºC for one hour. For this and the last step the centrifuge Megafuge, Heraeus, 16R was used. After centrifugation the supernatant was discarded, and the pellet was purified in 5 ml endotoxin-free 70% EtOH and centrifuged for another 30 min at the same setting. Afterwards the supernatant was discarded and the pellet was air dried. For storage, the pellet was dissolved in 100 µl TE buffer and the concentration was measured with NanoDrop.
Subsequent storage of the plasmids was at -20º.

2.2.6 *In Utero* Electroporation

2.2.6.1 *In Utero* Electroporation

The *in utero* electroporation (IUE) is a reliable method for temporary and permanent manipulation of gene expression in the embryonic mouse brain (112). Individually designed vectors including specific DNA sequences lead to changes only in the cells which incorporate the plasmid. When using a GFP-containing construct, the incorporating cells can then be distinguished under UV light from not-manipulated cells (112).
The electroporation was adapted from a protocol from Jan Baumgart, head of the TARC Mainz (113). The timed mated maternal C57B6/J mice were ordered from Janvier at E 12.5 and used for electroporation at E13.5. The *Mid1*^{lox}/*Mid2*^{lox} mice were timed mated in the TARC Mainz to guarantee for right pregnancy date E13.5. Surgery material was sterilized.
In the first step the plasmid was mixed with following protocol:

Table 25 Plasmid preparation for IUE

Plasmid with concentration of 4000 ng/µl	**Volume per maternal mouse [µl]**

pCAG-IG-MID1 or pCAG-IG-empty pCAGGS-Cre-IRES-GFP or pCAGGS-empty-IRES-GFP	13
pCAGGS-GFP	2

The mice were injected with analgesia (buprenorphin, 0,1mg/kg bodyweight) as a 3-4-hour depot in their nuchal fold 30 min before surgery. In the meantime, the set-up was prepared. The DNA was colored with 1 µl Fast Green solution per 10 µl of DNA. For the surgery special glass capillaries were used for injection. These borosilicate glass capillaries were pulled and grinded into a 35º angle and have a diameter of 0.8-0.9mm.

The mice were anesthetized with isoflurane 2.8% in a chamber. Depth of anesthesia was checked with unresponsiveness to toe pinch. During the surgery the mice inhaled 2.5% isoflurane over a face mask and lay on a thermal support device. Eye ointment was applied to protect the eyes.

The surgical area was sterilized with 70% EtOH and the mouse covered with a sterile gauze. The abdominal cavity was opened with a longitudinal cut and the area moistened with isotonic solution. The uterine horns were extracted with a ring forceps and the number and position of the embryos noted.

The colored DNA was pulled up into the capillary and injected into the ventricle of the embryo. On E13.5 around 1,5 µl could be injected. The electroporation paddles were placed anterior of the ear primordia and a voltage of 35 V with an interval cycle length of 50 msec and pause of 950 msec was applied. This was repeated twice.

Depending on position and number up to 8 embryos per mouse were electroporated. After the electroporation the uterine horns were replaced in the abdominal cavity and the muscle and skin incision sutured separately. The mouse was then put in a single housing cage and supervised during recovery.

2.2.6.2 Preparation of Embryonic Brains

Embryos at E14.5 (pCAG-IG-MID1 and pCAG-IG-empty) or E15.5 (pCAGGS-Cre-IRES-GFP or pCAGGS-empty-IRES-GFP) were dissected. For this purpose, the mothers were killed by cervical dislocation and the uterus was removed. After checking the position of the embryos, they were killed by cutting off the head. The brains were dissected.

The exposed brains were placed in ice-cold PBS and fixed in 3 ml 4% paraformaldehyde (PFA) for 8 hr at 4°C. PFA leads to a reversible cross-linking by methylene bridges between the proteins and thus fixes the tissue. In the next step the brains were cryoprotected by overnight immersion in 15% sucrose in PBS. This extracts water from the tissue so that no crystals are formed during freezing, which would destroy the structure. During storage at 4° C the brain sinks in the Falcon. Once this has occurred, the 15% solution can be replaced by a 30% sucrose in PBS. Finally, the brain was placed in 30% sucrose in PBS 1:1 with Tissue-Tek® O.C.T. (optimum cutting temperature) TM for 10 minutes at room temperature. All subsequent steps were performed under the fume hood. 100% EtOH was added to dry ice in a weighing dish. This creates temperatures down to -72°C as the dry ice extracts heat from the alcoholic solution. The embryonic brain was embedded in a Cryomold® dish filled with Tissue-Tek® O.C.T.TM and left on the dry ice-alcohol mixture until the embedding medium turned white. Storage was then carried out at -80°C.

Before cutting, the brains were stored at -20°C for at least one night for better processing. The brains were cryosectioned at 20 µm. For the experiment coronal sections of the cortex were prepared. The cutting was performed at the Leica Cryostat CM3050S. They were positioned on SuperFrost Plus® slides. The sections were stored at -20ºC.

2.2.6.3 Immunofluorescence Staining

The cryosections of the electroporated brains were examined under the fluorescence microscope. The GFP-positive cells appeared green. This allowed to check which sections contained electroporated cells at the right location of the neocortex.

Indirect Immunofluorescence (IF) uses two antibodies to visualize specific structures in cells and tissues. The primary antibody binds specifically to the protein of interest. This antibody has species-specific epitopes with which the secondary antibody can react in the next step. The secondary antibody acts as a fluorochrome and can therefore be detected under a fluorescence microscope. Immunofluorescence was carried out using the following antibodies: mouse anti-GFP (1:1500; 11814460001; Sigma-Aldrich), rabbit anti-GFP (1:500; **#**MA5-15256; ThermoScientific), rat anti-Ki67 (1:50; #14-5698-82;ThermoScientific), chicken anti-Tbr2 (1:200; #AB15894; Millipore), rabbit anti-Pax6 (1:200;

#AB2237; Millipore), mouse anti-HA-tag (1:500; AB20084), rabbit anti-Satb2 (1:200; # AB34735), rabbit anti-Cleaved-Caspase3 (1:500; #9661; Cell Signaling Technology®).

First the slides were washed in 0.2% PBS-Triton X 100 for 15 min. This solution was used for all washing steps. Afterwards antigen retrieval was carried out by boiling the sections at 85ºC for 20 min in pH 6 sodium citrate solution. Antigen retrieval is needed as the formalin fixation influences most antigens inducing cross-linkages between formalin and proteins. These can be reversed by high-temperature heating (114).

After a short washing step, 2% sheep serum was pipetted on the slides and incubated at RT for one hour. The antibody was diluted in 2% sheep serum, added on the samples and incubated overnight at 4ºC in the dark. The first antibody binds specifically on the target protein.

The next day the tissue sections were washed three times for 15 min. The secondary antibody was diluted in 2% sheep serum and incubated on the slides for three hours at RT. The secondary antibody binds to the species-specific region of the first antibody. The slides were again washed 3 times for 15 min and then mounted with Fluoromount-G™ with DAPI (4′,6-diamidino-2-phenylindole). DAPI is a blue-fluorescent staining for DNA and used as a nuclear counterstain. The dried slides were stored at 4ºC.

2.2.6.4 Analysis

The stained tissue sections were visualized using a Leica LSM SP5 confocal microscope. The area of the neocortex with the electroporated cells was recorded with a 25x magnification.

The image processing program ImageJ was used for cell counting. Before cell counting started the layers of VZ, IZ and CP were marked manually with the image processing program. Colored cells were checked for an existing nucleus. Only the electroporated cells with a visible nucleus were included and marked with a number. The cells were counted together and separately for each layer and antibody. The percentages of stained cells per layer were calculated and documented. Statistical analysis was done with GraphPad Prism8.

2.2.7 Control of the Overexpression in Cell Culture

To verify expression of MID1 from the plasmid, HeLa cells were transfected with the pCAG-IG-MID1 construct followed by Western blot analysis with specific MID1 antibodies.

2.2.7.1 Transfection of HeLa Cells with pCAG-IG-MID1

HeLa cells were cultivated in Dulbecco's Modified Eagle Medium (DMEM) containing 10% fetal bovine serum (FBS) and 1% penicillin streptomycin (PenStrep) in an incubator at 37 °C and at 5% CO_2 concentration for stabilization of the pH-value.

HeLa cells were counted, diluted to 100.000 cells/ml and seeded onto a 6-well plate. Per well 1.5 µg of the plasmid pCAG-IG-MID1 or pCAG-IG-empty were mixed with 12 µl PolyFect and filled up with 100 µl pure DMEM. After resuspension, incubation for 10 min at RT was performed. Meanwhile, the medium of the cells was discarded, and 3 ml fresh medium was added.

After incubation, 600 µl DMEM containing FBS and PenStrep were added to the transfection mixture and the total volume of approx. 712 µl per well was added to the HeLa cells. The cells were then cultivated again in the incubator as described above.

2.2.7.2 Protein Lysate

The medium was removed from the cells approximately 48h after transfection and washed once with PBS.Subsequently, trypsin was added and incubated for 5 min at 37°. Due to this treatment, the cells detached from the bottom and could be resuspended in DMEM containing FBS, which stopped the trypsin reaction.

The resulting cell suspension was centrifuged for 5 min at 200 rpm, after which the medium was discarded and the cells were resuspended in 1 ml fresh culture medium. After transfer to a 1.5 ml Eppendorf tube, the suspension was centrifuged again for 5 min at 1000 rpm, the medium was removed, and the pellet was washed in 1 ml PBS and centrifuged for 5 min at 1000 rpm. After removing the PBS, the pellet was resuspended in 50-200 µl MagicMix with 1% β-mercaptoethanol.

The dissolved pellet was pipetted onto a Qia shredder column (Qiagen) and centrifuged for 2 min at 13.500 rpm. The filtered lysate was transferred into a 1.5 ml Eppendorf tube and stored at -20°C.

2.2.7.3 Western Blot

Western blot is a common method for the detection of specific proteins. Two antibodies, which are incubated on a membrane, are used for the detection of the protein of interest.

First, all proteins from the protein lysate have to be separated by size. Therefore, Sodium dodecyl sulfate polyacrylamide gel electrophoresis (SDS-PAGE) works on the principle of protein separation according to molecular weight.

After measuring the protein concentration of the described lysate with the Qubit™, the first step was to denature the lysate together with 3 µl MagicMix containing bromophenol blue at 95°C for 5 min. Thus, the proteins are not only denatured but also dissociated and can bind to SDS, giving them a negative charge.

20 µg of each protein lysate were applied to 10% SDS-polyacrylamide gels and a voltage of 199 V was applied for 45 to 60 min. The proteins now migrated in the gel according to their charge, whereby the proportion of negative charges is proportional to the molecular weight, thus superimposing their own protein charge. Correspondingly, the proteins can be separated indirectly based on molecular weight. A ladder was inserted into the outermost pocket of the gel to control the size.

The next working step is to transfer (blot) the separated proteins from the SDS gel onto a polyvinylidene fluoride (PVDF) membrane.

To prepare membranes and filter paper, they are plunged into an EtOH bath for a few seconds until they appear transparent and then placed in 10% Towbin buffer. In a Trans-Blot SD semidry Transfer Cell from Bio-Rad the layering was done starting with filter paper and membrane on the side of the anode followed by the SDS gel and finally another filter paper on the side of the cathode. The chamber was closed and 25 V were applied for 30min. The negatively charged proteins could migrate towards the anode and were blotted in the membrane.

Afterwards, the membranes were blocked in 5% milk powder in PBS-T for 30 min. This was done in a 50 ml vessel while rotating continuously on a rolling plate.

The primary antibodies for MID1 (1:1000, selfmade) and for the housekeeping protein GAPDH (1:2000, AB8245) were incubated overnight at 4°C in 3 ml of milk blocking buffer.
The next day, three washing steps in PBS-T were performed for 10 min each. The secondary antibody anti-rabbit conjugated to HRP (horseradish peroxidase) was added at a 1:6000 dilution for one hour in 5% milk in PBS-T. This was again followed by three washing steps of 10 min each.
The detection of antibodies was performed on a ChemiDoc MP Imaging System. Using the Western Lightning Plus ECL Kit (PerkinElmer Inc.) a total of 600 µl of reaction solutions were added to the membrane and a fluorescence signal was recorded. The HRP enzyme, which is conjugated to the secondary antibody, reacts with the substrates from the kit to produce a chemiluminescent reaction and release light. The exposure times must be adapted to the specific antibody.

2.2.8 **Control of Conditional Knock-out via RT-qPCR**

As the KO only occurs in electroporated cells due to the electroporated Cre-plasmid, these cells should be specifically checked for *Mid1* and *Mid2* expression. Therefore, GFP-positive cells were separated and analyzed via RT-qPCR (reverse transcriptase quantitative polymerase chain reaction) for RNA levels of *Mid1* and *Mid2*.

2.2.8.1 FACS

FACS, short for automated fluorescence activated cell sorting, uses fluorescent labeling of cells to separate them from non-fluorescent cells or cells with different fluorescent labeling. A FACS machine is designed in a way that each individual cell can enter in a single droplet. Determined by the fluorescence staining of the cell in the drop is given a different electronic charge. The deflection plates attract or repel these cells then depending on the charge into collection tubes.
To collect the GFP-positive cells from the embryonic brain the embryos were removed as described in Chapter 2.2.6.2 on E15.5. The brains were prepped and observed under UV-light. Brains with the best GFP-signal in the cortex where chosen and the green fluorescent part was cut out. This section should include

a high concentration of GFP-positive cells. To continue with the FACS, which would sort out only GFP-positive cells, a single-cell solution had to be generated. Therefore, the protocol was established by our own working group. Up to three brain sections were put in 10 ml DMEM on ice until trypsin was heated to 37ºC. Then the medium was aspirated, 1 ml of trypsin was pipetted on the tissue and incubated for six minutes at 37ºC. Afterwards 3 ml of stopping medium were added and the solution centrifuged for two minutes with 200g at RT. The cell pellet was washed twice with PBS and centrifuged for 3 min. In the last step the cell pellet was resuspended in 1 ml PBS and decanted through a 100 µm filter for mechanical separation of the cells into a special FACS tube.

The FACS machine then would sort the cells into a GFP-positive fraction and the other cells were discarded. GFP-positive cells were collected in 100 µl RLT buffer from the following RNA isolation kit RNease® MicroKit. 1 µl of β-mercaptoethanol was added to the buffer to denature RNase.

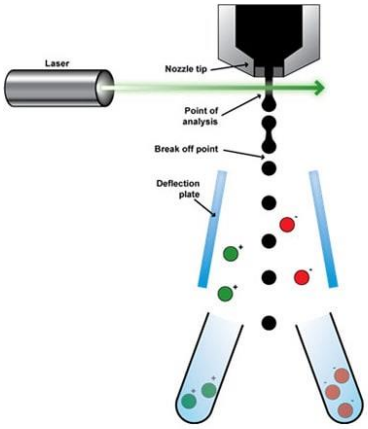

Figure 13 Scheme of FAC-Sorting (https://www.abcam.com/protocols/fluorescence-activated-cell-sorting-of-live-cells retrieved on 21.09.2020)

2.2.8.2 RNA Isolation

From the sorted cells, RNA was isolated and purified from DNA and proteins due to their different solution parameters using RNeasy® MicroKit.

In the first step 1 volume of 70% EtOH was added to the cell lysate and mixed by pipetting. The sample was then transferred to a RNeasy MinElute spin column placed in a 2 ml collection tube and centrifuged for 15 sec at 10.000 rpm. This and all following centrifugation steps were conducted at RT using the centrifuge Peqlab PerfectSpinP.

After discarding the flow-through, 350 µl buffer RW1 were added to the column and centrifuged to wash the membrane of the column. Flow-through was discarded and 10 µl of DNase I incubation mix was pipetted on the membrane and incubated for 15 min. Afterwards, again 350 µl RW1 buffer were added to the column for washing and centrifugated for 15 sec.

The column was placed in a new collection tube and 500 µl buffer RPW were added and centrifuged for 15 sec to wash the membrane following discarding the flow-through. Furthermore, 500 µl of 80% EtOH were pipetted on the column to wash the membrane via centrifugation for 2 min. To avoid carryover of ethanol, the column must be removed carefully from the collection tube into a new collection tube. To dry the membrane, the open column was centrifuged at full speed for 5 min.

With the last step, again the column was placed in a new 1.5 ml Eppendorf tube and 14 µl RNase-free water were pipetted on the membrane. The centrifugation for 1 min at full speed elutes the RNA into the collection tube. Storage had to be immediately at -80ºC.

To quantify the RNA concentration, Qubit RNA HS assay kit was used for measurement. The technique is based on a fluorescing dye, which binds to RNA and emits its fluorescence. The Qubit Fluorometer can detect the signal and calculate the RNA concentration in the sample.

A working solution was prepared, containing 199 µl buffer per sample and 1 µl reagent per sample. After mixing the solution, 190µl of it were pipetted into a 0.5ml tube and 10µl of standard 1 and standard 2 solution were added to separate tubes. 2µl of each sample were mixed with 198µl of the working solution. The tubes were vortexed for a few seconds and incubated at RT for 2min. The measurement was done with Qubit fluorometer.

2.2.8.3 cDNA Synthesis

To check for the gene expression via RT-qPCR the isolated RNA had to be transcribed into cDNA. The RevertAid First Strand cDNA Synthesis Kit was used for this purpose. The primers included in the kit bind randomly to the RNA, while the reverse transcriptase attaches to these primers and transcribes the RNA into cDNA.

For the subsequent RT-qPCR samples must have the exact same amount of cDNA. Knowing the concentration from Qubit measurement, the amount to gain

10 ng RNA was used. The components shown in the table were added together in a PCR-tube on ice.

Table 26 Components of the RevertAid First strand cDNA synthesis kit

Component	Quantity
RNA	10 ng
Random hexamer primers	1 µl
Oligo (dT)$_{18}$ primer	1 µl
5x reaction buffer	4 µl
RiboLock RNase inhibitor (20U/µL)	1 µl
10mM dNTP Mix	2 µl
RevertAid M-MulVRT (200U/µL)	1 µl
H_20	Add 20 µl

After mixing and centrifuging the solution, the tube was placed into a thermal cycler and a program with 20°C for 5 min and 42°C for 60 min was run. To terminate the reaction the sample was heated to 70°C for 5 min.

2.2.8.4 RT-qPCR

RT-qPCR is a method of nucleic acid amplification for the detection or quantification of gene expression (115). The method is intended to show whether the IUE of the Cre-plasmid has led to the deletion of the floxed regions of *Mid1* and *Mid2* genes in *Mid1*^{lox}/*Mid2*^{lox} mice.

The principle is based on intercalation between SYBR green dye and cDNA releasing a fluorescent signal. Via PCR the cDNA doubles its amount with every cycle. The more cycles pass, the higher the fluorescent signal will be. *Gapdh* served as reference housekeeping gene, against which the target genes need to be normalized.

To quantify the expression of *Mid1* and *Mid2,* specific primers were designed. Therefore, the template sequence of both genes was taken from the online database RefSeq. Furthermore, to find the primers specific to the template the online tool Primer-BLAST was used. Three primer pairs suggested by the program were ordered for each gene commercially from Sigma-Aldrich. The primers were designed in a way spanning an exon-exon junction, which can only be amplified after intron splicing. Therefore, gDNA could not be detected.

In preparation for RT-qPCR, one *master mix* per primer pair was prepared. dH_20 was pipetted into 1.5 ml tubes, the primers were vortexed and added to the water. SYBR Green was added shortly before using the master mix. The cDNA was diluted to a concentration of 0.5 ng/µl to gain enough volume for all reactions. A 96- well plate was placed on a cooling block and 2 µl cDNA were pipetted into the plate. Now, 8µl of the well mixed master mix were pipetted into the wells. A negative control without cDNA per primer pair was performed.

Table 27 Master mix protocol

Component	**Quantity [µl] per sample**
dH_20	26,4
Primer (1:10) For + Rev	4,4
SYBR Takara Green	57,2
cDNA (0,5 ng/µl)	2

The plate was sealed with a foil and centrifuged shortly. In the end it was placed in the cycler and program was started.
The cycling program conducted is shown below.

Table 28 RT-qPCR program

Temperature [ºC]	**Duration [sec]**
95	30
95	30
60 **40x**	30
72	40

To analyze the results the Ct values were compared after applying the ΔΔCt-method. First the Ct values had to be normalized to the reference genes. In the second step these values were normalized to the sample defined as control.

3 Results

3.1 Preparatory Work for the functional analysis of the MID1/MID2 genes

3.1.1 Confirmation of Breeding Results for *Mid1*^{lox}/*Mid2*^{lox}

The *Mid1*^{lox}/*Mid2*^{lox} mouse strain is the first to enable potential experiments with a double KO of the sister proteins to research whether the proteins could take over each other's functions. As the mouse line was first established in our lab the success of correct breeding had to be confirmed.

To guarantee the correct genotype of the *Mid1*^{lox}/*Mid2*^{lox} mice, litters were genotyped. Both the Mid1 and Mid2 genes are located on the X-chromosome, Mid1 on Xp22.2 and Mid2 on Xq22.3 in humans with comparable locations in mouse genome (55, 91). To avoid the possibility of crossing overs during breeding, homozygous *Mid1*^{lox}/*Mid2*^{lox} females were mated with hemizygous *Mid1*^{lox}/*Mid2*^{lox} males (37). This breeding strategy should result exclusively in hemizygous floxed males and homozygous floxed females.

To confirm the offsprings' genotypes, DNA was isolated from tail or ear punch biopsies. PCR was performed with primers (Lf and Lr, see primer table) specifically detecting the *Mid1* and *Mid2* wildtype and floxed genes.

The expected size (in bp) of the PCR fragments is shown in table 15. The targeted allele is longer due to the inserted LoxP sequence.

Table 29 Expected size of the PCR fragments of Mid1 and Mid2

Gene	Wildtype allele size (bp)	Targeted allele size (bp)
Mid1	457	534
Mid2	209	265

Figure 14 shows an example of the PCR products from four hemi- or homozygous mice embryos and the control (one heterozygous female (Ctrl.)). In the heterozygous control, the lower band represents the shorter fragment from the wildtype allele while the upper band represents the floxed allele.

Figure 14 Genotyping of four Mid1^{lox}/Mid2^{lox} mice. These are embryo samples, which is why the sex is not known and one cannot distinguish between hemi- or homozygous. Ctrl. Hom. is a homozygous Mid1lox/Mid2lox female mouse. The fragment of Mid1lox gene is 534 bp long, the wildtype allele 457 bp. The Mid2lox fragment is 265 bp long, wildtype allele 209 bp.

All descendants of this breeding were homo- or hemizygous floxed animals and showed only one band for the *Mid1* and *Mid2* genes with the correct size.

3.1.2 **Confirmation of Breeding Results for Heterozygous *Mid1*^{lox}/*Mid2*^{lox}**

As a preparation for further experiments and breedings, heterozygous *Mid1*^{lox}/*Mid2*^{lox} mice should be established.

The mating of homozygous *Mid1*^{lox}/*Mid2*^{lox} females with C57BL/6N males should result in heterozygous *Mid1*^{lox}/*Mid2*^{lox} female or hemizygous male offspring. To confirm this, the pubs were genotyped. The mating of homozygous *Mid1*^{lox}/*Mid2*^{lox} females with wildtype C57BL/6N should not be disturbed by crossing over (37).

To confirm the offsprings' genotypes, DNA was isolated from tail or ear punch biopsies. PCR was performed with primers (Lf and Lr, see primer table) specifically detecting the *Mid1* and *Mid2* wildtype and floxed genes.

The expected size (in bp) of the PCR fragments is shown in table 15. The targeted allele is longer due to the inserted LoxP sequence.

PCR was performed with primers Lf and Lr as described above. The expected size (in bp) of the PCR fragments using the Lf and Lr primer is shown in table 15.

Figure 15 shows one litter with heterozygous and hemizygous offspring as well as a heterozygous control. Two bands for *Mid1* can be seen, the shorter fragment displays the wildtype allele. The same applies for *Mid2*^{lox} and *Mid2*^{wt} alleles. It could be confirmed that all female offspring of the breeding were heterozygous *Mid1*^{lox}/*Mid2*^{lox}.

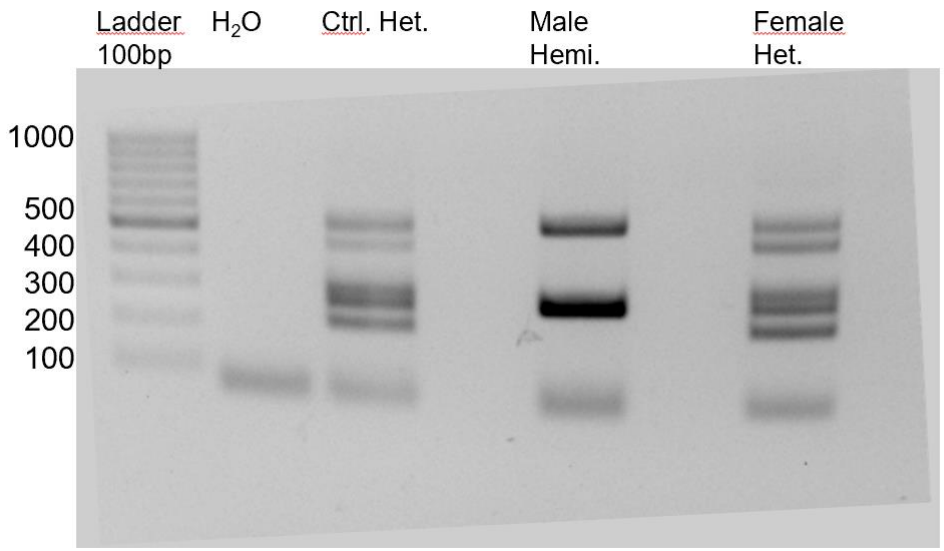

Figure 15 Genotyping of two mice from a breeding of a Mid1^{lox}/Mid2^{lox} female with C57BL/6N male. Ctrl. Het. is a known heterozygous Mid1^{lox}/Mid2^{lox} mouse from a breeding during establishment of the parental mouse strain. The fragment of Mid1^{lox} gene is 534 bp long, the wildtype allele 457 bp. The Mid2^{lox} fragment is 265, wildtype allele is 209 bp.

3.1.3 **Confirmation of Breeding Results for *Mid1*^{lox} and *Mid2*^{lox}**

Mid1 0 mice were described as a KO model in literature (21). For Mid2, on the other hand, no KO mouse model has been established so far. To research possible effects of a single KO of these genes, single conditional KO lines for *Mid1* and *Mid2* should be established. The advantage of *Mid1*^{lox} and *Mid2*^{lox}strains is the possibility to generate conditional KO in different tissues by pairing with specific Cre-expressing strains.

To generate a single conditional KO lines for *Mid1* and *Mid2,* the breedings would span over four generations (Fig. 17). In the parental generation a homozygous *Mid1*^{lox}/*Mid2*^{lox} female and a C57BL/6N male were mated. The female offspring of this breeding were heterozygous *Mid1*^{lox}/*Mid2*^{lox} (F1 generation). An example of the genotypings' PCR results is given in Chapter 3.2. The heterozygous female offspring were then bred with C57BL/6N male mice. This breeding aimed for

crossing over to result in a single conditional KO line either for *Mid1* or Mid2 as both genes are x-linked and separated by 29 Mb. To proof the genotype of these offspring (F2 generation), PCR was performed with the specific primers Lf and Lr to detect wildtype and floxed for the *Mid1* and *Mid2 gene*. The expected size (in bp) of the PCR fragments using the Lf and Lr primer is shown in table 15. Figure 16 shows the results of the genotyping of the F2 generation as well as a heterozygous (a) and homozygous (b) control samples. For both genes, the wildtype band is slightly smaller than the targeted allele resulting in the further migrated lower band. Lanes 5-7 show three males which carry the *Mid1/Mid2* wildtype alleles (c). One male mouse with only the targeted alleles in *Mid1* and *Mid2* is identified as hemizygous *Mid1*^{lox}/*Mid2*^{lox} (d). One female mouse is identified as homozygous *Mid1*^{wt}/*Mid2*^{wt} (f). Lane e) shows the results of a female mouse with only a wildtype allele of *Mid2*, but two bands for the *Mid1* gene. This mouse is therefore a heterozygous single *Mid1*^{lox} containing a targeted allele and a wildtype allele for the *Mid1* gene. This shows that a crossing over between the wildtype and targeted X-chromosome in the heterozygous mother happened and led to this genotype.

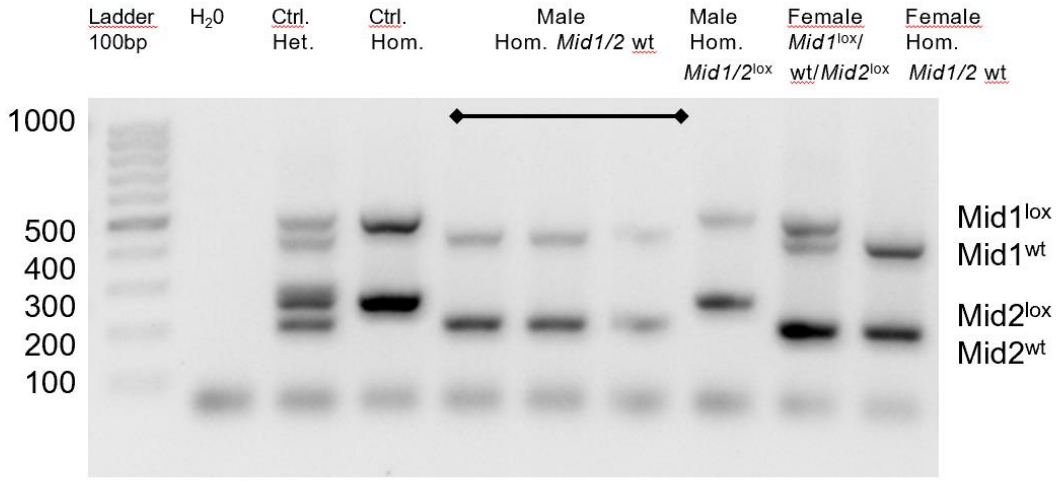

Figure 16 Genotyping of offspring of the third generation (III) with the aim to generate single conditional KO lines. Lane 3 Ctrl Heterozygous, 4 Ctrl Homozygous, 5-7 Male *Mid1*wt/*Mid2*wt, 8 Male *Mid1*^{lox}/*Mid2*^{lox}, 9 Female *Mid1*^{lox}/wt/*Mid2*^{lox}, 10 Female *Mid1*wt/*Mid2*wt

To generate a homozygous or hemizygous single conditional KO line for *Mid1* and *Mid2*, the breeding of a fourth (IV) of even fifth (V) generation is needed (Fig. 17). We showed that crossing over in breeding of *Mid1*^{lox}/*Mid2*^{lox} is capable of creating new mouse lines.

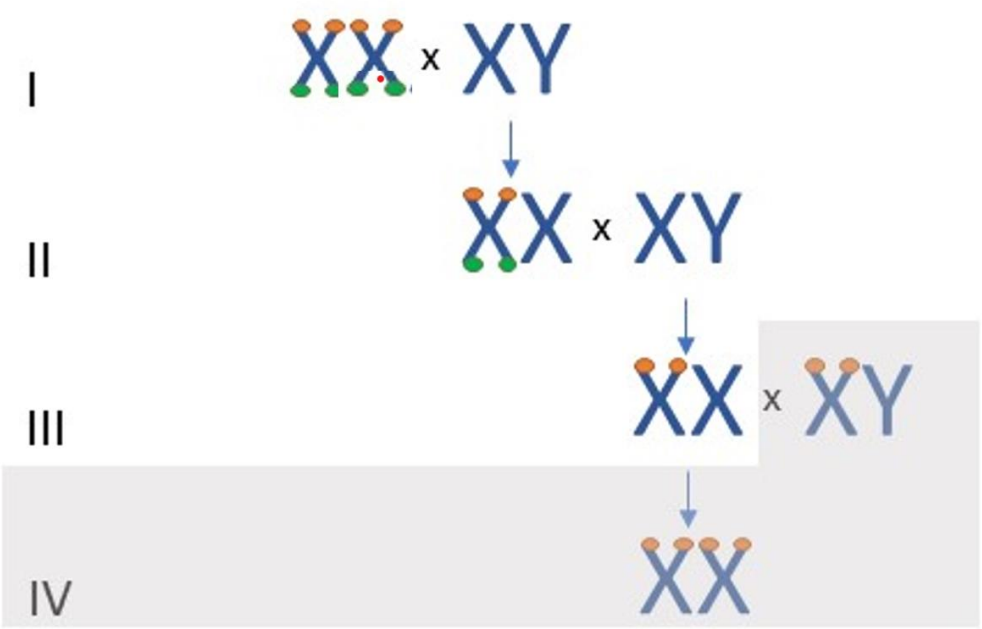

Figure 17 Excert of breeding procedure for single floxed mice. Breeding was not continued after crossing over was proofed (grey overlay).

3.1.4 Control of Cre-expression and functionality in *Mid1*^{lox}/*Mid2*^{lox} mice via breeding with Deleter-Cre mice

The *Mid1*^{lox}/*Mid2*^{lox} mice were used for *in utero* electroporation (IUE) with *Cre* containing plasmids, as described in Chapter 2.2.6. Due to the novelty of this mouse line the first step was to verify the Cre-Lox-system's functionality. Therefore, homozygous *Mid1*^{lox}/*Mid2*^{lox} females were mated with Deleter-Cre males. The Deleter strain expresses Cre recombinase in every tissue, even stem cells and is therefore a good strain to research consequences of gene deletion during embryogenesis (104). Cre expression is X-linked.

The first generation of this breeding should generate heterozygous cKO females and hemizygous *Mid1*^{lox}/*Mid2*^{lox} males. Table 16 shows the expected sizes of the PCR fragments.

Table 30 Expected size of the PCR fragments of Mid1 and Mid2

Gene	Wildtype allele size (bp)	Targeted allele size (bp)	Knock-Out allele size (bp)
Mid1	1380	~1480	~ 300
Mid2	768	~ 830	~ 300

The PCR products were transferred to an agarose-gel and separated. Figure 18 shows representative results of the PCR products for *Mid2* genotyping separately.

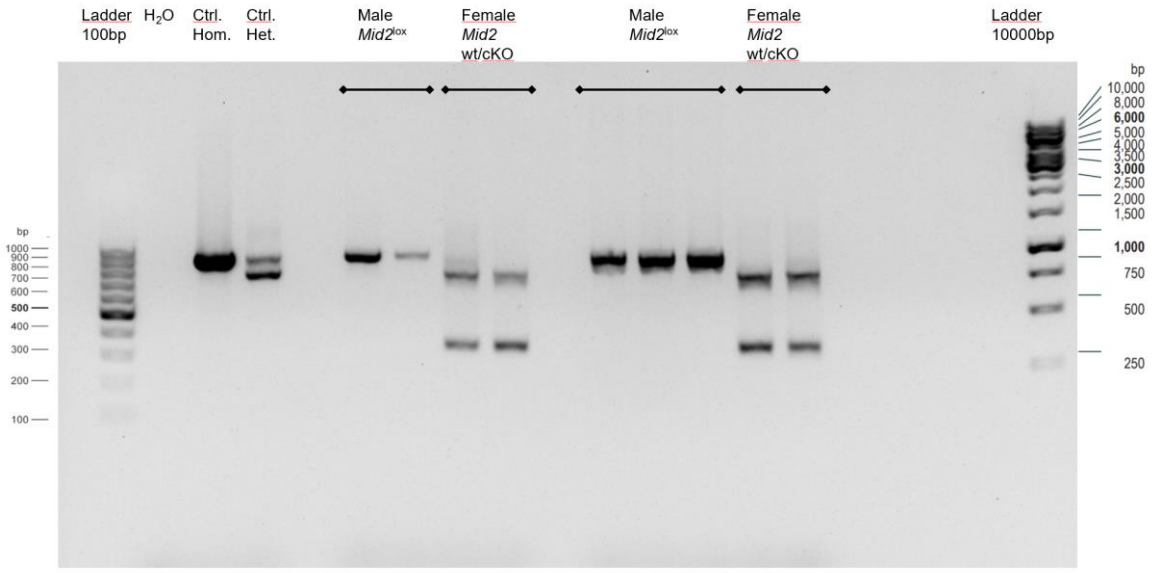

Figure 18 Genotyping of MID2 of the first generation after breeding Mid1^{lox}/Mid2^{lox} mice with Deleter Cre. Ctrl. Hom. is a known homozygous Mid1^{lox}/Mid2^{lox} mouse, Ctrl. Het. A known heterozygous Mid1^{lox}/Mid2^{lox} mouse. The longest fragments with a length of 830 bp represent the floxed sequences. The wildtype sequences are only slightly shorter. The cKO sequence is significantly shorter with around 300 bp.

The results were similar for *Mid1* and female mice were shown to be heterozygous *Mid1*$^{cKO/wt}$/*Mid2*$^{cKO/wt}$. The male offspring inherited the floxed genes from their mothers and therefore are hemizygous *Mid1*^{lox}/*Mid2*^{lox} males. The breeding showed, that the mouse line *Mid1*^{lox}/*Mid2*^{lox} is functional for recombination with Cre.

3.1.5 **Generation of a MID1 Overexpression Construct**

To investigate the effect of a cell-specific overexpression of *MID1* in embryonic mouse brains via *in utero* electroporation, a corresponding plasmid was

designed. At the beginning of this work, a construct containing the human *MID1* cDNA pCMV-tag 3A/MID1 was already available in the lab. For IUE, the *MID1* cDNA had to be subcloned into the plasmid pCAG-IG. The sequence of *MID1* was amplified from the above-mentioned construct by PCR using a specific primer pair (See Primer). These primers included recognition sequences for the restriction enzymes EcoRI and XhoI and the sequence for an HA-tag. The expected length of the PCR product (*MID1* cDNA plus restriction site and HA-tag sequences) was 2031 bp. The PCR samples were applied to a 1.5% agarose gel and separated according to size (Fig. 21). The gel image of the agarose gel electrophoresis shows the expected bands of the PCR product around 2000 bp (A-C). The circular plasmid pCMV-tag 2A and 3A are visible above the bands of MID1. Only pCMV-tag 2A was used in the end. As a control (C1) PCR of pCMV-tag 2A was done without polymerase, it shows a wide band from the circular plasmid in contrast to small bands after linearization.

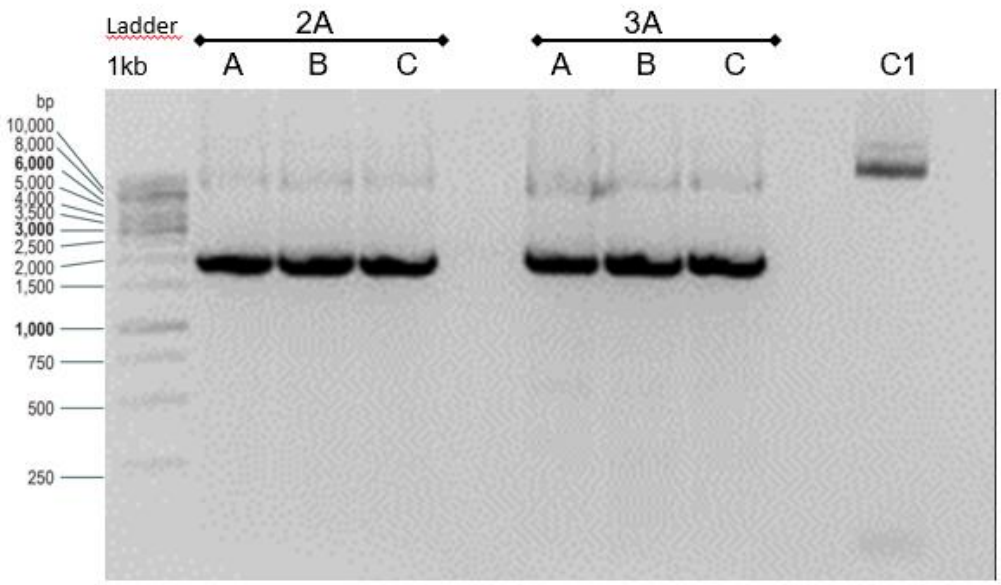

Figure 19: Agarose gel after amplification of MID1. The PCR was performed with three samples each of pCMV-ta 2A and pCMV-tag 3A and one plasmid control C1 without polymerase. The PCR products of MID1 show a band at 2000 bp. The circular plasmid pCMV-tag 2A with the MID1 sequence shows a band in the upper part of the gel image at C1 and 2A and 3A A to C.

The amplified *MID1* cDNA was isolated from the agarose gel and then digested together with the target plasmid pCAG-IG using the restriction enzymes EcoRI and XhoI. After ligation and transformation, in total 12 colonies could be picked for the samples pCAG-IG-MID1 2A and 3A. These samples were isolated and

purified using Miniprep. To check for the correct insert size, a control digestion of the 12 samples was performed with EcoRI and XhoI. Figure 23 shows the gel image of four of the twelve samples after the restriction digestion of the plasmid pCAG-IG and *MID1* 3A. Additionally, a control C1 is displayed, where no restriction enzymes were used. The wide band in the control represents the undigested plasmid pCAG-IG. All other columns show one band for the linearized plasmid pCAG-IG at 6000 bp. Noticeable is the sample 3A-B that shows a second band at around 2000 bp, representing the *MID1* sequence. Thus, the ligation of *MID1*-cDNA with pCAG-IG worked in this sample.

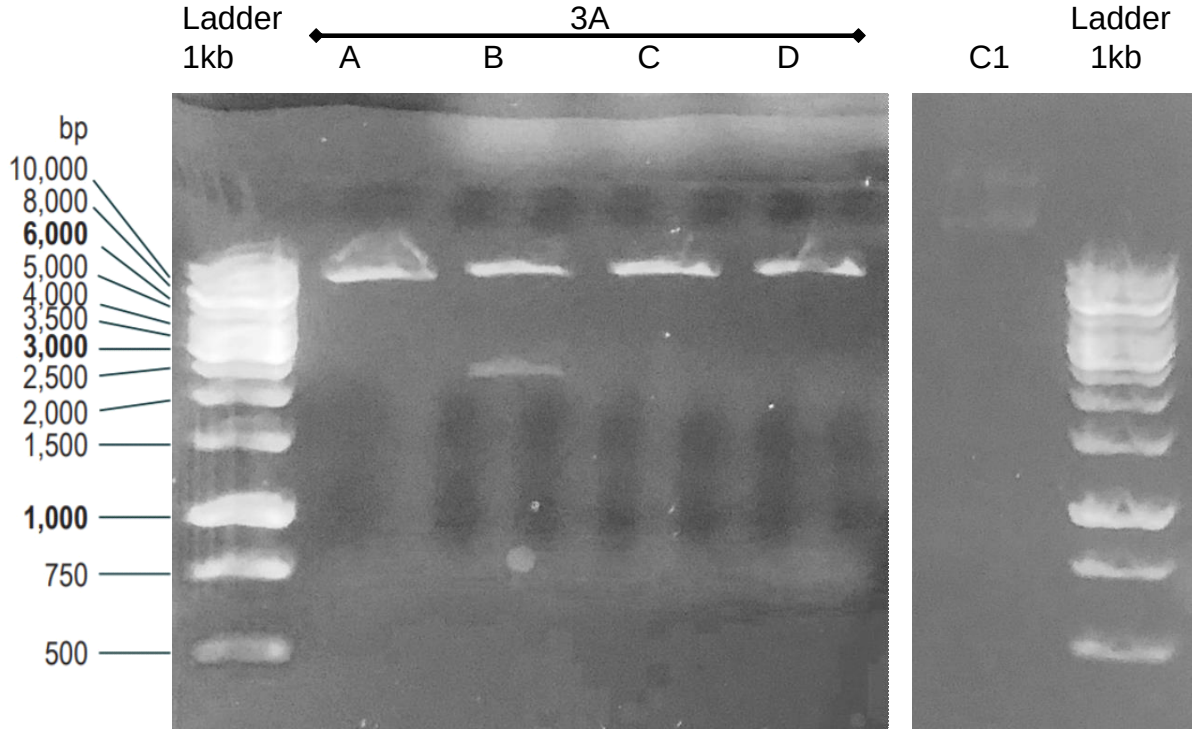

Figure 20 Agarose gel after control restriction digestion of pCAG-IG-MID1. The restriction digestion was performed with EcoRI and XhoI (A-D). In the control C1 no restriction enzymes were used. The sample 3A-B shows a band above 2000 bp and at 6000 bp. C1 shows a band in the upper part of the gel image.

To check if the sequence of *MID1*-HA-tag is correct in the samples that were tested positive in the control restriction digestion, two samples 3A-B (Fig. 22) and 3A-F (no picture) were sequenced by GATC Biotech. The primers *MID1* pCAG-IG R1, F2, F4 were used. The samples were checked for possible errors using the "BioEdit" program with the MID1 reference sequence (Transcript: MID1-201, ENST00000317552) from the "Genome Browser Ensembl" (Fig. 23). The sequence was evaluated as error-free if no mutation was present, e.g. insertion, deletion, base exchanges or duplication. Silent mutations could be

neglected, since in this case the mutated codon codes for the same amino acid as the non-mutated codon. Here, the first region of the sequenced sample is shown below. This sequence spans the plasmid pCAG-IG, the HA-tag, Kozak and the beginning of the *MID1* sequence with the start codon ATG. Figure 25 shows the MID1 sequence aligned to the sample from the positions 1800 to 2050. At c.1908C>T is a silent mutation in the sample sequence. Following the reading frame, the base triplet CTG changes to TTG. Both triplets encode for the same amino acid Leucine. This was the only mutation found in the sequence.

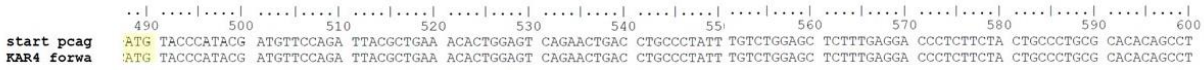

Figure 21: Alignment of the sample sequence (KAR4 forwa) and the reference sequence (start pcag) with the start codon, HA-tag and beginning of MID1 reference sequence. The bases adenine (A), guanine (G), cytosine (C) and thymine (T) form the base sequence. All bases match. The start codon (ATG) is marked in yellow.

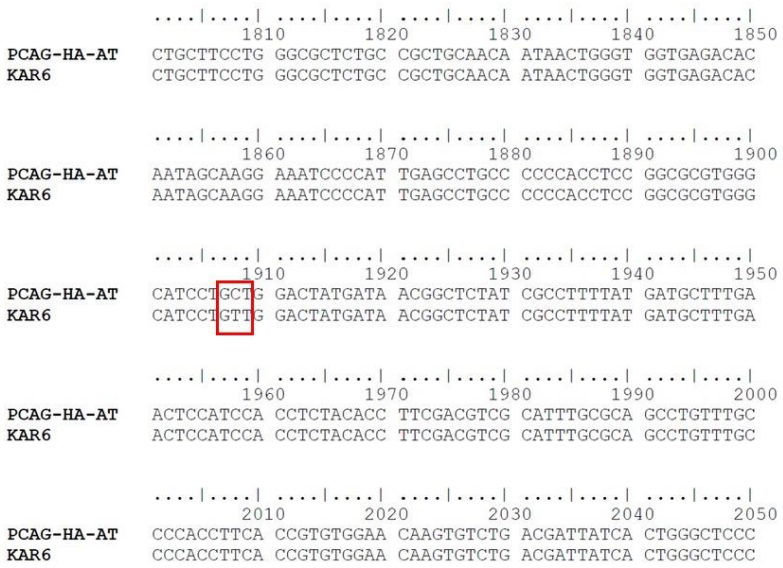

Figure 22: Alignment of the sample sequence (KAR6) with the MID1 reference sequence (PCAG-HA-AT) from position 1800 to 2050. The bases adenine (A), guanine (G), cytosine (C) and thymine (T) form the base sequence. The sequences match, on all but one position. The silent mutation c.1908C→T is marked in red.

Overall, two plasmids pCAG-IG-MID1 were evaluated as correct and one chosen for *in utero* electroporation.

3.1.6 Confirmation of MID1 expression from the pCAG-IG plasmid by westernblot analysis

The generated plasmid pCAG-IG-MID1 was checked for expression level of *MID1* to guarantee overexpression in electroporated brain cells. Therefore, HeLa cells were transfected with the plasmid pCAG-IG-MID1 and pCAG-IG-empty and incubated for 48h. Subsequently, protein lysates from transfected HeLa cells were generated and used for Western blot analysis. The primary antibodies anti-MID1 and anti-GAPDH as housekeeping protein were used. As secondary antibody HRP-linked anti-rabbit was used.

For the MID1 protein, a band at 72 kDa is expected, while the housekeeping protein GAPDH shows a band between 30 and 40 kDa. In the sample transfected with the control plasmid, no band at 72 kDa is visible for the eye. In comparison, the sample transfected with pCAG-IG-MID1 (OE) shows a band at around 72 kDa.

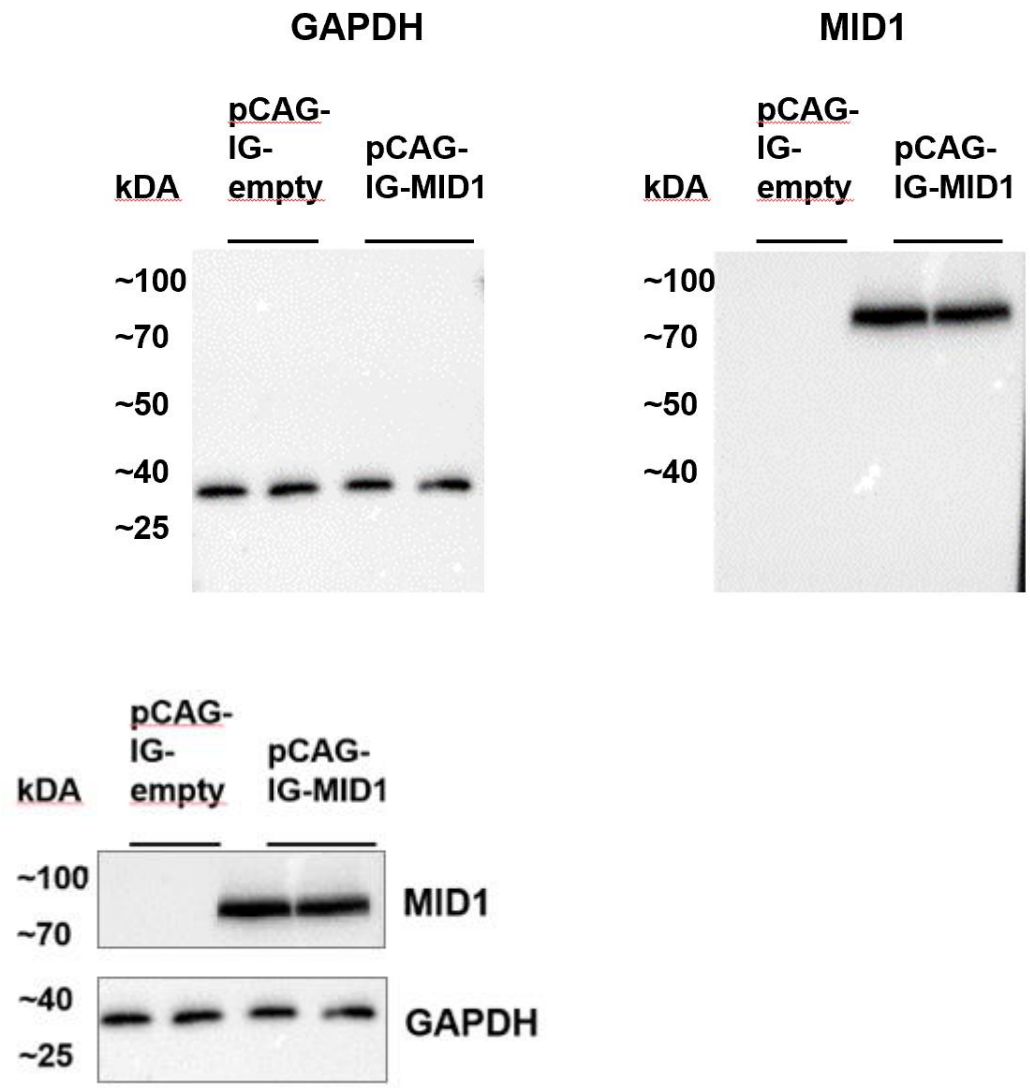

Figure 23 Western blot analysis of the overexpression construct pCAG-IG-MID1 in HeLa cells. Protein lysates of cells after transfection of PCAG-IG-MID1 and pCAG-IG-empty were used. As primary antibodies anti-MID1 and GAPDH were used. For the secondary antibody anti-rabbit HRP was used. The GAPDH bands for the control and the overexpression sample lie around 30 to 40 kDa. In the control no MID1 low expression could be observed. In the cells transfected with pCAG-IG MID1 the bands for MID1 lie around 70 kDa.

The results of the Western Blot were evaluated with the program "Image Lab" by normalizing the absolute values of the intensity of the respective anti-MID1 band to the corresponding anti-GAPDH band. The pCAG-IG-empty sample represents the endogenous protein of MID1 as control and shows an intensity of 0.022 for the anti-MID1 antibody but due to the short exposure time was not visible by eye in the picture. The sample transfected with the construct pCAG-IG MID1 for overexpression shows an intensity of 1.7541.

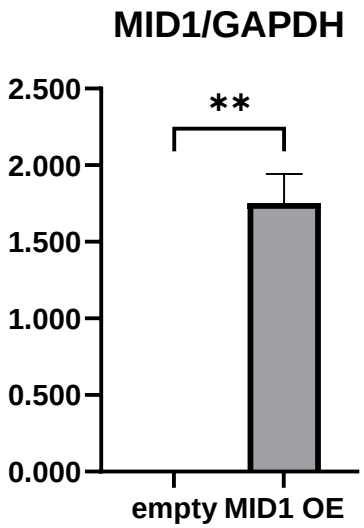

Figure 24 Normalized intensity of MID1 antibodies used in Western blot analysis. MID1 expression in HeLa cells transfected with the control plasmid pCG-IG-empty (empty) was 0,0022, in cells tranfected with pCAG-IG-MID1 (MID1 OE) 1,7541. The MID1 expression is significantly increased after transfection of pCAG-IG-MID1 (p = 0,0057)

The expression of MID1 was significantly increased in cells after transfection of pCAG-IG-MID1. Therefore, the capability of inducing an overexpression was proven in vitro.

3.2 In Utero Electroporation for the Overexpression of *MID1* at E14.5

The pathomechanism of genetic basis for OS is still not yet fully understood. Accumulation of the protein could also have an effect on the phenotype (22). Therefore, OE of MID1 is an interesting approach to understand cellular mechanisms during neurogenesis.

To achieve an overexpression of MID1 in embryonic mouse brains, a qualified member of our working group electroporated C57B6/J mice on E13.5 pCAG-IG-MID1 or pCAG-IG-empty into the lateral ventricles (See In Utero Electroporation) of the cerebrum. Twenty-four hours later the embryonic brains were harvested and fixed in 4% PFA, cryoprotected in sucrose and cut into 20 µm sections.

3.2.1 Validation of MID1 overexpression by staining for HA-tag in the electroporated E14.5 mouse neocortex

To verify the expression of MID1 from the pCAG-IG-MID1 plasmid in the electroporated cells of the E14.5 C57B6/J mouse neocortex, the brain sections were stained with an antibody against the HA-tag fused to MID1 (See Generation of an Overexpression Construct of MID1). The HA-tag is an epitope tag that can be used for labeling and detection of proteins. With only nine amino acids, its size is small and therefore it is unlikely to affect the tagged protein's reaction properties (116). Because the overexpressed MID1 protein is fused to the HA-tag N-terminal a HA staining can be used to visualize the expression of the overexpressed MID1. Additional to anti-HA, the cells were stained with anti-GFP antibody to detect the electroporated cells. Secondary antibodies Alexa Fluor® 594 Goat anti-Rabbit and 488 Goat anti-Mouse were used to visualize the primary antibodies. The mounting medium contained DAPI, a dye that binds to the DNA and therefore stains the nucleus blue. As the plasmid pCAG-IG-empty does not contain the sequence for HA, it served as a negative control.

Both brain sections show GFP-positive cells in green, defining them as electroporated cells (Fig. 28). The brain sections electroporated with the control plasmid pCAG-IG-empty do not show a red signal for the HA-tag. The brains containing the overexpression construct pCAG-IG-MID1 show a red signal. As the GFP-positive cells also carry the HA-signal, they occur yellow in the section shown (Fig. 27, left picture). This proves the expression of MID1 protein from the electroporated plasmid pCAG-IG-MID1 and ensures its expression *in vivo*.

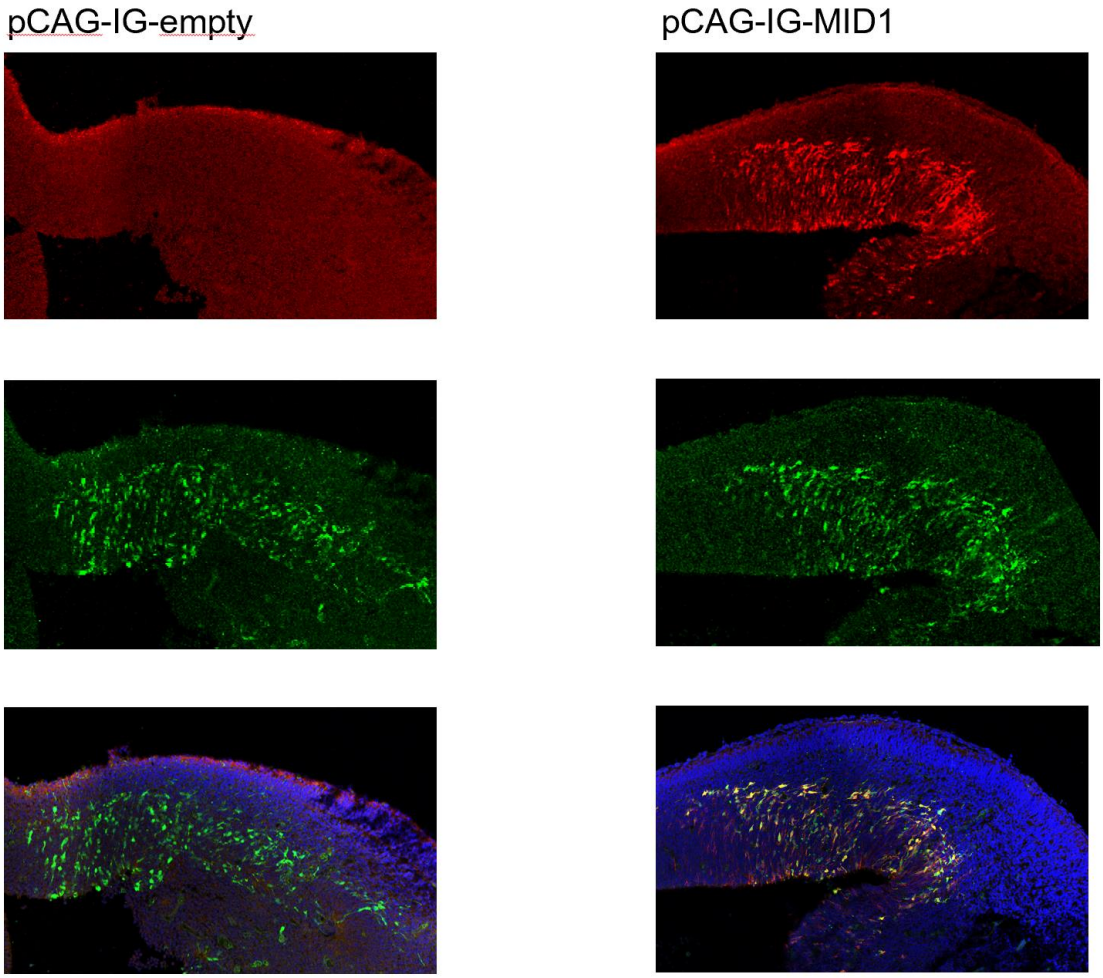

Figure 25 Representative picture of the HA-tag staining in the embryonic neocortex after IUE on E13.5. Brains dissected 24 h after electroporation an E14.5. Green cells are GFP+, HA-tag is stained in red, cells containing both constructs therefore appear yellow. On the left side the OE construct containing the HA-tag was electroporated. On the right side the control plasmid was used. Only in the brain on the left the HA-tag is expressed.

3.2.2 **Distribution and migration of neuronal progenitor cells after IUE of pCAG-IG-MID1 or pCAG-IG-empty**

To analyze changes in migration of neuronal progenitor cells in E14.5 embryos, the neuronal cells containing the electroporated construct were labeled with the anti-GFP antibody and visualized using the secondary antibody Alexa Fluor® 488 (Goat anti-Mouse IgG). Additionally, the nuclei were stained with DAPI. To quantify migration of the neuronal progenitor cells in the neocortex after electroporation, the distribution of cells in the VZ, SVZ/IZ and CP were counted.

The cell percentage per layer in proportion to all cells was calculated. The analysis was performed with the software ImageJ and Prism.

In the control 62,7% ± 0,02 of the cells were counted in VZ and 37,2% ± 0,02 in the SVZ/IZ. 49,1% ± 0,07 of the cells containing the MID1 OE plasmid could be found in the VZ and 50,6% ± 0,07 in the SVZ/IZ. In both groups no cells were seen in the CP due to the short time span of 24 h after electroporation. Therefore, a significant difference between the OE and control group could be found in the VZ and SVZ/IZ. In the VZ the amount of GFP+ cells after electroporation of pCAG-ID-MID1 was reduced compared to the control group and vice versa in the SVZ/IZ. The significant difference in the distribution of the cells could be a result of altered migration. But also altered cell proliferation and differentiation might play a role and will be discussed later. Figure 29 shows representative pictures of cortices after electroporation, while figure 30 displays the quantification of the counting.

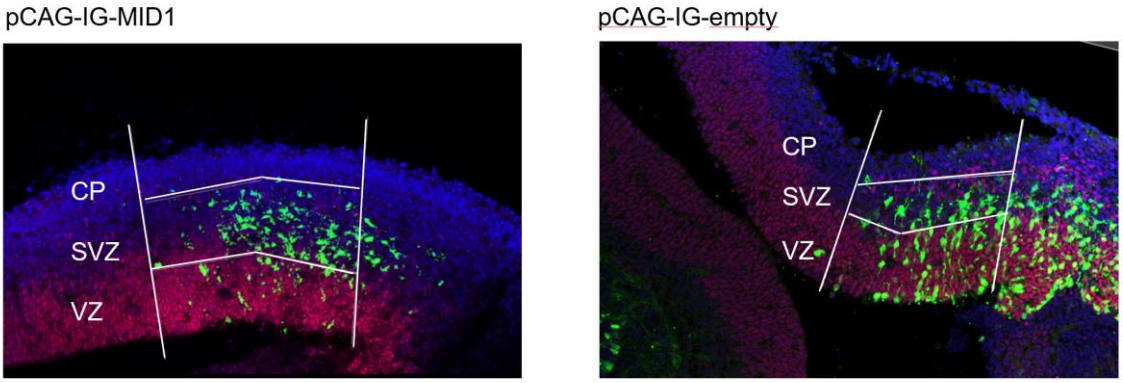

Figure 26 Representative picture of a staining in the embryonic neocortex after IUE on E13.5. Brains dissected 24 h after electroporation an E14.5. Here two brains stained with Pax6 are displayed. Green cells are GFP+, Pax6 is stained in red. White lines mark the border between the different layers. On the left side the OE construct, on the right side the control plasmid was used. Only cells lying in the region of interest, the cortex were counted.

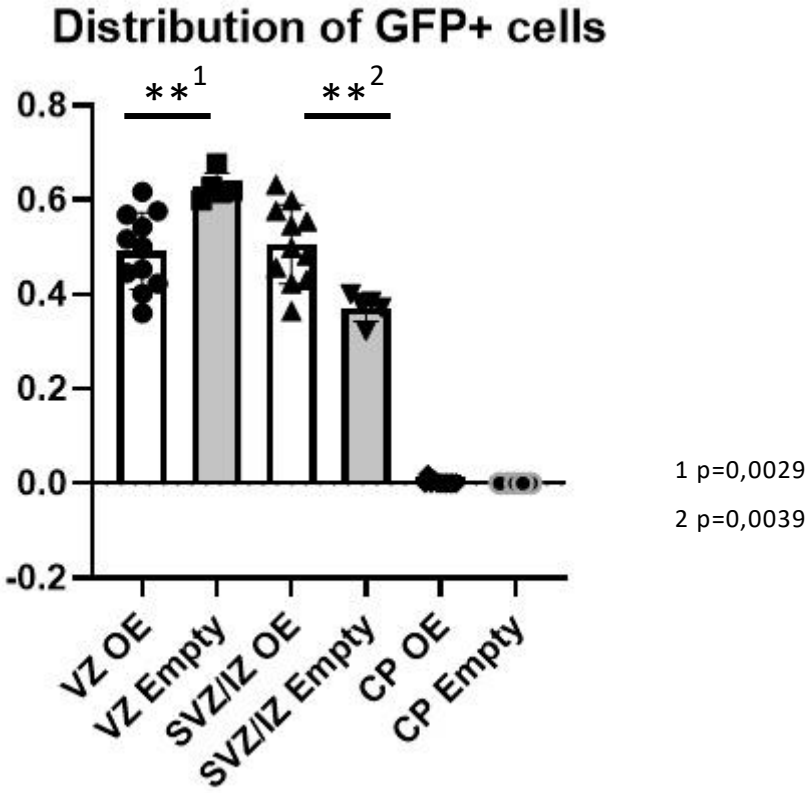

Figure 27 Results of the IUE of control and MID1 OE in the embryonic neocortex on E14.5. Quantification of stained cells in VZ, SVZ/IZ and CP. Data are mean ± SD. VZ: ventricular zone, IZ: intermediate zone, CP: cortical plate (VZ: OE vs. Empty ** p=0.003, SVZ/IZ OE vs. Empty ** p=0.0041, unpaired t-test, N_{OE}=11 N_{Empty}=5).

3.2.3 **Cell distribution of Pax6+ cells as a marker for VZ radial glia cells**

Staining for Pax6 was performed as a marker for VZ radial glia cells. The Pax6 positive cells lie in the VZ and are called RGCs. For the primary antibody rabbit anti-Pax6, for the secondary antibody Alexa Fluor® 594 (Goat anti-rabbit IgG) was used. Pax6 positive cells appear red, GFP positive cells green. Figure 31 displays representative stainings. GFP positive cells lying within Pax6+ zone were counted for the VZ. Additionally, staining with DAPI in blue.

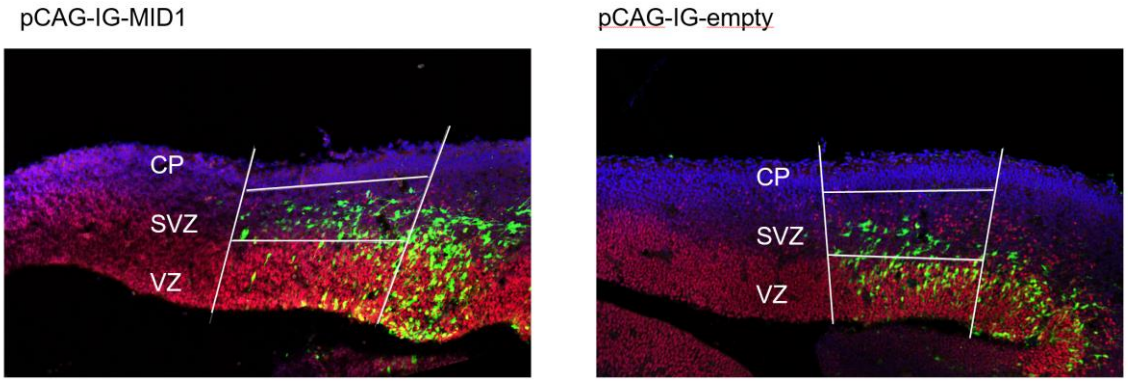

Figure 28 Representative pictures of the cell distribution in embryonic neocortex after IUE on E13.5. Brains dissected 24 h after electroporation on E14.5. Here two brains stained with Pax6 are displayed. Green cells are GFP+, Pax6 is stained in red. White lines mark the border between the dofferent layers. On the left side the OE construct, on the right side the control plasmid was used. Only cells lying in the region of interest, the cortex were counted.

In the control group 71,8% ± 0,02 of the GFP+ cells were positive for Pax6. The neocortex electroporated with the MID1 OE construct contained significantly less Pax6+ cells with 54,2 % ± 0,12 of all GFP+ cells being Pax6+. The cellular distribution is depicted in Figure 31. This is in line with the result of the distribution analysis. The IUE of pCAG-IG-MID1 leads to a decreased cell number in the VZ 24 h after electroporation.

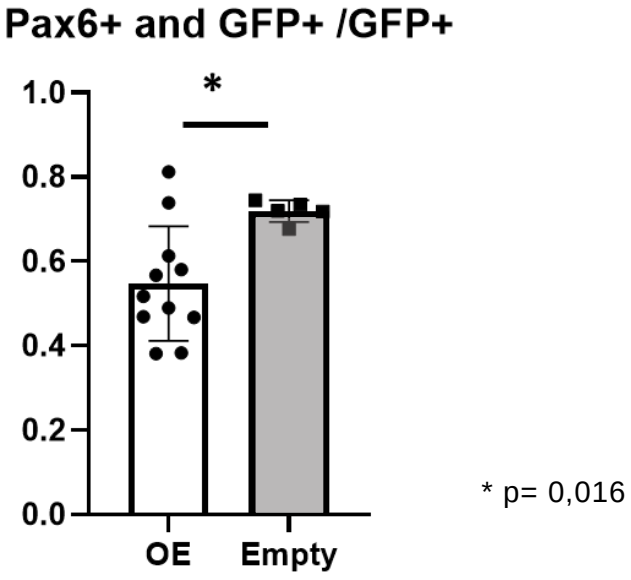

Figure 29 Results of the IUE of control- and MID1 OE-plasmids in the embryonic neocortex on E14.5 and staining for Pax6. Quantification of Pax6+ cells in dependence of GFP+ cells. Data are mean ± SD. (OE vs. Empty * p=0.016 unpaired t-test, N_{OE}=11, N_{Empty}=5).

3.2.4 Cell distribution of Tbr2+ cells as a marker for intermediate progenitors

Tbr2 is expressed by iPCs that are located in the SVZ. Therefore, it can be used as a marker for the SVZ. For the primary antibody chicken anti-Tbr2, for the secondary antibody Alexa Fluor® 594 (Goat anti-rabbit IgG) was used. Figure 32 shows two staining examples. Red cells are Tbr2 positive. Green cells are GFP positive electroporated cells.

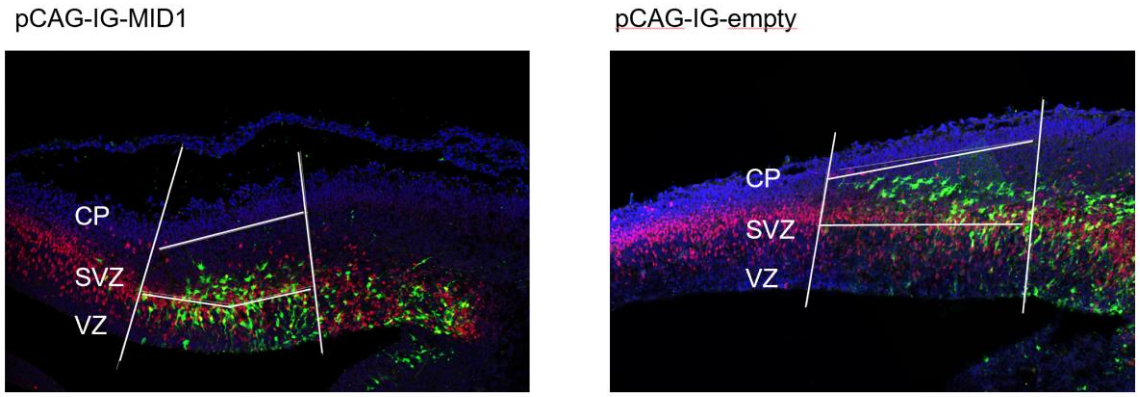

Figure 30 Exemplary representation of the cell distribution in embryonic neocortex after IUE on E14.5 24 h after electroporation. Here two brains staines with Tbr2 are displayed. Green cells are GFP+, Tbr2 is stained in red.

In the control brains 38,4% ± 0,03 of the GFP+ cells were positive for Tbr2+, while in the brains electroporated with the MID1 OE construct 49,1% ± 0,08 of all GFP+ cells were Tbr2+. This was significant. This is in line with the result of the distribution analysis. The IUE of pCAG-IG-MID1 leads to more Tbr2 positive cells 24 h after electroporation.

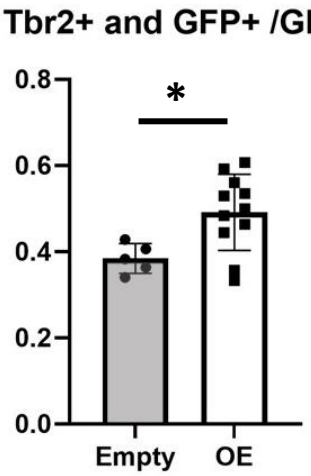

* p=0,0216

Figure 31 Results of the IUE of control and MID1 OE in the embryonic neocortex on E14.5 and staining for Tbr2. Quantification of Tbr2+ cells in dependence of GFP+ cells. Data are mean ± SD. (OE vs. Empty * p=0.0216 unpaired t-test, N_{OE}=11, N_{Empty}=5).

3.2.5 **Proliferation analysis by Ki67 staining**

To analyze changes in cell proliferation, the proliferation marker Ki67 was stained. For the primary antibody rat anti-Ki67, for the secondary antibody Alexa Fluor® 594 (Goat anti-rat IgG) was used. In figure 35 two representative pictures are depicted. Red cells are Ki67 positive. Green cells are GFP positive electroporated cells. Proliferating cells can be seen in different layers.

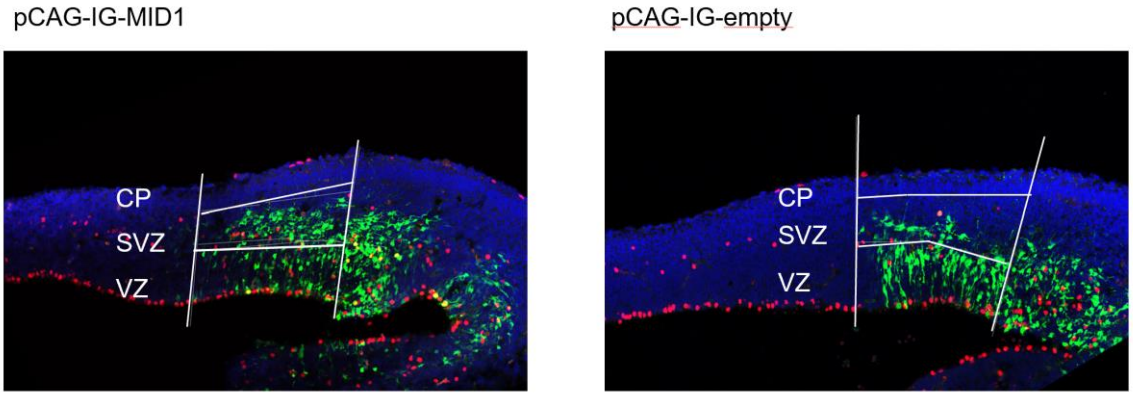

Figure 32 Representative pictures of the cell distribution in the embryonic neocortex on E14.5 24 h after electroporation. Here, two brains stained with Ki67 are displayed. Green cells are GFP+, Ki67 is stained in red.

In the brains electroporated with the MID1 OE construct 24 hr after electroporation significantly more KI67+ cells were counted in the VZ. In the control group only 8,6% ± 0,02 of the GFP+ cells were positive for the proliferation marker, while the mean value in the intervention group was 26,4% ± 0,11. In the SVZ/IZ 13,5% ± 0,07 (MID1 OE) vs. 6% ± 0,02 (ctrl) of the GFP+

cells were positive for Ki67, however, the difference was not significant. In summary, the overexpression leads to a higher proliferation rate in the VZ, but not in the SVZ/IZ compared to control.

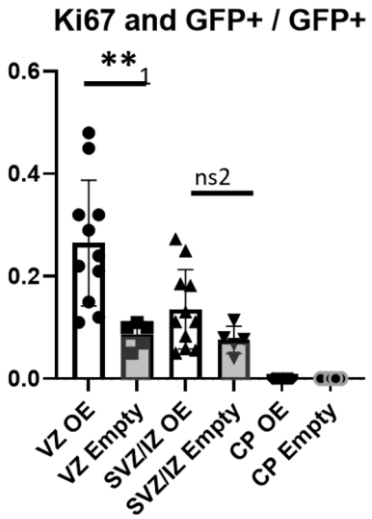

[1] p=0,007; [2] p= 0,11

Figure 33 Results of the IUE of control and MID1 OE in the embryonic neocortex on E14.5 and staining for Ki67. Quantification of Ki67+ cells in dependence of GFP+ cells. Data are mean ± SD. (OE vs. Empty [1] p=0.007, [2] p=0.11, unpaired t-test, N_{OE}=11, N_{Empty}=5)

It should be noted that the Ki67 staining in our experiment showed typical cells with very bright signals, but they seemed to be less than in other publications (117, 118). It is likely that only cells during mitosis are positive for the staining. RGCs undergo mitosis on the ventricular surface, BPs at a more basal localization (98). In our experiment the Ki67+ cells are located at these spots. To proof this staining with a specific mitosis marker (e.g. PHH3-antibody) should be performed.

3.2.6 **Apoptosis Analysis by Casp3 staining**

Apart from proliferation and specific layer markers, the brain sections were stained with Cleaved Caspase3 (cCasp3). Casp3 can be used as a marker for apoptotic cells as it is a primary executioner of apoptotic cell death in the cytochrome c pathway and contributes to the majority of cleavage during apoptosis, as well as chromatin condensation and DNA fragmentation (119). Apart from its role as a marker for apoptosis, Casp3 is also essential for normal brain development (120). Casp3 is cleaved and therefore activated, the antibody used thus detects only the active form of the marker protein Casp3 (121).

Staining was performed with Rabbit-Anti-cCasp3, for the secondary antibody Alexa Fluor® 594 (Goat anti-rabbit IgG) was used.

Figure 37 shows two brains stained with Casp3.

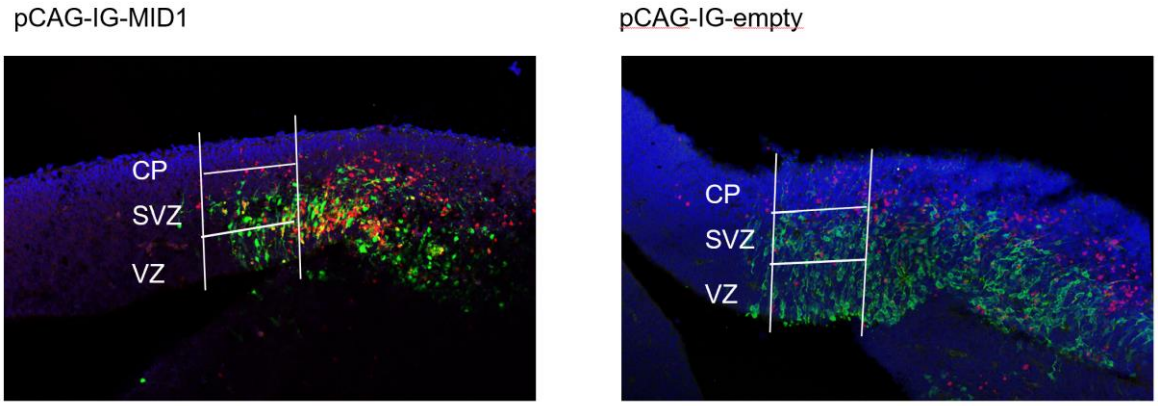

Figure 34 Exemplary representation of the cell distribution in embryonic neocortex after IUE on E14.5 24 h after electroporation. Here two brains stained with Casp3 are displayed. Green cells are GFP+, Casp3 is stained in red.

In the control neocortices 37,5% ± 0,21 cCasp3+/GFP+ cells were found in the VZ, while 60,1% ± 0,37 electroporated with the MID1 OE construct were counted. Analysis of SVZ/IZ showed that 62,5% (ctrl) vs. 39,8% (MID OE) of the GFP+ cells were positive for the apoptosis marker. The differences were, however, not significant in the layer specific analysis.

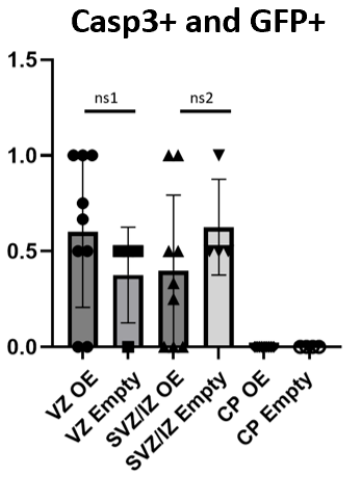

[1] p=0,3183;
[2] p= 0,3183

Figure 35 Results of the IUE of control and MID1 OE in the embryonic neocortex on E14.5 and staining for Casp3. Quantification of distribution of Casp3+ and GFP+ cells. Data are mean ± SD. (OE vs. Empty [1] p=0.3183, [2] p=0.3183, unpaired t-test, N_{OE}=9, N_{Empty}=4)

When the proportion of Casp3+/GFP+ cells in the total number of GFP+ cells is analyzed, no significant difference can be detected either. In the control 6,1% ± 0,01 of the GFP+ cells were co-stained with Casp3 vs. 12,3% ± 0,07 (MID1 OE).

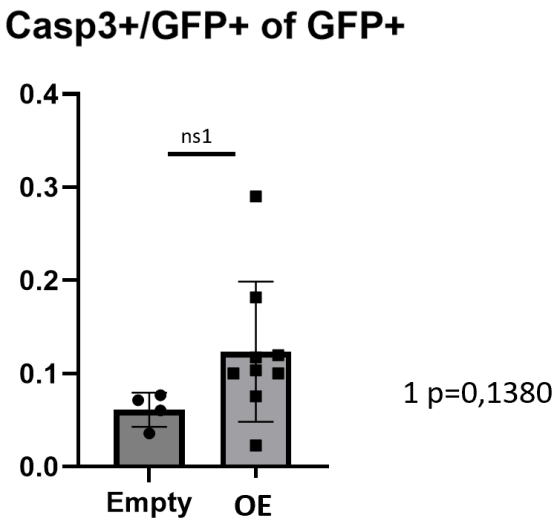

Figure 36 Results of the IUE of control and MID1 OE in the embryonic neocortex on E14.5 and staining for Casp3. Quantification all Casp3+/GFP+ cells divided through all GFP+ cells. Data are mean ± SD. OE vs. Empty ([1] p=0.1380, unpaired t-test, N_{OE}=9, N_{Empty}=4)

3.3 *In Utero* Electroporation for Generating a Conditional double KO of *MID1* and *MID2* on E15.5

Mid1^{lox}/*Mid2*^{lox} embryos were electroporated on embryonal day E13.5 to generate a cKO of the marked genes. Therefore, pCAGGS-Cre-IRES or pCAGGS-empty-IRES-GFP were used. Around 48hr later the embryos were sacrificed, and the brains prepared. After slicing and staining for neuronal markers, GFP positive cells were counted.

3.3.1 Control of Conditional Knock-out via rtPCR

The functioning of the floxed genes was proofed in breeding with conditional KO mice (See Control of Cre-Expression). Additionally, a control of cKO in electroporated cells in embryonic mice brains should be carried out. Therefore, rtPCR of GFP+ cells for gene expression of *Mid1* and *Mid2* was performed. As calibrator the cell samples collected from IUE of pCAGGS-empty-IRES-GFP were calculated and defined as RQ value of 1. RQ of cKO samples is fold change compared to the calibrator.

For *Mid1* RQ was calculated with 0,30. Due to extremely limited sample volume and number only one run could be performed. Statistical analysis was therefore not possible. A RQ value of 0,30 means a clear reduction of gene expression, yet we would expect an even smaller expression due to cKO via electroporated Cre-recombinase. Figure 51 shows results of rtPCR of *Mid1* and *Mid2*.

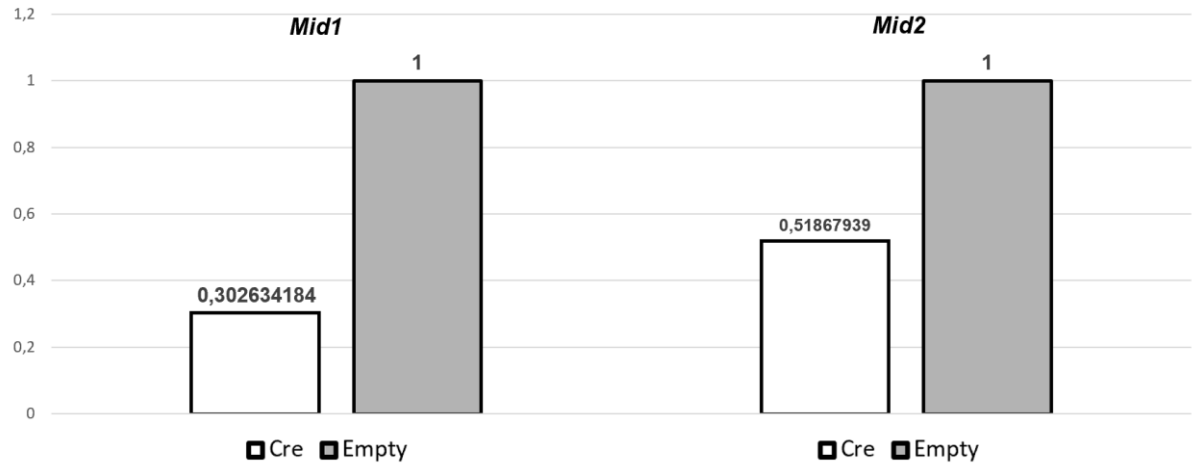

Figure 37 Results of rtPCR of Mid1 and Mid2 in GFP+ cells after IUE. RQ values are visible above the columns. A reduced expression can be seen for Mid1 and Mid2.

Possible reasons may be limits of technique of FACS and rtPCR. Also, cells could be GFP+ but could not contain pCAGGS-Cre-IRES-GFP due to co-electroporation of a GFP-plasmid. At last airborne contamination cannot be excluded either.

These arguments apply on rtPCR of *Mid2.* Here rtPCR showed a decrease of RQ in cells after electroporation of pCAGGS-Cre-IRES-GFP to 0,51. Complicating analysis of *Mid2* is the low expression in embryonic brains on E15.5, making it hard to detect differences.

Nevertheless, the rtPCR showed a decrease of gene expression for both genes of interest due to IUE of pCAGGS-Cre-IRES-GFP in embryonic mice brain cells. Whereby the existing data should probably be read as a cKD more than a cKO.

3.3.2 **Distribution and migration of neuronal progenitor cells in the *MID1/MID2* double KO neocortex**

To analyze changes in migration of neuronal progenitor cells in E15.5 embryos, staining of the cortical layers in embryonic cortex was performed. Different marker proteins were used to visualize distinct layers. The neuronal cells containing the electroporated construct were labeled with the antibody anti-GFP and visualized using the secondary antibody Alexa Fluor® 488 (Goat anti-Mouse IgG). Additionally, the cells were treated with DAPI. To quantify migration of the neuronal progenitor cells in the neocortex after electroporation, cells were counted. The cell percentage per layer in proportion to all cells was calculated.

The analysis was performed with the software ImageJ and Prism. The evaluation was always carried out identically and is therefore not further described in the following chapters.

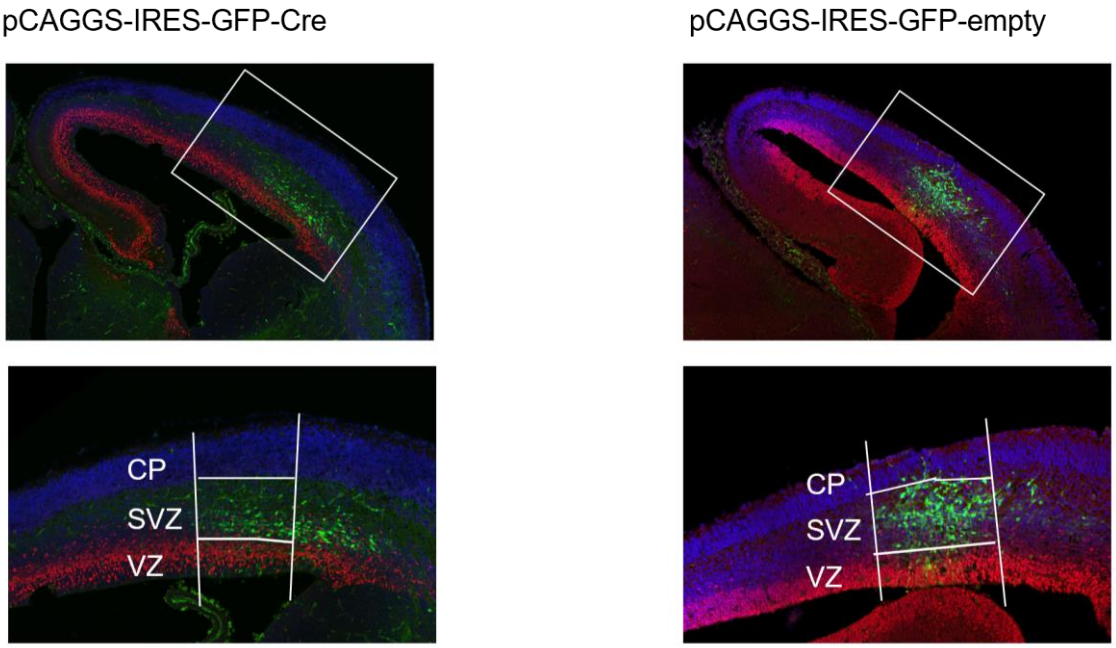

Figure 38 Exemplary representation of the cell distribution in embryonic neocortex after IUE on E15.5 48 h after electroporation. The brain on the left side is stained with Tbr2, on the right side with Pax6 for the reason of presentation. The white box shows in the upper picture indicates the zoom frame in the picture below.

At E15.5 GFP+ cells were found in all cortical layers of the cerebrum. 12,8% ± 0,06 of the GFP+ cells containing the pCAGGS-Cre-IRES-GFP lay in the VZ. In the control group 26,6 % ± 0,04 of the cells lay in VZ. This difference was statistically significant. Analyzing the SVZ/IZ the percentage share of cells containing cKO was 60,7% ± 0,09 vs. 56,9% ± 0,04 of all GFP+ cells after IUE of pCAGGS-empty-IRES-GFP. No statistically significant difference was calculated. In the CP in both groups a smaller percentage of GFP+ cells were found. After IUE of the Cre construct 26,4% ±0,05 of the cells were counted in the upper layer, in the control group the percentage was 16,4% ± 0,04. Also, in the CP the difference was statistically significant. The significant difference in the distribution of the cells could be a result of altered migration. But also altered cell proliferation might play a role.

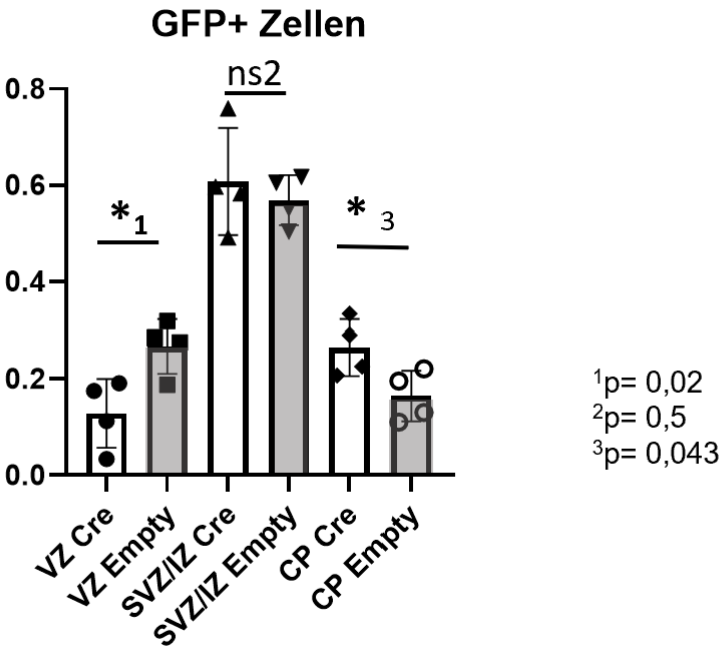

Figure 39 Results of the IUE of cKO and control construct in the embryonic neocortex on E15.5. Quantification of cells in dependence of GFP+ cells. Data are mean ± SD. (Cre vs. Empty 1 p=0.02, 2 p=0.5, 3 p=0.043, unpaired t-test, N_{Cre}=4, N_{Empty}=4).

3.3.3 Cell distribution of Pax6+ cells as a marker for radial glia cells

Staining for Pax6 was performed as a marker for VZ. For the primary antibody rabbit anti-Pax6, for the secondary antibody Alexa Fluor® 594 (Goat anti-rabbit IgG) was used. Pax6 positive cells appear red, GFP positive cells green. Figure 40 displays exemplary stainings. GFP positive cells co-stained with Pax6 were counted. The DAPI staining in blue confirms that it is a nucleus containing cell.

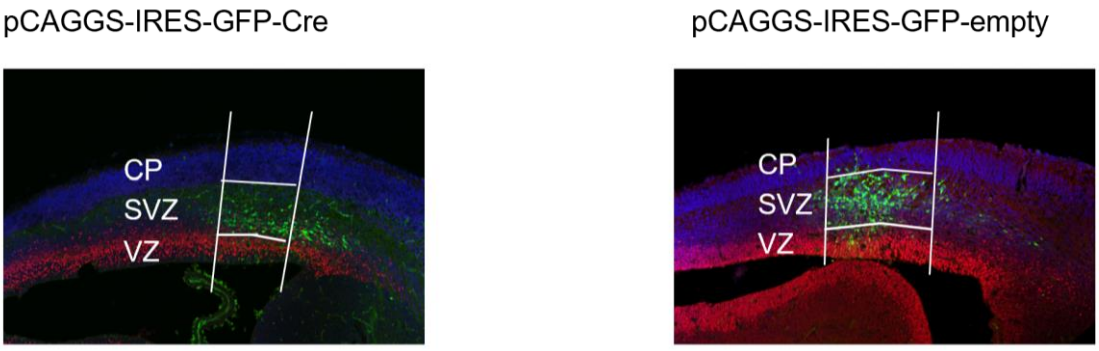

Figure 40 Exemplary representation of the cell distribution in embryonic neocortex after IUE on E15.5 48 h after electroporation. Here two brains stained with Pax6 are displayed. Green cells are GFP+, Pax6 is stained in red. On the left side the cKO construct, on the right side the control plasmid was used. Only cells lying in the region of interest of the cortex were counted.

In the brains electroporated with the cKO construct there was no significant difference in any layer compared to control. The distribution of the cells can be seen in Figure 41. In the intervention group 82,9% ± 0,17 of all GFP+ cells in the VZ were Pax6+, in the control group also 82,9% ± 0,14 were counted. In the SVZ/IZ also a lower amount of Pax6+ cells were found. The percentages were almost identical with 17,0% ± 0,17 (Cre) vs. 17,1% ± 0,14 (Empty) in the two groups.

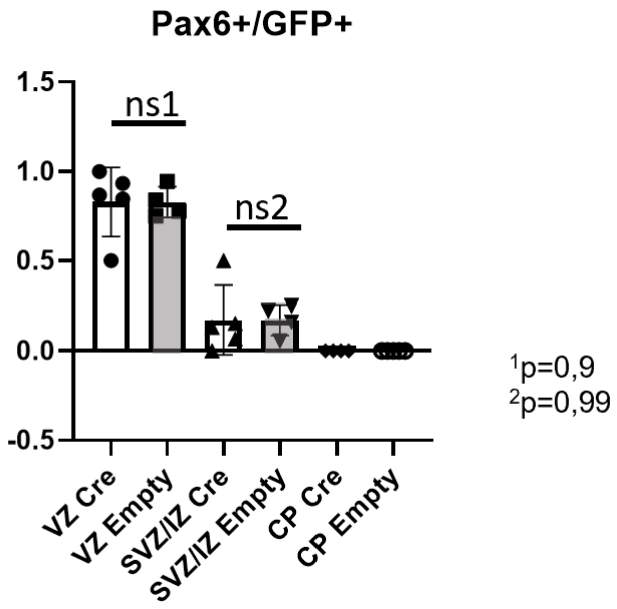

Figure 41 Results of the IUE of cKO and control construct in the embryonic neocortex on E15.5. Quantification of cells in dependence of GFP+ cells and layer specific. Data are mean ± SD. Cre vs. Empty 1 p=0.9, 2 p=0.99, CP not evaluable, unpaired t-test, N_{Cre}=4, N_{Empty}=4).

Analysing the total number of Pax6+ cells in the selected areas of the cortex, no significant difference could be shown either. 20,8% ± 0,1of GFP+ cells after IUE of pCAGGS-Cre-IRES-GFP were co-stained for Pax6 vs. 25,2% ± 0,03 in the control group. This is in line with the layer-specific analysis as Pax6 is a marker for RGCs in the VZ.

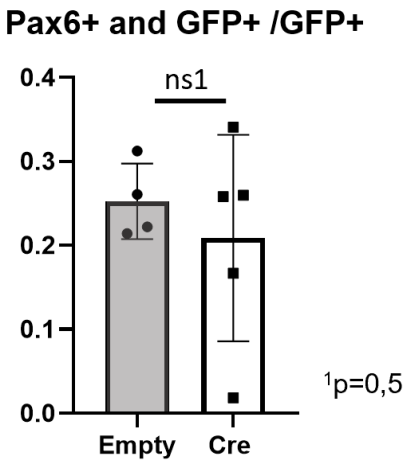

Figure 42 Results of the IUE of cKO and control construct in the embryonic neocortex on E15.5. Quantification of the total number of Pax6+ cells in dependence of GFP+ cells. Data are mean ± SD. (Cre vs. Empty 1 p=0.5, unpaired t-test, N_{Cre}=5, N_{Empty}=4).

3.3.4 Cell distribution of Tbr2+ cells as a marker for intermediate progenitor cells

Tbr2 is expressed by iPCs that lie in the SVZ. Therefore, it can be used as a marker for the SVZ. For the primary antibody chicken anti-Tbr2, for the secondary antibody Alexa Fluor® 594 (Goat anti-chicken IgG) was used. In figure 43 two staining examples are shown.

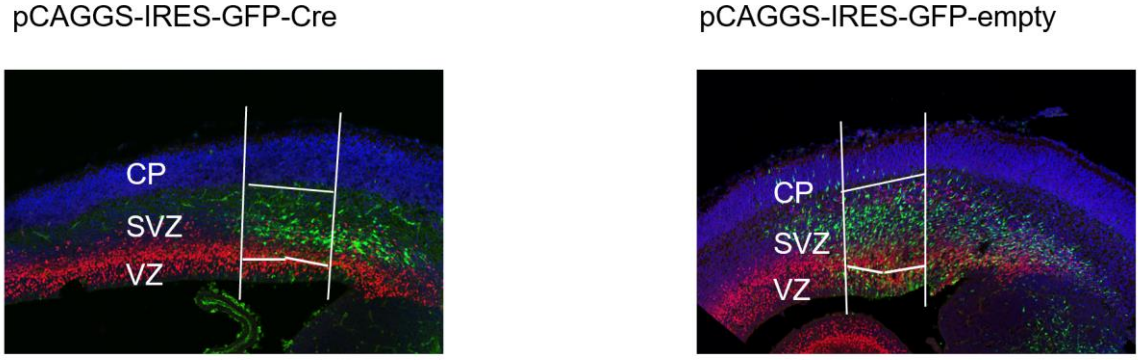

Figure 43 Exemplary representation of the cell distribution in embryonic neocortex after IUE on E15.5 48 h after electroporation. Here two brains stained with Tbr2 are displayed. Green cells are GFP+, Tbr2 is stained in red. On the left side the cKO construct, on the right side the control plasmid was used. Only cells lying in the region of interest of the cortex were counted.

At E15.5 GFP+ cells the Tbr2+ cells were counted in each layer. 24,5% ± 0,14 of the Tbr2+/GFP+ cells containing the pCAGGS-Cre-IRES-GFP lay in the VZ. In the control group 27,1% ± 0,13 of the cells lay in VZ. There was no significant difference. Analyzing the SVZ/IZ the percentage share of cells containing cKO

was 75,5% ± 0,14 (Cre) vs. 72,3% ± 0,13 (Empty). No statistically significant difference was calculated. In the CP no cells were detected.

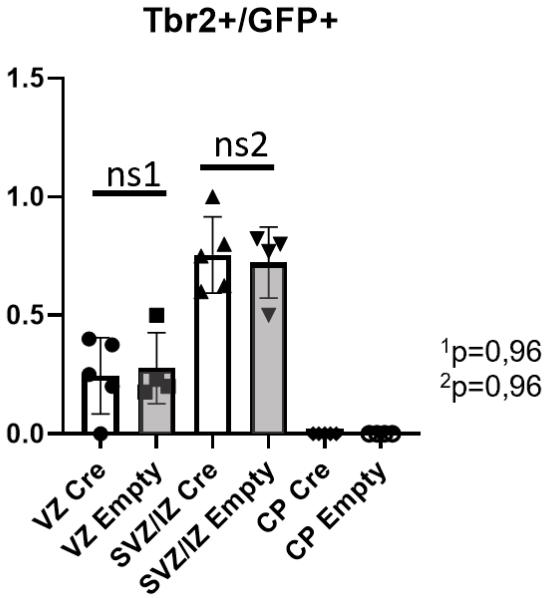

Figure 44 Results of the IUE of cKO and control construct in the embryonic neocortex on E15.5 and staining for Tbr2. Quantification of cells in dependence of GFP+ cells and layer specific. Data are mean ± SD. (Cre vs. Empty 1 p=0.96, 2 p=0.96, CP not evaluable, Mann-Whitney test, N_{Cre}=4, N_{Empty}=4).

Analysis of the total number of Tbr2+ cells in the selected areas of the cortex, showed no significant difference either. 33% ± 0,15 of GFP+ cells after IUE of pCAGGS-Cre-IRES-GFP were Tbr2+, in the control group 46,8% ± 0,14.

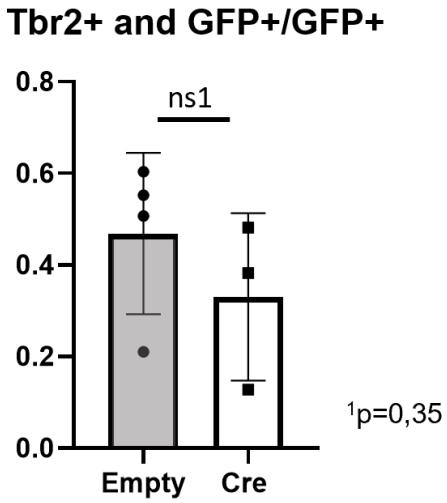

Figure 45 Results of the IUE of cKO and control construct in the embryonic neocortex on E15.5 and staining for Tbr2. Quantification of the total number of Tbr2+ cells in dependence of GFP+ cells. Data are mean ± SD. (Cre vs. Empty 1 p=0.35, unpaired t-test, N_{Cre}=4, N_{Empty}=3).

3.3.5 Cell distribution of Satb2+ cells as a marker for CP

Satb2 (Special AT-rich sequence-binding protein 2) is a TF expressed in immature, newborn neurons (85). For the primary antibody rabbit anti-Satb2, for the secondary antibody Alexa Fluor® 594 (Goat anti-rabbit IgG) was used. In figure 46 two staining examples are shown. The cells shown in red, are positive for Satb2. The green cells are GFP positive and contain the electroporated construct.

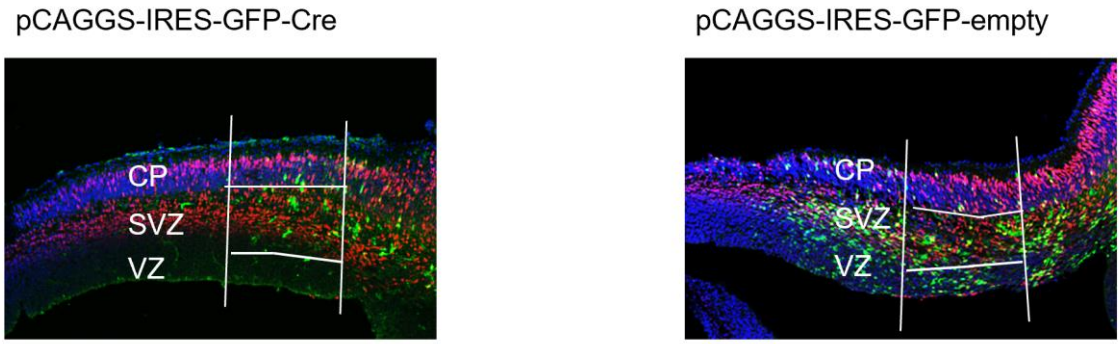

Figure 46 Exemplary representation of the cell distribution in embryonic neocortex after IUE on E15.5 48 h after electroporation. Here two brains stained with Satb2 are displayed. Green cells are GFP+, Satb2 is stained in red. On the left side the cKO construct, on the right side the control plasmid was used. Only cells lying in the region of interest of the cortex were counted.

In the brains electroporated with the cKO construct there was no significant difference in any layer compared to control. The distribution of the cells can be seen in figure 47. In the both groups no relevant number of the Satb2+ cells were found in the VZ. 72,3% ± 0,21 of the cells after electroporation of the Cre-plasmid were counted in the SVZ/IZ, compared to 83,8% ± 0,09 in the control group. At E15.5 a small amount of GFP+ cells were already differentiated into neurons and could be found in the CP. This applied to 21,9% ± 0,23 of the cKO containing cells and 14,1% ± 0,06 in the control group.

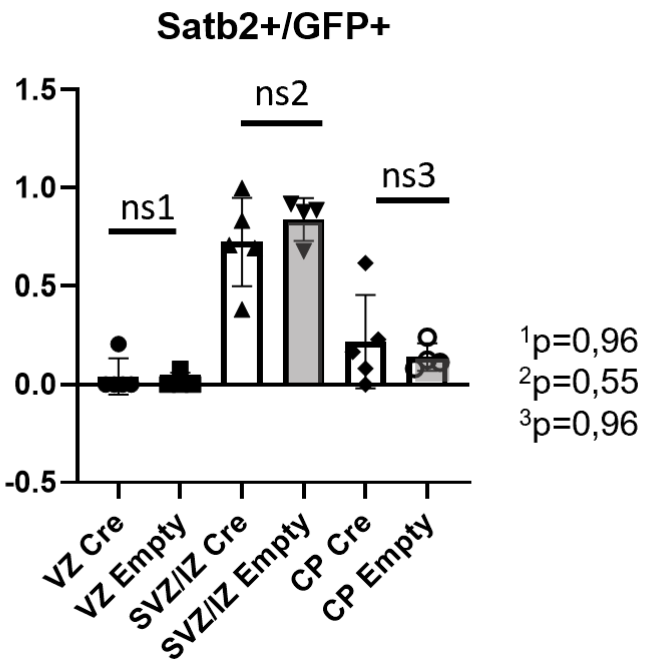

Figure 47 Results of the IUE of cKO and control construct in the embryonic neocortex on E15.5 and staining for Satb2. Quantification of cells in dependence of GFP+ cells and layer specific. Data are mean ± SD. (Cre vs. Empty 1 p=0.99, 2 p=0.55, 3 p=0.96, Mann-Whitney test, N_{Cre}=4, N_{Empty}=4).

Analysis of the total number of Satb2+ cells in the selected areas of the cortex, showed no significant difference either. 27,8% ± 0,20 of GFP+ cells after IUE of pCAGGS-Cre-IRES-GFP were Satb2+, in the control group 43,0% ± 0,14.

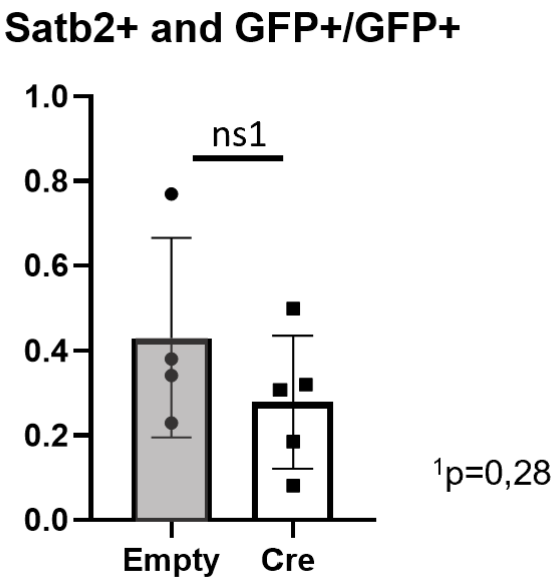

Figure 48 Results of the IUE of cKO and control construct in the embryonic neocortex on E15.5 and staining for Satb2. Quantification of the total number of Satb2+ cells in dependence of GFP+ cells. Data are mean ± SD. (Cre vs. Empty 1 p=0.35, unpaired t-test, N_{Cre}=5, N_{Empty}=4).

3.3.6 **Proliferation Analysis by Ki67 staining**

As described, Ki67 is a common proliferating cell marker. For the primary antibody rat anti-Ki67, for the secondary antibody Alexa Fluor® 594 (Goat anti-rat IgG) was used. In figure 49 two exemplary brain slices after staining are depicted. The cells shown in red, are positive for Ki67. The green cells are GFP positive and contain the electroporated construct.

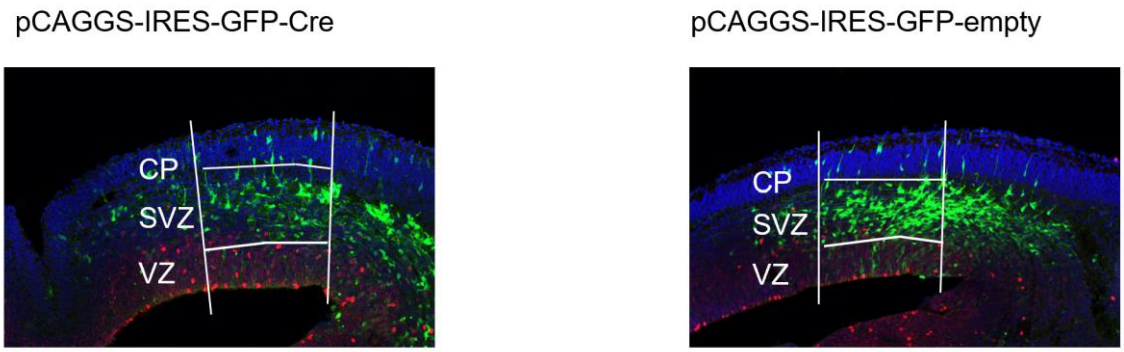

Figure 49 Exemplary representation of the cell distribution in embryonic neocortex after IUE on E15.5 48 h after electroporation. Here two brains stained with Ki67 are displayed. Green cells are GFP+, Ki67 is stained in red. On the left side the cKO construct, on the right side the control plasmid was used. Only cells lying in the region of interest of the cortex were counted.

The proportionate distribution of Ki67+ and GFP+ cells after IUE of the Cre-plasmid in *Mid1*^{lox}/*Mid2*^{lox} mice showed a high heterogeneity. In the VZ after IUE of pCAGGS-Cre-IRES-GFP 16,2% ± 0,17 of the co-stained cells could be detected in the VZ, while in the control group 75,4% ± 0,15 of the cells positive for proliferation marker were found in the VZ. The difference was statistically significant. In SVZ/IZ 66,2% ± 0,34 of the cKO-cells, while in the brains electroporated with pCAGGS-empty-IRES-GFP 24,5% ± 0,15 of KI67+ cells were counted. In the CP 17,5% ± 0,2 (Cre) vs. 0% ± 0 of the GFP+ cells were positive for Ki67, no significant difference was seen. In summary, the cKO leads to a lower proliferation rate in the VZ, but not in the SVZ/IZ and CP compared to control.

It should be noted that the Ki67 staining in our experiment showed typical cells with very bright signals, but they seemed to be less than in other publications (117, 118).

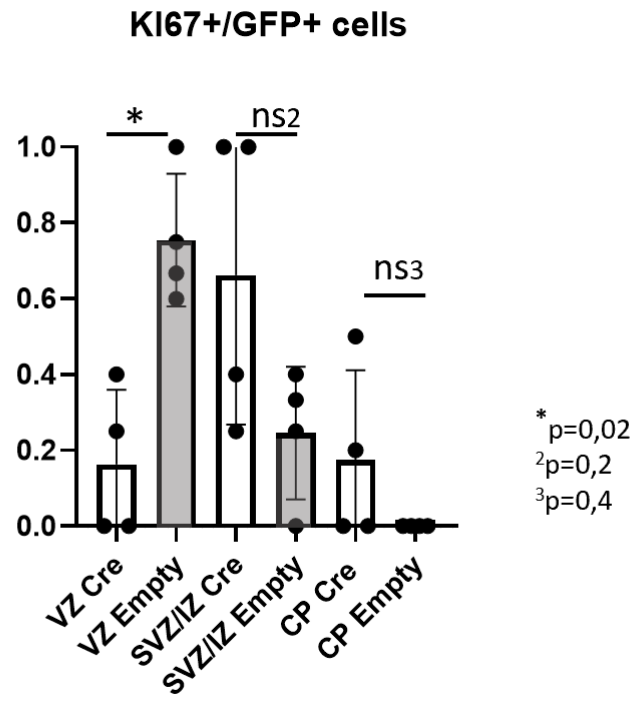

Figure 50 Results of the IUE of cKO and control construct in the embryonic neocortex on E15.5. Quantification of cells in dependence of GFP+ cells. Data are mean ± SD. (Cre vs. Empty 1 p=0,02, 2 p=0,2, 3 p=0,04, unpaired t-test, N_{Cre}=4, N_{Empty}=4).

3.3.7 **Apoptosis Analysis by Casp3 staining**

Caspase 3 (Casp3) is a common marker to show apoptosis. Due to limited effects of Cre-electroporation in the mice brains an effect via apoptosis should be examined. It is known, that Cre induces cell death. The portion of apoptotic cells depends on the number of targeted genes. As the *Mid1*^{lox}/*Mid2*^{lox} mice have two potential target genes, an apoptotic effect would be possible.

The analysis of Casp3+ cells was identical to analysis of Ki67, staining was performed with Rabbit-Anti-cCasp3, for the secondary antibody Alexa Fluor® 594 (Goat anti-rabbit IgG) was used.

Immunofluorescent staining with Casp3, GFP and DAPI was performed. Brains with an appropriate distribution of GFP-positive cells were chosen. Staining was performed with Rabbit-Anti-cCasp3, for the secondary antibody Alexa Fluor® 594 (Goat anti-rabbit IgG) was used.

Caspase 3 is cleaved and therefore activated, the antibody used thus detects only the active form of the marker protein Casp3 (121). Figure 51 shows an exemplary brain of a *Mid1*^{lox}/*Mid2*^{lox} E15.5 embryo after *in utero* electroporation of pCAGGS-Cre-IRES-GFP and pCAGGS-empty-IRES-GFP.

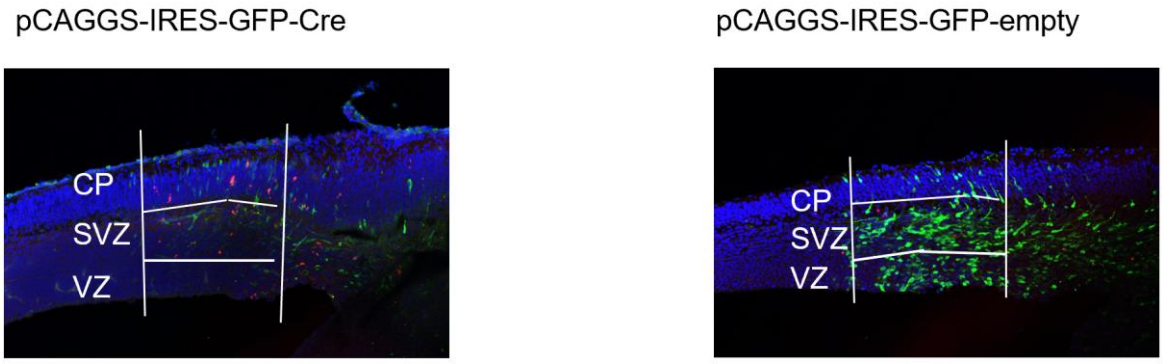

Figure 51 Exemplary representation of the cell distribution in embryonic neocortex after IUE on E15.5 48 h after electroporation. Here two brains stained with cCasp3 are displayed. Green cells are GFP+, cCasp3 is stained in red. On the left side the cKO construct, on the right side the control plasmid was used. Only cells lying in the region of interest of the cortex were counted.

Statistical analysis showed very limited cell numbers in both groups. Figure 52 shows the percentage of GFP+/Casp3+ of GFP+ cells and their distribution in different layers. In none of the layers a significant difference between electroporation of Cre or control plasmid could be seen. In the VZ 5,5% ± 0,07 of Casp3+ cells containing the Cre-plasmid were counted, 0,0% ± 0 were found in the control group. In the SVZ/IZ the ratio lay at 44,4% ± 0,31 (Cre) vs. 50,0%

± 0,5 (Empty). 50,0% ± 0,36 of the cells after electroporation of pCAGGS-Cre-IRES-GFP that were stained with Casp3 lay in the CP, compared to 0,0% ± 0 containing pCAGGS-empty-IRES-GFP. Due to a high standard deviation (SD) no significant difference was seen.

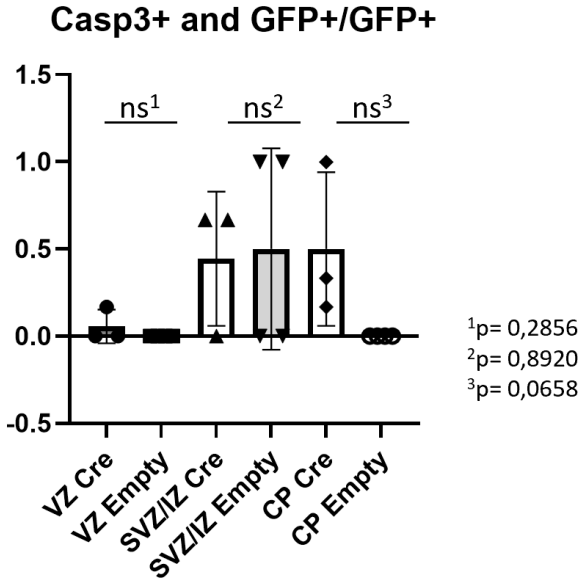

Figure 52 Results of the IUE of cKO and control construct in the embryonic neocortex on E15.5 and staining for Satb2. Quantification of cells in dependence of GFP+ cells and layer specific. Data are mean ± SD. (Cre vs. Empty 1 p=0.99, 2 p=0.55, 3 p=0.96, Mann-Whitney test, N_{Cre}=3, N_{Empty}=4).

Analysis of the total number of Casp3+ cells a significant difference could be seen. Of all GFP+ cells, 10,5% ± 0,03 of the cells after IUE of pCAGGS-Cre-IRES-GFP were Casp3+, in the control group 1,0% ± 0,01. The difference between significance in layer specific and total number analysis may be due to the limited cell numbers of Casp3+ cells. Figure 53 shows the results of the second analysis.

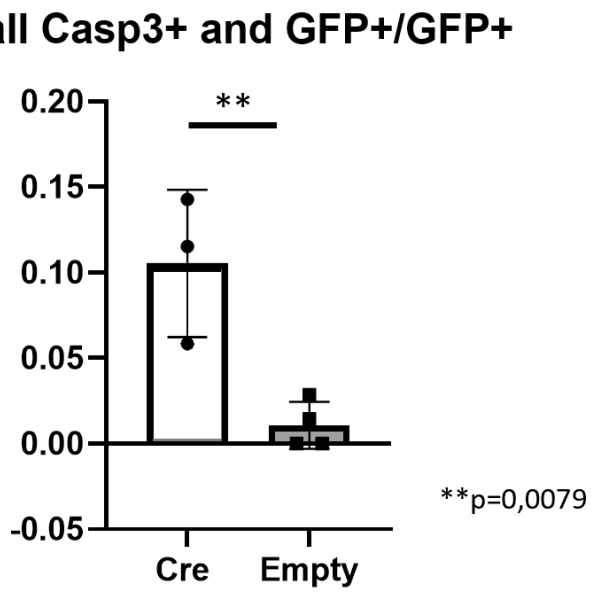

Figure 53 Results of the IUE of cKO and control construct in the embryonic neocortex on E15.5 and staining for Satb2. Quantification of the total number of Casp3+ cells in dependence of GFP+ cells. Data are mean ± SD. (Cre vs. Empty p=0.0079, unpaired t-test, N_{Cre}=3, N_{Empty}=4).

3.4 Generation of a Knock-Down Construct of *Pax6* as preparatory work for future experiments

When creating OE or KO of Mid1 in IUE to research effects in neurogenesis on the theory of interaction between Pax6 and Mid1, rescuing experiments with induced expression or knockdown of Pax6 could help understanding this theory. To prepare for future experiments KD constructs of Pax6 were generated with shRNA constructs. These were established from oligonucleotides (See Design of the Oligonucleotides). The double-stranded oligonucleotides of shRNA 1 to 6 for mouse *Pax6* were ligated with the linearized plasmid pSUPERIOR.puro.

Excerpt from Ensembl Pax6 cDNA

5´ACTTCCAGCGAAAGCCCGCGTCGGAGGGCGACGGTCCGCGCGAGCCACAACAGCGCGGAT
CTTCAGGCAGGCGGCTGGCTCTGCACCAGCGCAAGTGCGGCTGGAGCTCTCGGAGAGCAG
CTAGGCTGCAGGGCGCCCCCGCAAACCGCAGCTCTCAGCTTCAGCGCCTCCAAAAGCTCG
CGGTCAGCGCAAAGGGACGTAGAGGCTCCTCCGTGCCCCAGGCCGCGGAGAGCAGCCGCC
GGCGATGCTTTTGTCCAGCCCGGGCCGAGCCAGCGCGCAAAGAGCGCCCAACCAGCCGAC
TCTCCGCGCCGCCTCCCGCCAGCCCGCGCTCCGGCTTTGTGCAAGATTCTCCCGGCACAG
AACTGCCCGCAGCACTCGAGCACCAAAGGGTCATCGCGCCCTCCGCCAGCCGGAGCCGTC
TGGATGGGCACCACGGCCGTGCGCCGGAGGCCACGAGGGACCCAGAGCGAGAGCGGGCGG
TGAAAGAAGCCACTAGGCCGAGGCGGTCGGATGCGCTCTGCGAGGGAGCTCCGAGCCGAT
CGCAAGGACTGCCAGCTTCCATCCACCCCCCAGGGCCCTCGCCTCCAGCCTCAGCCGAGC
GCTGAGCTCAGATTTGGAAACAAACGCCCTAGCTCTCCCGGCTTCCCACAACTCTATCTT
GCGAAAGTTGGTGTGTTCCCTGTCCTGTGGACTCCCACCTCCAGCTCTTGGCAGAAGACT
TTAACCAAGGGCGGTGAGCAGATGTGTGAGATCTTCTATTCTAGAAGTGGACGTATATCC
CAGTTCTCAGAGCCCCGTATTCGAGCCCCGTGGGATCCGGAGGCTGCCAACCAGCTCCAG
CATGCAGAACAGTCACAGCGGAGTGAATCAGCTTGGTGGTGTCTTTGTCAACGGGCGGCC
ACTGCCGGACTCCACCCGGCAGAAGATCGTAGAGCTAGCTCACAGCGGGGCCCGGCCGTG
CGACATTTCCCGAATTCTGCAGGTATCCAACGGTTGTGTGAGTAAAATTCTGGGCAGGTA

Figure 54 Excerpt from Pax6 cDNA sequence. Positioning of the shRNAs 1 to 6 are marked in yellow, due to overlapping of the sequences only two regions are marked.

For linearization, the vector was digested with BGIII and HindIII. Agarose gel electrophoresis was used to check if the digestion worked and to purify the vector afterwards. Figure 19 shows the result of the agarose gel electrophoresis. The first sample (P1) is the linearized vector p.Superior.puro with a length of 4354 bp. As control, C1 shows the plasmid digested only with the restriction enzyme BglII, in C2 only HindIII was used and in C3 no restriction enzymes were added. As BglII and HindIII are only 6 bp apart, the size of C1 and C2 are very similar to P1. As expected, the undigested vector shows a blurred signal without a clear band.

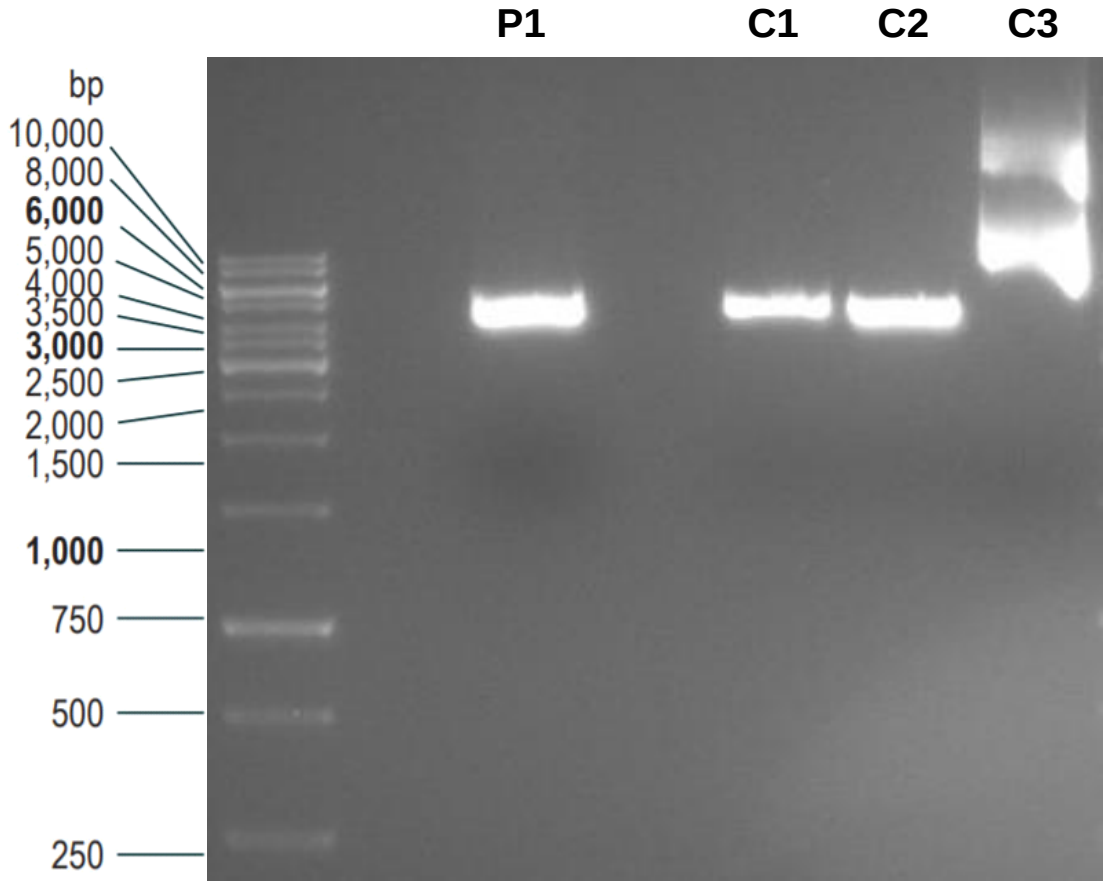

Figure 55 Agarose gel after restriction digestion of pSUPERIOR.puro. The restriction digestion was performed with BglII and HindIII. P1 shows the linearized and cut plasmid. C1 shows the plasmid pSUPERIOR.puro cut only with BglII, C2 it was only cut with HindIII and C3 is the circular, uncut plasmid pSUPERIOR.puro. P1: The sample has a size of around 4000 bp. C1 and C2: The samples show a similar size around 4000 bp. C3: The uncut sample shows no clear band.

The correct sample P1 was purified, ligated with *Pax6* shRNA and then multiplied by transformation into *E. coli* bacteria. Five colonies per shRNA construct were picked from the agar plates. After plasmid isolation and purification via Minipreparation, the samples were checked for the shRNA sequences using either H1_Primer or Bluescript primer. The sequencing results were then checked for the right sequence using the program BioEdit (Fig. 21). The program displays a match between sample sequence, here sample 1C, and reference sequence *Pax6* shRNA1 as a dot for the corresponding base. Figure 21 shows a complete match of the sample with the respective reference sequence.

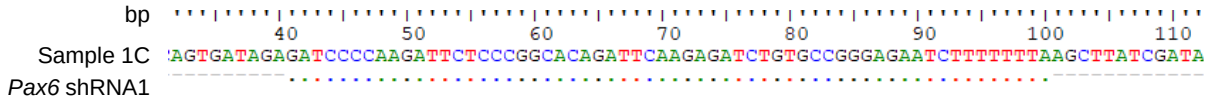

Figure 56: Alignment of the sample sequence for sample 1C with the reference sequences Pax6 shRNA1. The correspondence of the bases is indicated by a dot; thus, the sequence is error-free. The scale displays the base number in the sample.

Three sequenced plasmids with constructs from *Pax6* shRNA 1, 3 and 4 were used for Maxipreparation. After Maxipreparation further experiments for example IUE can be performed with the plasmids p.Superior.puro-Pax6 but were not part of this work.

4 Discussion

4.1 The potential of different mouse strains in the exploration of the function of *Mid1* and *Mid2*

Mid1 and *Mid2* are two homologous genes both encoding E3-ubiquitin ligase (56, 122). Both genes have different and overlapping functions in the regulation of cell growth and division.

To explore the function of Mid1 and Mid2, mouse models are a common strategy. There are several different strains of mice and different approaches that can be used in research, each with its own advantages and disadvantages.

Former experiments displayed that *Mid1* KO mice do not show typical signs of midline defects unlike patients with OS (123). More detailed analysis of the C. callosum in these mice showed, that axon length and branch number increased in cortical neurons, while cell proliferation, neuronal migration and dendritic arborization were stable (22).

One of the possible explanations of the inadequate *Mid1* KO model is the role of *Mid2* in vertebrate species, as *Mid1* and *Mid2* have redundant functions and could compensate for the loss of function (59, 124). A recent literature search gave no evidence of an existing *Mid2* KO mouse model.

Therefore, the question arises what phenotype a KO of both genes would generate. In order to perform different experiments with a conditional or constitutive KO of the sister genes *Mid1* and *Mid2*, the breeding of the genetically modified mouse strain *Mid1*^{lox}/*Mid2*^{lox} was essential. As expected, the genotyping showed stable expression of the genes flanked with loxP sites (see Confirmation of Breeding Results for Mid1^{lox}/Mid2^{lox}). It allows to investigate tissue-specific effects of gene knockout, as different promoters can be used to drive Cre recombinase expression in different tissues or organs (105).

For this work, two different approaches will be discussed. One attempt was to breed a homozygous or hemizygous single conditional KO line for *Mid1* and *Mid2* to provide the basis for further experiments (Confirmation of Breeding). The probability of crossing over between a wildtype *Mid1* or *Mid2* and their corresponding floxed genes in hemizygous mice could be calculated (125). In our experiment only hemizygous single KO females could be bread. This may be caused by limited animal number, but also recombination frequency is known to

be highly variable as summarized by Dumont (126). However, the technique turned out to be functioning and further experiments to establish two distinct *Mid1*^{lox} and *Mid2*^{lox} mouse should be performed.

The other attempt was to generate *Mid1*^{cKO}/*Mid2* ^{cKO}. Therefore, Deleter-Cre males were mated with *Mid1*^{lox}/*Mid2*^{lox} homozygous females. In Deleter-Cre mice all tissues express the Cre recombinase, even germ cells. Schwenk and Baron stated that the Cre expression is X-linked (104). This led to hemizygous cKO females. Genotyping (See Control of Cre-expression and functionality in Mid1lox/Mid2lox mice via breeding with Deleter-Cre mice) showed that the cKO is possible. This proves that the established *Mid1*^{lox}/*Mid2*^{lox} mouse strain is capable to generate distinct cKO lines when bred with Cre expressing mouse strains (127).

In conclusion, the basis for further experiments was provided in this work.

4.2 The MID1 Ubiquitin-Protein Ligase in Neuronal Migration and Proliferation

The E3-ubiquitin ligase MID1 is known to play a role in neuronal development. In our experiment, we overexpressed MID1 in neuronal progenitor cells via IUE. We also generated a cKO of *MID1* and *MID2* via IUE. This will be discussed separately.

During neuronal development, neurons migrate from their place of origin to their destination in the brain. This process requires a complex, balanced interplay of cellular and molecular mechanisms, including cytoskeletal rearrangements, adhesion, and signaling pathways to control neural progenitor maintenance and neuron production. However, the regulatory mechanisms of neural progenitor homeostasis are yet to be fully understood. The MID1 protein has been shown to play a key role in regulating the stability of proteins involved in cytoskeletal dynamics, cell adhesion and signaling and is therefore an interesting target in neural developmental research (22).

The discussion is complicated by the fact that only some of the existing research is specific to neuronal systems. In our experiment we saw that the OE of Mid1 in the embryonic mouse brain leads to a higher proportion of cells in the SVZ/IZ.

This effect could be due to faster migration, premature differentiation or altered apoptosis rate.

Staining with Ki67, a proliferation marker, showed an increased expression in VZ after OE, while our staining seems to show not all proliferating cells, but only cells during mitosis. In the neonatal cortex mitosis occurs in different cell types. RGCs divide in the VZ, while the cell division of BPs happens in the SVZ/IZ. Mitosis of RGCs in the VZ can occur in different modes. Through symmetric proliferation RGCs form a pool of these progenitor cells in the VZ. When RGCs undergo asymmetric differentiative cell division they could become postmitotic neurons, BPs or apical intermediate progenitor cells (63, 84). In our experiment we cannot distinguish between the different modes, a higher amount of Ki67+ cells in the VZ could therefore be associated with more asymmetric division. The postmitotic cells could then migrate into the SVZ and explain the higher cell proportion in the SVZ after OE of MID1. In future experiments a specific staining for mitotic cells in comparison to a different Ki67 antibody could confirm the assumption.

Checking for apoptosis via Casp3 staining showed no significant difference between the two groups.

In vitro experiments of MID1 OE in HeLa cells showed that OE leads to faster migration, while proliferation was unchanged. Willam even speaks of a “overdriven migration behavior”. In a KD model of MID1 with around 65% effectivity in HeLa cells, no significant effect on migration and proliferation could be seen (93).

Looking at possible underlying mechanisms, the effect of MID1 in cell cycle control appears complex. A pathway well researched in context of MID1 is ubiquitination of PP2Ac and thereafter regulating levels of PP2Ac in the cell (47). PP2Ac is described to be a central catalysator of MID1 cellular function, regulating mTORC1 signaling pathway and Shh network (128). PP2Ac has multiple roles and target points in the cell cycle and distinct effects depending on the phase during cell cycle (summarized in (129, 130)). Yet, Tang et al. saw no changes in cell cycle analysis when PP2Ac was overexpressed (131). The influence on mTOR pathway is a key regulatory mechanism as mTOR is highly activated in proliferating RGCs and a deletion of mTOR leads to decreased proliferation and subsequently defects in brain structure (132, 133).

Overactivation of mTOR has been linked to promoting proliferation, differentiation and migration in neural progenitor cells and also accelerating their cell cycle exit (134-136).

A conclusive finding was, that in neuronal cells from WT mice after IUE overexpression of Mid1 led to a reduction of endogenous PP2Ac to around 50% (22). For Lu et al. the effect of MID1 OE on PP2Ac was used as a proof of principle, while the aim of their work was focused on MID1 KD. In MID1 KD through Mid1 RNAi in hippocampal and cortical cultured neurons they saw promoted axon growth and branching, but no effect on neuronal precursor-cell proliferation. This could be confirmed through IUE of Mid1 RNAi construct leading to an in vivo KD and analysis of cultured neurons. No effect on neuronal precursor-cell proliferation or neuronal migration on P3 was observed. This might support the thesis, that our findings from Ki67-staining are due tot analysis of mitosis and not proliferation.

While arguing with the antagonistic experiment to describe MID1 OE phenotype is limited, Lu et al. gained important evidence that MID1 KD and PP2Ac OE show similar phenotypes. This further supports argumentation based on PP2Ac mediated effects on cell cycle. Yet, while PP2Ac is a central player in cell regulation, there is limited evidence on migration effects, but it is known that lower levels of PP2Ac enhance cell proliferation in hemangioma cells, while they suppress it in osteosarcoma cells (137-139).

One hypothesis partly connected to the previous discussion is that effects on cell proliferation or migration are mediated by regulation of cytoskeleton (22). But also other signaling pathways may play a role like Wnt signaling (29) and especially important in brain development Pax6 (51). Pax6 will be discussed separately. Further research is needed to understand the effect of MID1 in these pathways in neuronal development.

In conclusion – using a PP2Ac mediated effect as an argument – it does not resolve conclusively whether the changed cell distribution after Mid1 OE in embryonic mice brain is due to proliferation or migration changes. Yet it is interesting to note that in the experiments performed in our laboratory, OE had a more pronounced effect than the KD of Mid1.

Further research into the molecular mechanisms underlying the function of MID1 could lead to new insights into the regulation of neuronal development and

potential therapeutic targets for the treatment of developmental disorders. Therefore, different staining markers and longer experimental intervals could be used. Especially the FACS sorting of GFP positive cells after IUE followed by transcriptome analysis could give interesting insights into gene expression changes in vivo.

4.3 MID1 and MID2 Ubiquitin-Protein Ligases in Neuronal Migration and Proliferation

MID1 and MID2 can heterodimerize and are known to have common binding partners, like the alpha4 subunit of PP2Ac and Astrin (37, 60, 61). It is therefore often discussed whether and to what extend defects of one protein can be compensated by the other (60).

Mid1 KD or KO experiments in the developing mouse brain caused impairments in brain development but could not explain midline defects of OS patients (21, 22, 93).

One important difference between human and mouse is the location of *MID1* gene. In humans the gene is located close to the pseudoautosomal region. In mice the gene overarches the pseudoautosomal boundary (140). This region is responsible during male meiosis for X and Y chromosomes to pair and recombine (141). *MID2* is not located in this region in both species. Genes located in the pseudoautosomal region are affected by higher rate of recombination than genome average and increased mutations (142). One hypothesis is that the role of Mid1 is therefore distinct between mouse and human. A logical explanation could be a better capability of Mid2 to compensate for Mid1 defects in mice than in humans. Yet, this is only a hypothesis.

In our experiment we created a cell specific cKO of Mid1 and Mid2, yet qPCR showed only reduced expression of these genes. This may be due to cells being transfected only with the GFP-plasmid that was co-electroporated. Also, we cannot proof, that Cre was active in all GFP+ cells. This might lead to a dilution of the KD effect. After IUE of Cre less cells were found in the VZ and more in the CP, proliferation analysis showed a lower rate of Ki67+ cells in Cre+ cells, while in our staining probably only the mitotic cells were stained (See The MID1 Ubiquitin-Protein Ligase in Neuronal Migration and Proliferation). Also, a higher apoptosis rate could be seen.

The increase in apoptosis could be caused by the reduced expression of Mid1/Mid2 in the knockout cells. In HeLa cells, the interaction of Mid1 and Mid2 with Astrin, a microtubule-associated protein was analyzed. The reduction of Mid1 or Mid2 levels caused small defects in mitosis but clear defects in cytokinesis. Interestingly, they showed that Mid2 regulates Astrin stabilization through ubiquitination. Cells lacking Mid2 showed increased stabilization of astrin during cell division, causing cytokinetic arrest and finally generating binucleate cells entering apoptosis (61).

Therefore, it might be interesting to create Mid2 single KO or KD experiments with IUE to answer the question whether the higher apoptosis rate could be induced by the lack of Mid2.

However Cre expression itself can also induce apoptosis (143). A qualitative evaluation of the cell configuration and morphology showed an atypical form in VZ, being supported by higher Casp3+ rate after IUE. To verify that changes in apoptosis are caused by Mid1/Mid2 depletion, it would be necessary to establish a second control group. Additionally, to *Mid1*^{lox}/*Mid2*^{lox} mice electroporated with a control GFP-plasmid, C57BL/6N wildtype mice should be electroporated with the Cre-plasmid. Yet, the meaningfulness of this experiment is also limited as it has been shown that Cre-mediated apoptosis increases with the level of floxed target genes (143).

While Cre-mediated apoptosis could describe the reduced cell number in VZ. The higher cell number in the CP might be due to statistical analysis, as all GFP+ cells were defined as 100% and the distribution to the layers was calculated proportionately. Less percentage in the VZ, means a higher percentage in the SVZ/IZ and/or CP. Yet, a migration, differentiation or proliferation defect still might be relevant.

It is interesting that KO of both genes seems to create a similar distribution phenotype as OE. However, the specific stainings show different results. While in the OE more Pax6 and Tbr2 positive cells were seen, no effect was identified in the KO experiment. Opposing results were described in Ki67-staining, OE led to more cells, KO led to less Ki67+ cells. Therefore, the differences in the distribution pattern of the cells appear to be of different pathomechanism.

Astonishing is the comparison between our Mid1/Mid2 double KO and experiments performed by Willam that created a single Mid1 KD in IUE via

shRNA constructs. This Mid1 KD showed no effect on cell distribution after 48h, while only the cell distribution was analyzed (93). Interestingly, the simultaneous KO of Mid2 leads to a defect in the distribution of cells. Apoptosis and cell division cannot be compared as the markers were not stained in the single KD experiment. Also, shRNA led to a KD, therefore a residual function of Mid1 might be responsible for the overserved phenotype.

But the following experiment speaks in favor of a compensation function of Mid2. In cytotoxic T-cells an upregulation of MID2 was observed after MID1 KD (60).

At E14.5 Mid2 is expressed ubiquitously in the mouse embryo, although higher levels can be found in the heart. While the expression level is not as high as Mid1, which is highly expressed in the developing cortex of different species, missing upregulation of Mid2 could explain migration or proliferation defects in the cKO in *Mid1*^{lox}/*Mid2*^{lox} mice (22, 34, 60, 128).

This supports evidence that Mid1 might play a role in RGC development, but loss-of-function could be rescued by Mid2. For future experiments with the mouse line *Mid1*^{lox}/*Mid2*^{lox}, a ubiquitous cKO of both target genes should be generated to test this hypothesis.

Looking at the effect on migration or proliferation in our cKO experiment, there seems to be a higher apoptosis, less proliferation but more migration pattern.

Interestingly MID1 OE lead to a similar cellular distribution pattern in the cortical zones as the Mid1/Mid2 cKO.

As MID1 KD experiments before didn´t show significant effects on migration and proliferation, causal pathways have not yet been described. Our results suggest, that MID2 may rescue the MID1 KD. However, future experiments have to be carried out to prove this hypothesis.

As described above PP2Ac is a central player in cell regulation and an important binding partner of MID1 and MID2 (139). Lower levels of MID1 and MID2 could lead to higher PP2Ac levels in the cell (37, 39). It is known, that lower levels of PP2Ac enhance cell proliferation in hemangioma cells, while they suppress it in osteosarcoma cells (137, 138).

Chen et al. saw that lower expression of Mid1 leads to an accumulation of PP2Ac in the cell. They found increased autophagy in liver cells by dephosphorylating TFEB as a downstream target. TFEB is an important regulator of lysosome biogenesis and autophagy (144). In what way this pathway could play a role in

the developing brain is not known. Future experiments looking more into this pathway should give more insight into this pathway.

Curiously, research has not yet answered the question of the pathomechanism behind OS. A variety of mutations in the Mid1 gene has been identified with a variety of protein expression changes (12, 16, 91, 145). Generally acknowledged is that a loss-of-function mechanism is responsible for the phenotype in OS patients, supported by patients showing whole gene deletions (12). In literature Mid1 KO mice showed structural brain defects comparable to OS patients' anatomy, like hypoplasia of the cerebellar vermis (21). On a more detailed level MRI studies of patients with OS showed no obvious neuronal migration defects (12). In line with this, fibroblasts from an OS patient carrying a 4bp deletion in Exon 9 of *MID1* showed no clear migration defect but only had a tendency to migrate slower than control fibroblasts (93). This is not in line with the results of Mid1/Mid2 KO, where one might discuss a faster migration. There is also evidence a gain-of-function mechanisms might play a role in OS pathogenesis. Experiments with mutations found in OS patients leading to truncated MID1 proteins described a migration defect when the protein was overexpressed (22). Some OS patients carrying truncating mutations also show brain anomalies (12). In our OE of MID1 we saw a migration defect in the neocortex, but the protein is not truncated. This is contrary to findings, that OE of wild type Mid1 led not to a migration defect while the truncated protein did (22).
In the future, studies with different in cellular and animal models will elucidate the effects of these mutations on MID1 expression and function in detail.
Rarely discussed is the compensating role of MID2 in pathogenesis of OS and to what extend MID2 could save possible MID1 deficiency. Showing that a KO of both genes leads to an effect in cell distribution that is alike the effect in OE of MID1, supports the idea that gain-of-function and loss-of-function mutations might exist in OS patients. To give insight on the role of MID2 more studies in this field are necessary and might help to understand pathogenesis of OS. Especially, the mouse line *Mid1*^{lox}/*Mid2*^{lox} could be used to create a ubiquitous KO to see whether these mice show midline defects as these symptoms were not visible in Mid1 KO mice (12).

Moreover, the experiment should be repeated with a higher n number and shorter and longer time span between IUE and dissection of the brains.

4.4 The impact of MID1 on PAX6

In this work a KD construct of Pax6 was established which is suitable for future IUE experiments (see Generation of a Knock-Down Construct of Pax6). Pfirrman et al. were the first to show that Mid1 and Pax6 interact in the eye of Xenopus. Pax6 is a target protein of Mid1 ubiquitin ligase activity. Pfirrman et al. could even see that Mid1 usually being found in the cytosol was localized in the nucleus. In the eyestalk of Xenopus a lack of Mid1 led to an expansion of the region with deviant retinal folds and loss of sharp boundaries between retinal layers (51). As Pax6 is a major TF in brain development with no universally consistent role and a very complex regulation (summarized in (63)), the discussion on the impact of MID1 on PAX6 based on literature is complex. However, the results from the eyestalk provide evidence to broaden the arguments and ask if apart from PP2Ac also Pax6 is responsible for MID1-mediated effects.

PAX6 is a highly conserved TF throughout species (reviewed by (146)). Yet, there are differences in expression and function of PAX6 between primates and rodents (reviewed by (63)). As described in Chapter *Embryonic Development of the Cortex* the developed cortices also differ in their structure. Posttranslational regulation such as ubiquitin mediated degradation of PAX6 levels could be mechanisms responsible for inter-species variability.

Prior to Pfirrmann, Tuoc et al. demonstrated proteasomal degradation of Pax6 by Trim11 in embryonal neurons generated from mice. As a reminder, *Mid1* corresponds to *Trim18*. *Trim11* does not exist in Xenopus. Therefore, it would be interesting to study the interaction of Mid1 and Pax6 in the mouse (147).

In our IUE experiments we created an OE of Mid1 in embryonic mouse cortex, that should lead to lower levels of Pax6, while Mid1 (and Mid2) KO should lead to higher Pax6 levels. Therefore, the KD construct of Pax6 could be used to design rescue experiments in the future to validate whether the KO effect is mediated by Pax6.

4.4.1 **Does the KO of Mid1/Mid2 cause increased Pax6 expression?**

Research on the role of Pax6 on neuronal progenitors in the cortex showed a significant role for a normal development, while the highest impact of Pax6 is on early RGCs (148). KO or KD of Mid1 should lead to increased levels of Pax6 in theory. In our experiment we induced a KO of Mid1 and Mid2, if Mid2 and Pax6 interact is not known. Our results showed differences in cell distribution, with a reduced percentage in the VZ after double KO. For the VZ we used Pax6 as a marker protein. Yet, the analysis of Pax6+ cells in the different layers and cumulatively did show no significant difference. Therefore, in our experiment we could see no direct effect on Pax6 due to KO of Mid1 and Mid2.

OE of Pax6 in experiments looking at similar embryonic days as in this work gave evidence, that cell cycle is shortened and a higher amount of hells can be found in S- or M-phase (66, 96). In neuronal stem cells no effect on proliferation or migration *in vitro* was found, while showing increase in neurogenesis (149). The effects of Pax6 OE seem to be small and very region dependent. In this context, it is described that Pax6 OE leads to its negative autoregulation (66, 99, 149, 150).

Depletion of Trim11 in embryonal neurons generated from mice lead to accumulation of Pax6 and increased apoptosis in the VZ. The study indicated, that proteosomal degradation at E14 was needed to modulate Pax6 levels, as mRNA levels of *Pax6* do not change as fast as protein levels. Interestingly, Tuoc et al. could describe an autoregulatory feedback loop, were high levels of Pax6 induced Trim11 expression (147).

Further experiments, especially analyzing Pax6 levels after Mid1 or Mid1/Mid2 KO are needed to understand, if changes in neuronal distribution may be due to an impact on Pax6.

4.4.2 **Does the overexpression of Mid1 cause reduced Pax6 expression?**

In contrast, overactivation of Mid1 should lead to decreased Pax6 expression due to increased Pax6 ubiquitination and degradation (51). In our work we used Pax6 staining as a marker for the VZ. We saw a decrease in Pax6+ cells, yet at this point we have no evidence if this is due to an interaction between Mid1 and Pax6 or changed migration and differentiation behavior due to other pathways.

Pax6 downregulation has no clear dosage-dependent effect on the cell cycle exit rate in progenitors, also the effect depends on the region of the cortex (63, 99). Some studies found that a decrease of Pax6 leads to shortening of the cell cycle and premature cell cycle exits found in spinal cord of chicken embryos (151-153). Pax6 KO mice generate significantly less neuronal clones, also a KD in human RGCs showed a decreased production of neurons, stressing the effect of Pax6 on neuronal fate (97, 154).

Trim11, from the same protein family of E3- ubiquitin ligases as Mid1, showed that its OE leads to a decrease in Pax6 expression in the VZ. Ki67+ cells significantly decreased, when Trim11 was overexpressed on E12.5, also Pax6-dependent neurogenesis was repressed in vivo and in vitro. The effect seemed to be cell-autonomously (147). Trim 11 and Mid1 might have a redundant function.

IUE of an OE construct of Mid1 on E14.5 caused a higher rate of cells in SVZ/IZ and less cells in the VZ. In theory, this could be due cell cycle shortening and faster cell cycle exit, leading to an enhanced differentiation into an IPC. In contrary, IPCs or BPs divide into neurons, so that one could argue that a higher ratio of cells in SVZ/IZ is a marker for increased neurogenesis, which would not be in line with the described reduction of neurons due to lower Pax6 levels. Yet, if this increased premature exhaustion of the stem cell pool it would lead to fewer neurons ultimately.

Therefore, Future experiments with a longer incubation period after IUE should be performed to determine neuronal fate of electroporated cells.

Future experiments should investigate the possible degradation of PAX6 by MID1 mediated ubiquitination in the mammalian cortex. In addition, it would be important to also study a possible interaction of MID2 and PAX6.

5 Abstract

Mid1 and *Mid2* are two homologous genes encoding E3-ubiquitin ligases. This work explores the functions of the sister proteins Mid1 and Mid2 in the context of mouse models and their impact on neuronal development in the embryonic neocortex of mice. The work involves the establishment of genetically modified mouse strains, including *Mid1*^{lox}/*Mid2*^{lox}, to investigate tissue-specific effects of gene knockout.

Previous experiments of a knockdown of Mid1 via *in utero* electroporation in the embryonic neocortex showed no differences in cell distribution, leading to the idea that Mid2 can compensate for Mid1. In this work we saw an effect of the double knockout via in-utero electroporation on neuronal cell distribution with a reduced percentage of GFP+ cells in the ventricular zone and an increased presence in the cortical plate in the *Mid1*/*Mid2* double knockout. Alterations in cell distribution might be due to a potential impact on migration, proliferation or differentiation. Fewer cells positive for Ki67+ were observed, while apoptosis analysis via Casp3 staining showed a higher number of Casp3+ cells after knockout. RtPCR confirmed reduced gene expression of Mid1 and Mid2 in GFP+ cells after electroporation, supporting the effectiveness of conditional knockout. Overall, these findings shed light on the role of *Mid1* and *Mid2* in neurogenesis, indicating their involvement in regulating cell distribution and proliferation during embryonic neocortical development.

The work further explores the effects of Mid1 overexpression in neuronal progenitor cells. The Mid1 overexpression group exhibited significant alterations in cell distribution, with fewer cells in the ventricular zone and more in the subventricular/intermediate zone compared to the control group. Ki67 staining revealed a higher proliferation rate in the ventricular zone of Mid1 overexpressed brains, while apoptosis analysis using Caspase3 staining showed no difference. Additionally, the impact on Pax6, a key transcription factor in brain development, is also investigated. The need for further research on this topic is emphasized.

6 Bibliography

1. Organization WH. ICD-10 guide for mental retardation. World Health Organization; 1996.
2. Maulik PK, Mascarenhas MN, Mathers CD, Dua T, Saxena S. Prevalence of intellectual disability: a meta-analysis of population-based studies. Research in developmental disabilities. 2011;32(2):419-36.
3. Häßler F, Bienstein P, Buscher M, Caby F, Hennicke K, Hoffmann K. Intelligenzminderung: S2k-Leitlinie; AWMF-Register Nr. 028-042: Medizinisch Wissenschaftliche Verlagsgesellschaft; 2016.
4. van Bokhoven H. Genetic and epigenetic networks in intellectual disabilities. Annual review of genetics. 2011;45:81-104.
5. Musante L, Ropers HH. Genetics of recessive cognitive disorders. Trends in Genetics. 2014;30(1):32-9.
6. Ilyas M, Mir A, Efthymiou S, Houlden H. The genetics of intellectual disability: advancing technology and gene editing. F1000Research. 2020;9.
7. https://nhsgms-panelapp.genomicsengland.co.uk/panels/285/v5.0 [
8. Akhtar F, Bokhari SRA. Down Syndrome. StatPearls. Treasure Island (FL) ineligible companies. Disclosure: Syed Rizwan Bokhari declares no relevant financial relationships with ineligible companies.: StatPearls Publishing Copyright © 2023, StatPearls Publishing LLC.; 2023.
9. Ropers HH, Hamel BC. X-linked mental retardation. Nature reviews Genetics. 2005;6(1):46-57.
10. Hagerman RJ, Berry-Kravis E, Hazlett HC, Bailey DB, Moine H, Kooy RF, et al. Fragile X syndrome. Nature Reviews Disease Primers. 2017;3(1):17065.
11. Geetha TS, Michealraj KA, Kabra M, Kaur G, Juyal RC, Thelma BK. Targeted deep resequencing identifies MID2 mutation for X-linked intellectual disability with varied disease severity in a large kindred from India. Human mutation. 2014;35(1):41-4.
12. Fontanella B, Russolillo G, Meroni G. MID1 mutations in patients with X-linked Opitz G/BBB syndrome. Human mutation. 2008;29(5):584-94.
13. Opitz J FJ, Gutenberger J, Pellet J The G-syndrome of multiple congenital anomalies. BD:OAS 1969;V:95–101.
14. Opitz J SR, Smith D (1969b) . BD:OAS V:86–94. The BBB syndrome Familial telecanthus with associated congenital anomalies. BD. 1969.
15. Cordero JF, Holmes LB. Phenotypic overlap of the BBB and G syndromes. Am J Med Genet. 1978;2(2):145-52.
16. Winter J, Basilicata MF, Stemmler MP, Krauss S. The MID1 protein is a central player during development and in disease. Frontiers in bioscience (Landmark edition). 2016;21:664-82.
17. Trainor PA. Neural crest cells : evolution, development and disease: Amsterdam : Elsevier/AP; 2014.
18. Kalluri R, Weinberg RA. The basics of epithelial-mesenchymal transition. The Journal of clinical investigation. 2009;119(6):1420-8.
19. Köhler A, Demir U, Kickstein E, Krauss S, Aigner J, Aranda-Orgillés B, et al. A hormone-dependent feedback-loop controls androgen receptor levels by limiting MID1, a novel translation enhancer and promoter of oncogenic signaling. Mol Cancer. 2014;13:146-.

20. Meroni G. X-Linked Opitz G/BBB Syndrome. In: Adam MP, Ardinger HH, Pagon RA, Wallace SE, Bean LJH, Stephens K, et al., editors. GeneReviews((R)). Seattle (WA): University of Washington, Seattle
University of Washington, Seattle. GeneReviews is a registered trademark of the University of Washington, Seattle. All rights reserved.; 1993.
21. Lancioni A, Pizzo M, Fontanella B, Ferrentino R, Napolitano LM, De Leonibus E, et al. Lack of Mid1, the mouse ortholog of the Opitz syndrome gene, causes abnormal development of the anterior cerebellar vermis. The Journal of neuroscience : the official journal of the Society for Neuroscience. 2010;30(8):2880-7.
22. Lu T, Chen R, Cox TC, Moldrich RX, Kurniawan N, Tan G, et al. X-linked microtubule-associated protein, Mid1, regulates axon development. Proc Natl Acad Sci U S A. 2013;110(47):19131-6.
23. Kruszka P, Li D, Harr MH, Wilson NR, Swarr D, McCormick EM, et al. Mutations in SPECC1L, encoding sperm antigen with calponin homology and coiled-coil domains 1-like, are found in some cases of autosomal dominant Opitz G/BBB syndrome. Journal of medical genetics. 2015;52(2):104-10.
24. Robin NH, Feldman GJ, Aronson AL, Mitchell HF, Weksberg R, Leonard CO, et al. Opitz syndrome is genetically heterogeneous, with one locus on Xp22, and a second locus on 22q11.2. Nature genetics. 1995;11(4):459-61.
25. Fryburg JS, Lin KY, Golden WL. Chromosome 22q11.2 deletion in a boy with Opitz (G/BBB) syndrome. Am J Med Genet. 1996;62(3):274-5.
26. McDonald-McGinn DM, Driscoll DA, Bason L, Christensen K, Lynch D, Sullivan K, et al. Autosomal dominant "Opitz" GBBB syndrome due to a 22q11.2 deletion. Am J Med Genet. 1995;59(1):103-13.
27. Latta EJ, Golding JP. Regulation of PP2A activity by Mid1 controls cranial neural crest speed and gangliogenesis. Mechanisms of development. 2012;128(11-12):560-76.
28. Granata A, Quaderi NA. The Opitz syndrome gene MID1 is essential for establishing asymmetric gene expression in Hensen's node. Developmental biology. 2003;258(2):397-405.
29. Qiao Y, Zhou Y, Song C, Zhang X, Zou Y. MID1 and MID2 regulate cell migration and epithelial-mesenchymal transition via modulating Wnt/β-catenin signaling. Annals of translational medicine. 2020;8(16):1021.
30. Winter J, Lehmann T, Krauss S, Trockenbacher A, Kijas Z, Foerster J, et al. Regulation of the MID1 protein function is fine-tuned by a complex pattern of alternative splicing. Human genetics. 2004;114(6):541-52.
31. Landry JR, Mager DL. Widely spaced alternative promoters, conserved between human and rodent, control expression of the Opitz syndrome gene MID1. Genomics. 2002;80(5):499-508.
32. Winter J, Kunath M, Roepcke S, Krause S, Schneider R, Schweiger S. Alternative polyadenylation signals and promoters act in concert to control tissue-specific expression of the Opitz Syndrome gene MID1. BMC molecular biology. 2007;8:105.
33. Cox TC. The Microtubule-Associated C-I Subfamily of TRIM Proteins and the Regulation of Polarized Cell Responses. In: Meroni G, editor. TRIM/RBCC Proteins. New York, NY: Springer New York; 2012. p. 105-18.
34. Dal Zotto L, Quaderi NA, Elliott R, Lingerfelter PA, Carrel L, Valsecchi V, et al. The mouse Mid1 gene: implications for the pathogenesis of Opitz syndrome and the evolution of the mammalian pseudoautosomal region. Human molecular genetics. 1998;7(3):489-99.

35. Meroni G. Preface. TRIM/RBCC proteins. Advances in experimental medicine and biology. 2012;770:vii-viii.
36. Meroni G. Genomics and Evolution of the TRIM Gene Family. In: Meroni G, editor. TRIM/RBCC Proteins. New York, NY: Springer New York; 2012. p. 1-9.
37. Short KM, Hopwood B, Yi Z, Cox TC. MID1 and MID2 homo- and heterodimerise to tether the rapamycin-sensitive PP2A regulatory subunit, alpha 4, to microtubules: implications for the clinical variability of X-linked Opitz GBBB syndrome and other developmental disorders. BMC cell biology. 2002;3:1.
38. Aranda-Orgilles B, Aigner J, Kunath M, Lurz R, Schneider R, Schweiger S. Active transport of the ubiquitin ligase MID1 along the microtubules is regulated by protein phosphatase 2A. PloS one. 2008;3(10):e3507.
39. Trockenbacher A, Suckow V, Foerster J, Winter J, Krauss S, Ropers HH, et al. MID1, mutated in Opitz syndrome, encodes an ubiquitin ligase that targets phosphatase 2A for degradation. Nature genetics. 2001;29(3):287-94.
40. Schweiger S, Schneider R. The MID1/PP2A complex: a key to the pathogenesis of Opitz BBB/G syndrome. Bioessays. 2003;25(4):356-66.
41. Schweiger S, Foerster J, Lehmann T, Suckow V, Muller YA, Walter G, et al. The Opitz syndrome gene product, MID1, associates with microtubules. Proc Natl Acad Sci U S A. 1999;96(6):2794-9.
42. Aranda-Orgilles B, Trockenbacher A, Winter J, Aigner J, Kohler A, Jastrzebska E, et al. The Opitz syndrome gene product MID1 assembles a microtubule-associated ribonucleoprotein complex. Human genetics. 2008;123(2):163-76.
43. Müller M, Graeve L. Proteine – Transport, Modifikation und Faltung. In: Heinrich PC, Müller M, Graeve L, editors. Löffler/Petrides Biochemie und Pathobiochemie. Berlin, Heidelberg: Springer Berlin Heidelberg; 2014. p. 615-28.
44. Gotz J, Probst A, Ehler E, Hemmings B, Kues W. Delayed embryonic lethality in mice lacking protein phosphatase 2A catalytic subunit Calpha. Proc Natl Acad Sci U S A. 1998;95(21):12370-5.
45. Kinoshita K, Nemoto T, Nabeshima K, Kondoh H, Niwa H, Yanagida M. The regulatory subunits of fission yeast protein phosphatase 2A (PP2A) affect cell morphogenesis, cell wall synthesis and cytokinesis. Genes to cells : devoted to molecular & cellular mechanisms. 1996;1(1):29-45.
46. Nanahoshi M, Tsujishita Y, Tokunaga C, Inui S, Sakaguchi N, Hara K, et al. Alpha4 protein as a common regulator of type 2A-related serine/threonine protein phosphatases. FEBS letters. 1999;446(1):108-12.
47. Du H, Huang Y, Zaghlula M, Walters E, Cox TC, Massiah MA. The MID1 E3 ligase catalyzes the polyubiquitination of Alpha4 (alpha4), a regulatory subunit of protein phosphatase 2A (PP2A): novel insights into MID1-mediated regulation of PP2A. The Journal of biological chemistry. 2013;288(29):21341-50.
48. Liu E, Knutzen CA, Krauss S, Schweiger S, Chiang GG. Control of mTORC1 signaling by the Opitz syndrome protein MID1. Proc Natl Acad Sci U S A. 2011;108(21):8680-5.
49. Liu J, Prickett TD, Elliott E, Meroni G, Brautigan DL. Phosphorylation and microtubule association of the Opitz syndrome protein mid-1 is regulated by protein phosphatase 2A via binding to the regulatory subunit alpha 4. Proc Natl Acad Sci U S A. 2001;98(12):6650-5.
50. Schweiger S, Dorn S, Fuchs M, Kohler A, Matthes F, Muller EC, et al. The E3 ubiquitin ligase MID1 catalyzes ubiquitination and cleavage of Fu. The Journal of biological chemistry. 2014;289(46):31805-17.

51. Pfirrmann T, Jandt E, Ranft S, Lokapally A, Neuhaus H, Perron M, et al. Hedgehog-dependent E3-ligase Midline1 regulates ubiquitin-mediated proteasomal degradation of Pax6 during visual system development. Proc Natl Acad Sci U S A. 2016;113(36):10103-8.
52. Krauss S, Griesche N, Jastrzebska E, Chen C, Rutschow D, Achmuller C, et al. Translation of HTT mRNA with expanded CAG repeats is regulated by the MID1-PP2A protein complex. Nature communications. 2013;4:1511.
53. Kickstein E, Krauss S, Thornhill P, Rutschow D, Zeller R, Sharkey J, et al. Biguanide metformin acts on tau phosphorylation via mTOR/protein phosphatase 2A (PP2A) signaling. Proc Natl Acad Sci U S A. 2010;107(50):21830-5.
54. Arigoni M, Barutello G, Riccardo F, Ercole E, Cantarella D, Orso F, et al. miR-135b coordinates progression of ErbB2-driven mammary carcinomas through suppression of MID1 and MTCH2. The American journal of pathology. 2013;182(6):2058-70.
55. Perry J, Short KM, Romer JT, Swift S, Cox TC, Ashworth A. FXY2/MID2, a gene related to the X-linked Opitz syndrome gene FXY/MID1, maps to Xq22 and encodes a FNIII domain-containing protein that associates with microtubules. Genomics. 1999;62(3):385-94.
56. Buchner G, Montini E, Andolfi G, Quaderi N, Cainarca S, Messali S, et al. MID2, a homologue of the Opitz syndrome gene MID1: similarities in subcellular localization and differences in expression during development. Human molecular genetics. 1999;8(8):1397-407.
57. Yates AD, Achuthan P, Akanni W, Allen J, Allen J, Alvarez-Jarreta J, et al. Ensembl 2020. Nucleic acids research. 2020;48(D1):D682-d8.
58. Petrera F, Meroni G. TRIM Proteins in Development. In: Meroni G, editor. TRIM/RBCC Proteins. New York, NY: Springer New York; 2012. p. 131-41.
59. Suzuki M, Hara Y, Takagi C, Yamamoto TS, Ueno N. MID1 and MID2 are required for Xenopus neural tube closure through the regulation of microtubule organization. Development (Cambridge, England). 2010;137(14):2329-39.
60. Boding L, Hansen AK, Meroni G, Levring TB, Woetmann A, Odum N, et al. MID2 can substitute for MID1 and control exocytosis of lytic granules in cytotoxic T cells. APMIS : acta pathologica, microbiologica, et immunologica Scandinavica. 2015;123(8):682-7.
61. Gholkar AA, Senese S, Lo YC, Vides E, Contreras E, Hodara E, et al. The X-Linked-Intellectual-Disability-Associated Ubiquitin Ligase Mid2 Interacts with Astrin and Regulates Astrin Levels to Promote Cell Division. Cell reports. 2016;14(2):180-8.
62. Holm PC, Mader MT, Haubst N, Wizenmann A, Sigvardsson M, Gotz M. Loss- and gain-of-function analyses reveal targets of Pax6 in the developing mouse telencephalon. Molecular and cellular neurosciences. 2007;34(1):99-119.
63. Manuel MN, Mi D, Mason JO, Price DJ. Regulation of cerebral cortical neurogenesis by the Pax6 transcription factor. Frontiers in Cellular Neuroscience. 2015;9:70.
64. Ton CC, Miwa H, Saunders GF. Small eye (Sey): cloning and characterization of the murine homolog of the human aniridia gene. Genomics. 1992;13(2):251-6.
65. Haubst N, Berger J, Radjendirane V, Graw J, Favor J, Saunders GF, et al. Molecular dissection of Pax6 function: the specific roles of the paired domain and homeodomain in brain development. Development (Cambridge, England). 2004;131(24):6131-40.

66. Manuel M, Georgala PA, Carr CB, Chanas S, Kleinjan DA, Martynoga B, et al. Controlled overexpression of Pax6 in vivo negatively autoregulates the Pax6 locus, causing cell-autonomous defects of late cortical progenitor proliferation with little effect on cortical arealization. Development (Cambridge, England). 2007;134(3):545-55.
67. Davis LK, Meyer KJ, Rudd DS, Librant AL, Epping EA, Sheffield VC, et al. Pax6 3' deletion results in aniridia, autism and mental retardation. Human genetics. 2008;123(4):371-8.
68. Englund C, Fink A, Lau C, Pham D, Daza RA, Bulfone A, et al. Pax6, Tbr2, and Tbr1 are expressed sequentially by radial glia, intermediate progenitor cells, and postmitotic neurons in developing neocortex. The Journal of neuroscience : the official journal of the Society for Neuroscience. 2005;25(1):247-51.
69. Rohen JW, Lütjen-Drecoll E. Funktionelle Embryologie. Aufl Stuttgart: Schattauer. 2006.
70. Fotos J, Olson R, Kanekar S. Embryology of the brain and molecular genetics of central nervous system malformation. Seminars in ultrasound, CT, and MR. 2011;32(3):159-66.
71. Florio M, Heide M, Pinson A, Brandl H, Albert M, Winkler S, et al. Evolution and cell-type specificity of human-specific genes preferentially expressed in progenitors of fetal neocortex. eLife. 2018;7.
72. Wong FK, Fei JF, Mora-Bermúdez F, Taverna E, Haffner C, Fu J, et al. Sustained Pax6 Expression Generates Primate-like Basal Radial Glia in Developing Mouse Neocortex. PLoS Biology. 2015;13(8).
73. Noctor SC, Martinez-Cerdeno V, Kriegstein AR. Distinct behaviors of neural stem and progenitor cells underlie cortical neurogenesis. J Comp Neurol. 2008;508(1):28-44.
74. Smart IH. Proliferative characteristics of the ependymal layer during the early development of the mouse neocortex: a pilot study based on recording the number, location and plane of cleavage of mitotic figures. Journal of anatomy. 1973;116(Pt 1):67-91.
75. Smart IH, Dehay C, Giroud P, Berland M, Kennedy H. Unique morphological features of the proliferative zones and postmitotic compartments of the neural epithelium giving rise to striate and extrastriate cortex in the monkey. Cerebral cortex (New York, NY : 1991). 2002;12(1):37-53.
76. Lukaszewicz A, Savatier P, Cortay V, Giroud P, Huissoud C, Berland M, et al. G1 phase regulation, area-specific cell cycle control, and cytoarchitectonics in the primate cortex. Neuron. 2005;47(3):353-64.
77. Gilmore EC, Herrup K. Cortical development: Layers of complexity. Current Biology. 1997;7(4):R231-R4.
78. Shen Q, Wang Y, Dimos JT, Fasano CA, Phoenix TN, Lemischka IR, et al. The timing of cortical neurogenesis is encoded within lineages of individual progenitor cells. Nature neuroscience. 2006;9(6):743-51.
79. Marin-Padilla M. Early prenatal ontogenesis of the cerebral cortex (neocortex) of the cat (Felis domestica). A Golgi study. Zeitschrift für Anatomie und Entwicklungsgeschichte. 1971;134(2):117-45.
80. Luskin MB, Shatz CJ. Neurogenesis of the cat's primary visual cortex. Journal of Comparative Neurology. 1985;242(4):611-31.
81. Ishii K, Kubo KI, Nakajima K. Reelin and Neuropsychiatric Disorders. Front Cell Neurosci. 2016;10:229.
82. Gil-Sanz C, Franco SJ, Martinez-Garay I, Espinosa A, Harkins-Perry S, Müller U. Cajal-Retzius cells instruct neuronal migration by coincidence signaling

between secreted and contact-dependent guidance cues. Neuron. 2013;79(3):461-77.
83. Pollen AA, Nowakowski TJ, Chen J, Retallack H, Sandoval-Espinosa C, Nicholas CR, et al. Molecular identity of human outer radial glia during cortical development. Cell. 2015;163(1):55-67.
84. Florio M, Huttner WB. Neural progenitors, neurogenesis and the evolution of the neocortex. Development (Cambridge, England). 2014;141(11):2182-94.
85. Zhang J, Jiao J. Molecular Biomarkers for Embryonic and Adult Neural Stem Cell and Neurogenesis. BioMed research international. 2015;2015:727542.
86. Britanova O, de Juan Romero C, Cheung A, Kwan KY, Schwark M, Gyorgy A, et al. Satb2 is a postmitotic determinant for upper-layer neuron specification in the neocortex. Neuron. 2008;57(3):378-92.
87. De Falco F, Cainarca S, Andolfi G, Ferrentino R, Berti C, Rodríguez Criado G, et al. X-linked Opitz syndrome: novel mutations in the MID1 gene and redefinition of the clinical spectrum. Am J Med Genet A. 2003;120a(2):222-8.
88. Goldstein A, Covington BP, Mahabadi N, Mesfin FB. Neuroanatomy, Corpus Callosum. StatPearls. Treasure Island (FL): StatPearls Publishing
Copyright © 2020, StatPearls Publishing LLC.; 2020.
89. Hadeball B, Borchers A, Wedlich D. Xenopus cadherin-11 (Xcadherin-11) expression requires the Wg/Wnt signal. Mechanisms of development. 1998;72(1):101-13.
90. Xi M, Lui F. Neuroanatomy, Neural Crest. StatPearls. Treasure Island (FL): StatPearls Publishing
Copyright © 2020, StatPearls Publishing LLC.; 2020.
91. Quaderi NA, Schweiger S, Gaudenz K, Franco B, Rugarli EI, Berger W, et al. Opitz G/BBB syndrome, a defect of midline development, is due to mutations in a new RING finger gene on Xp22. Nature genetics. 1997;17(3):285-91.
92. Pinson L, Augé J, Audollent S, Mattéi G, Etchevers H, Gigarel N, et al. Embryonic expression of the human MID1 gene and its mutations in Opitz syndrome. Journal of medical genetics. 2004;41(5):381-6.
93. Willam M. Die Ubiquitin-Protein-Ligase MID1 und ihre Funktion in Zellproliferation und -migration sowie bei der Entstehung der Huntington-Krankheit: Johannes Gutenberg-Universität Mainz; 2018.
94. Aranda-Orgilles B, Rutschow D, Zeller R, Karagiannidis AI, Kohler A, Chen C, et al. Protein phosphatase 2A (PP2A)-specific ubiquitin ligase MID1 is a sequence-dependent regulator of translation efficiency controlling 3-phosphoinositide-dependent protein kinase-1 (PDPK-1). The Journal of biological chemistry. 2011;286(46):39945-57.
95. Kaddour H, Coppola E, Di Nardo AA, Le Poupon C, Mailly P, Wizenmann A, et al. Extracellular Pax6 Regulates Tangential Cajal-Retzius Cell Migration in the Developing Mouse Neocortex. Cerebral cortex (New York, NY : 1991). 2019.
96. Heins N, Malatesta P, Cecconi F, Nakafuku M, Tucker KL, Hack MA, et al. Glial cells generate neurons: the role of the transcription factor Pax6. Nature neuroscience. 2002;5(4):308-15.
97. Mo Z, Zecevic N. Is Pax6 critical for neurogenesis in the human fetal brain? Cerebral cortex (New York, NY : 1991). 2008;18(6):1455-65.
98. Georgala PA, Carr CB, Price DJ. The role of Pax6 in forebrain development. Developmental neurobiology. 2011;71(8):690-709.
99. Georgala PA, Manuel M, Price DJ. The generation of superficial cortical layers is regulated by levels of the transcription factor Pax6. Cerebral cortex (New York, NY : 1991). 2011;21(1):81-94.

100. Shaham O, Menuchin Y, Farhy C, Ashery-Padan R. Pax6: a multi-level regulator of ocular development. Progress in retinal and eye research. 2012;31(5):351-76.
101. Van Cruchten S, Vrolyk V, Perron Lepage MF, Baudon M, Voute H, Schoofs S, et al. Pre- and Postnatal Development of the Eye: A Species Comparison. Birth Defects Res. 2017;109(19):1540-67.
102. She Q, Fu F, Guo X, Tan W, Liao C. Genetic testing in fetuses with isolated agenesis of the corpus callosum. The journal of maternal-fetal & neonatal medicine : the official journal of the European Association of Perinatal Medicine, the Federation of Asia and Oceania Perinatal Societies, the International Society of Perinatal Obstet. 2019:1-201.
103. Birling MC, Dierich A, Jacquot S, Hérault Y, Pavlovic G. Highly-efficient, fluorescent, locus directed cre and FlpO deleter mice on a pure C57BL/6N genetic background. Genesis (New York, NY : 2000). 2012;50(6):482-9.
104. Schwenk F, Baron U, Rajewsky K. A cre-transgenic mouse strain for the ubiquitous deletion of loxP-flanked gene segments including deletion in germ cells. Nucleic acids research. 1995;23(24):5080-1.
105. Van Duyne GD. Cre Recombinase. Microbiology spectrum. 2015;3(1):Mdna3-0014-2014.
106. Abremski K, Hoess R. Bacteriophage P1 site-specific recombination. Purification and properties of the Cre recombinase protein. The Journal of biological chemistry. 1984;259(3):1509-14.
107. Svoboda DS, Clark A, Park DS, Slack RS. Induction of protein deletion through in utero electroporation to define deficits in neuronal migration in transgenic models. Journal of visualized experiments : JoVE. 2015(95):51983.
108. Lobo I, Shaw K. Thomas Hunt Morgan, genetic. 2008.
109. Jensen SM, Schmitz A, Pedersen FS, Kjems J, Bramsen JB. Functional selection of shRNA loops from randomized retroviral libraries. PloS one. 2012;7(8):e43095.
110. Paddison PJ, Caudy AA, Bernstein E, Hannon GJ, Conklin DS. Short hairpin RNAs (shRNAs) induce sequence-specific silencing in mammalian cells. Genes & development. 2002;16(8):948-58.
111. Griffith F. The Significance of Pneumococcal Types. The Journal of hygiene. 1928;27(2):113-59.
112. Pacary E, Guillemot F. In utero electroporation to study mouse brain development. Methods in molecular biology (Clifton, NJ). 2014;1082:285-93.
113. Baumgart J, Grebe N. C57BL/6-specific conditions for efficient in utero electroporation of the central nervous system. Journal of neuroscience methods. 2015;240:116-24.
114. Shi S-R, Cote RJ, Taylor CR. Antigen Retrieval Immunohistochemistry: Past, Present, and Future. Journal of Histochemistry & Cytochemistry. 1997;45(3):327-43.
115. Hawkins SF, Guest PC. Multiplex Analyses Using Real-Time Quantitative PCR. Methods in molecular biology (Clifton, NJ). 2017;1546:125-33.
116. Field J, Nikawa J, Broek D, MacDonald B, Rodgers L, Wilson IA, et al. Purification of a RAS-responsive adenylyl cyclase complex from Saccharomyces cerevisiae by use of an epitope addition method. Molecular and cellular biology. 1988;8(5):2159-65.
117. Zhang W, Ma L, Yang M, Shao E, Xu J, Lu Z, et al. Cerebral organoid and mouse models reveal a RAB39b–PI3K–mTOR pathway-dependent dysregulation

of cortical development leading to macrocephaly/autism phenotypes. Genes & development. 2020;34.
118. Chittka A. Dynamic Distribution of Histone H4 Arginine 3 Methylation Marks in the Developing Murine Cortex. PloS one. 2010;5(11):e13807.
119. Brentnall M, Rodriguez-Menocal L, De Guevara RL, Cepero E, Boise LH. Caspase-9, caspase-3 and caspase-7 have distinct roles during intrinsic apoptosis. BMC cell biology. 2013;14(1):32.
120. Porter AG, Jänicke RU. Emerging roles of caspase-3 in apoptosis. Cell Death & Differentiation. 1999;6(2):99-104.
121. Fernandes-Alnemri T, Litwack G, Alnemri ES. CPP32, a novel human apoptotic protein with homology to Caenorhabditis elegans cell death protein Ced-3 and mammalian interleukin-1 beta-converting enzyme. The Journal of biological chemistry. 1994;269(49):30761-4.
122. Meroni G, Diez-Roux G. TRIM/RBCC, a novel class of 'single protein RING finger' E3 ubiquitin ligases. Bioessays. 2005;27(11):1147-57.
123. Perry J, Palmer S, Gabriel A, Ashworth A. A short pseudoautosomal region in laboratory mice. Genome research. 2001;11(11):1826-32.
124. Granata A, Savery D, Hazan J, Cheung BM, Lumsden A, Quaderi NA. Evidence of functional redundancy between MID proteins: implications for the presentation of Opitz syndrome. Developmental biology. 2005;277(2):417-24.
125. Stapley J, Feulner PGD, Johnston SE, Santure AW, Smadja CM. Variation in recombination frequency and distribution across eukaryotes: patterns and processes. Philosophical transactions of the Royal Society of London Series B, Biological sciences. 2017;372(1736).
126. Dumont BL. X-Chromosome Control of Genome-Scale Recombination Rates in House Mice. Genetics. 2017;205(4):1649-56.
127. Friedel RH, Wurst W, Wefers B, Kühn R. Generating conditional knockout mice. Methods in molecular biology (Clifton, NJ). 2011;693:205-31.
128. Baldini R, Mascaro M, Meroni G. The MID1 gene product in physiology and disease. Gene. 2020;747:144655.
129. Ariño J, Velázquez D, Casamayor A. Ser/Thr protein phosphatases in fungi: structure, regulation and function. Microbial Cell. 2019;6:217-56.
130. Zolnierowicz S. Type 2A protein phosphatase, the complex regulator of numerous signaling pathways. Biochemical Pharmacology. 2000;60(8):1225-35.
131. Tang S, Liu Y, Wang X, Liang Z, Cai H, Mo L, et al. Characterization of overexpression of the alternatively spliced isoform of the protein phosphatase 2A catalytic subunit in cells. Biochemical and Biophysical Research Communications. 2017;494(3):491-8.
132. Poduri A, Evrony GD, Cai X, Elhosary PC, Beroukhim R, Lehtinen MK, et al. Somatic activation of AKT3 causes hemispheric developmental brain malformations. Neuron. 2012;74(1):41-8.
133. Ka M, Condorelli G, Woodgett JR, Kim WY. mTOR regulates brain morphogenesis by mediating GSK3 signaling. Development (Cambridge, England). 2014;141(21):4076-86.
134. Fishwick KJ, Li RA, Halley P, Deng P, Storey KG. Initiation of neuronal differentiation requires PI3-kinase/TOR signalling in the vertebrate neural tube. Developmental biology. 2010;338(2):215-25.
135. Han J, Wang B, Xiao Z, Gao Y, Zhao Y, Zhang J, et al. Mammalian target of rapamycin (mTOR) is involved in the neuronal differentiation of neural progenitors induced by insulin. Molecular and cellular neurosciences. 2008;39(1):118-24.

136. Malagelada C, López-Toledano MA, Willett RT, Jin ZH, Shelanski ML, Greene LA. RTP801/REDD1 regulates the timing of cortical neurogenesis and neuron migration. The Journal of neuroscience : the official journal of the Society for Neuroscience. 2011;31(9):3186-96.
137. Xie F, Bao X, Yu J, Chen W, Wang L, Zhang Z, et al. Disruption and inactivation of the PP2A complex promotes the proliferation and angiogenesis of hemangioma endothelial cells through activating AKT and ERK. Oncotarget. 2015;6(28):25660-76.
138. Yang D, Okamura H, Morimoto H, Teramachi J, Haneji T. Protein phosphatase 2A Calpha regulates proliferation, migration, and metastasis of osteosarcoma cells. Laboratory investigation; a journal of technical methods and pathology. 2016;96(10):1050-62.
139. Sontag E. Protein phosphatase 2A: the Trojan Horse of cellular signaling. Cellular signalling. 2001;13(1):7-16.
140. Palmer S, Perry J, Kipling D, Ashworth A. A gene spans the pseudoautosomal boundary in mice. Proc Natl Acad Sci U S A. 1997;94(22):12030-5.
141. Simmler MC, Rouyer F, Vergnaud G, Nyström-Lahti M, Ngo KY, de la Chapelle A, et al. Pseudoautosomal DNA sequences in the pairing region of the human sex chromosomes. Nature. 1985;317(6039):692-7.
142. Raudsepp T, Chowdhary BP. The Eutherian Pseudoautosomal Region. Cytogenetic and genome research. 2015;147(2-3):81-94.
143. Zhu J, Nguyen MT, Nakamura E, Yang J, Mackem S. Cre-mediated recombination can induce apoptosis in vivo by activating the p53 DNA damage-induced pathway. Genesis (New York, NY : 2000). 2012;50(2):102-11.
144. Chen L, Wang K, Long A, Jia L, Zhang Y, Deng H, et al. Fasting-induced hormonal regulation of lysosomal function. Cell research. 2017;27(6):748-63.
145. Van den Veyver IB, Cormier TA, Jurecic V, Baldini A, Zoghbi HY. Characterization and physical mapping in human and mouse of a novel RING finger gene in Xp22. Genomics. 1998;51(2):251-61.
146. Walther C, Gruss P. Pax-6, a murine paired box gene, is expressed in the developing CNS. Development (Cambridge, England). 1991;113(4):1435-49.
147. Tuoc TC, Stoykova A. Trim11 modulates the function of neurogenic transcription factor Pax6 through ubiquitin-proteosome system. Genes & development. 2008;22(14):1972-86.
148. Quinn JC, Molinek M, Martynoga BS, Zaki PA, Faedo A, Bulfone A, et al. Pax6 controls cerebral cortical cell number by regulating exit from the cell cycle and specifies cortical cell identity by a cell autonomous mechanism. Developmental biology. 2007;302(1):50-65.
149. Kallur T, Gisler R, Lindvall O, Kokaia Z. Pax6 promotes neurogenesis in human neural stem cells. Molecular and Cellular Neuroscience. 2008;38(4):616-28.
150. Pinson J, Simpson TI, Mason JO, Price DJ. Positive autoregulation of the transcription factor Pax6 in response to increased levels of either of its major isoforms, Pax6 or Pax6(5a), in cultured cells. BMC developmental biology. 2006;6:25.
151. Mi D, Manuel M, Huang YT, Mason JO, Price DJ. Pax6 Lengthens G1 Phase and Decreases Oscillating Cdk6 Levels in Murine Embryonic Cortical Progenitors. Front Cell Neurosci. 2018;12:419.

152. Mi D, Carr CB, Georgala PA, Huang YT, Manuel MN, Jeanes E, et al. Pax6 exerts regional control of cortical progenitor proliferation via direct repression of Cdk6 and hypophosphorylation of pRb. Neuron. 2013;78(2):269-84.
153. Bel-Vialar S, Medevielle F, Pituello F. The on/off of Pax6 controls the tempo of neuronal differentiation in the developing spinal cord. Developmental biology. 2007;305(2):659-73.
154. Schmahl W, Knoedlseder M, Favor J, Davidson D. Defects of neuronal migration and the pathogenesis of cortical malformations are associated with Small eye (Sey) in the mouse, a point mutation at the Pax-6-locus. Acta neuropathologica. 1993;86(2):126-35.

7 Appendix

7.1 Declaration

Ich, Katharina Anna Ruppert, erkläre hiermit, dass die vorgelegte Dissertation von mir selbstständig, ohne unzulässige Hilfe Dritter und ohne Benutzung anderer als der angegebenen Hilfsmittel, angefertigt wurde. Alle von mir benutzten Veröffentlichungen, ungedruckten Materialien, sonstige Hilfsmittel sowie Textstellen, die ich wörtlich oder inhaltlich aus gedruckten oder ungedruckten Arbeiten übernommen habe, habe ich als solche gekennzeichnet und mit den erforderlichen bibliographischen Angaben nachgewiesen. Unterstützungsleistungen, die ich von anderen Personen erhalten habe, wurden in der Dissertationsschrift als solche benannt.
Die Dissertation wurde bei keiner anderen Fakultät oder einem anderen Fachbereich vorgelegt, weder im In- noch im Ausland.
Überdies bin ich nicht im Besitz eines anderen Doktorgrades.
Ich habe bisher kein Promotionsverfahren erfolglos beendet.
Mir ist bekannt, dass die Zulassung zur Promotion zu versagen ist, wenn die Unterlagen unvollständig oder die Angaben unrichtig sind. Ich bin darüber informiert, dass ich zur Führung des Doktortitels erst mit Aushändigung der Promotionsurkunde berechtigt bin.

Mainz, 18.12.2023

7.2 Supplementary Data

Data MID1 OE GFP+/GFP + cells
Mean value from 3 different stainings

Animal	VZ	SVZ	CP
MI1 OE Empty 43	0,67695992	0,32304008	0
Mother B6/N 1			
MI1 OE Empty 45	0,62796232	0,38431013	0
Mother Mouse 1			
MI1 OE Empty 46	0,59953184	0,37203768	0
Mother Mouse 2			
MI1 OE Empty 47	0,61970651	0,40046816	0
Mother Mouse 2			
MI1 OE Empty 48	0,61568987	0,38029349	0
Mother Mouse 2			
MID1 OE 28	0,5167298	0,4832702	0
Mother B6/N 3			
MID1 OE 32	0,56867419	0,43132581	0
Mother B6/N 3			
MID1 OE 33	0,45380733	0,54619267	0
Mother B6/N 4			
MID1 OE 34	0,42268901	0,57731099	0
Mother B6/N 4			
MID1 OE 35	0,36025217	0,63234043	0,00740741
Mother B6/N 4			
MID1 OE 36	0,40088397	0,59911603	0
Mother B6/N 4			
MID1 OE 37	0,57614291	0,42385709	0
Mother B6/N 5			
MID1 OE 38	0,44523327	0,55476673	0
Mother B6/N 5			
MID1 OE 40	0,50132275	0,49867725	0
Mother B6/N 5			
MID1 OE 41	0,54327719	0,45672281	0
Mother B6/N 5			
MID1 OE 42	0,6172504	0,36423108	0,01851852
Mother B6/N 5			

Data Pax6+ and GFP+/GFP+
Animal

MI1 OE Empty 43	0,73469388		
Mother B6/N 1			
MI1 OE Empty 45	0,74418605		
Mother Mouse 1			
MI1 OE Empty 46	0,67647059		
Mother Mouse 2			
MI1 OE Empty 47	0,71794872		

Mother Mouse 2			
MI1 OE Empty 48	0,72		
Mother Mouse 2			
MID1 OE 28	0,38297872		
Mother B6/N 3			
MID1 OE 32	0,46875		
Mother B6/N 3			
MID1 OE 33	0,48979592		
Mother B6/N 4			
MID1 OE 34	0,61290323		
Mother B6/N 4			
MID1 OE 35	0,73913043		
Mother B6/N 4			
MID1 OE 36	0,38095238		
Mother B6/N 4			
MID1 OE 37	0,51724138		
Mother B6/N 5			
MID1 OE 38	0,58064516		
Mother B6/N 5			
MID1 OE 40	0,46666667		
Mother B6/N 5			
MID1 OE 41	0,56666667		
Mother B6/N 5			
MID1 OE 42	0,8125		
Mother B6/N 5			

Data Tbr2+ and GFP+/GFP+ cells

Animal

MI1 OE Empty 43	0,36363636		
Mother B6/N 1			
MI1 OE Empty 45	0,40625		
Mother Mouse 1			
MI1 OE Empty 46	0,34042553		
Mother Mouse 2			
MI1 OE Empty 47	0,42857143		
Mother Mouse 2			
MI1 OE Empty 48	0,38297872		
Mother Mouse 2			
MID1 OE 28	0,56		
Mother B6/N 3			
MID1 OE 32	0,59259259		
Mother B6/N 3			
MID1 OE 33	0,46341463		
Mother B6/N 4			
MID1 OE 34	0,35714286		
Mother B6/N 4			

MID1 OE 35	0,60714286		
Mother B6/N 4			
MID1 OE 36	0,48387097		
Mother B6/N 4			
MID1 OE 37	0,52941176		
Mother B6/N 5			
MID1 OE 38	0,53488372		
Mother B6/N 5			
MID1 OE 40	0,33333333		
Mother B6/N 5			
MID1 OE 41	0,5		
Mother B6/N 5			
MID1 OE 42	0,44444444		
Mother B6/N 5			

Data Ki67+ and GFP+/GFP+ cells

Animal	VZ	SVZ	CP
MI1 OE Empty 43	0,04878049	0,11428571	0
Mother B6/N 1			
MI1 OE Empty 45	0,1	0,07692308	0
Mother Mouse 1			
MI1 OE Empty 46	0,10526316	0,04	0
Mother Mouse 2			
MI1 OE Empty 47	0,0952381	0,06666667	0
Mother Mouse 2			
MI1 OE Empty 48	0,07142857	0,08	0
Mother Mouse 2			
MID1 OE 28	0,23529412	0,11111111	0
Mother B6/N 3			
MID1 OE 32	0,28571429	0,13043478	0
Mother B6/N 3			
MID1 OE 33	0,47826087	0,25	0
Mother B6/N 4			
MID1 OE 34	0,11764706	0,08333333	0
Mother B6/N 4			
MID1 OE 35	0,15	0,05882353	0
Mother B6/N 4			
MID1 OE 36	0,31818182	0,18518519	0
Mother B6/N 4			
MID1 OE 37	0,45454545	0,27272727	0
Mother B6/N 5			
MID1 OE 38	0,22222222	0,05555556	0
Mother B6/N 5			
MID1 OE 40	0,10714286	0,05	0
Mother B6/N 5			
MID1 OE 41	0,32	0,18181818	0
Mother B6/N 5			

MID1 OE 42	0,21428571	0,11111111	0
Mother B6/N 5			

Data Casp3+ and GFP

MI1 OE Empty 43	0,5	0,5	0
Mother B6/N 1			
MI1 OE Empty 45	0,5	0,5	0
Mother Mouse 1			
MI1 OE Empty 46	0,5	0,5	0
Mother Mouse 2			
MI1 OE Empty 47	0	1	0
Mother Mouse 2			
MID1 OE 28	0	1	0
Mother B6/N 3			
MID1 OE 32	0,666666667	0,33333333	0
Mother B6/N 3			
MID1 OE 33	1	0	0
Mother B6/N 4			
MID1 OE 35	0,5	0,5	0
Mother B6/N 4			
MID1 OE 36	0	1	0
Mother B6/N 4			
MID1 OE 37	1	0	0
Mother B6/N 5			
MID1 OE 38	1	0	0
Mother B6/N 5			
MID1 OE 40	0,5	0,5	0
Mother B6/N 5			
MID1 OE 41	0,75	0,25	0
Mother B6/N 5			

Data *MID1/MID2* double KO GFP+/GFP + cells

Mean value from 3 different stainings

Animal	VZ	SVZ	CP
M6E2 Empty	0,318220232	0,551632682	0,130147085
Mother Mid1lox/Mid2lox nr. 6			
M6E3 Empty	0,275517807	0,503700506	0,220781687
Mother Mid1lox/Mid2lox nr. 6			
M8E1 Empty	0,187425122	0,616804954	0,195769925
Mother Mid1lox/Mid2lox nr. 8			
M6E1 Empty	0,28464	0,60473	0,11062
Mother Mid1lox/Mid2lox nr. 6			
M9E5 CRE	0,174850657	0,491726404	0,333422939
Mother Mid1lox/Mid2lox nr. 9			
M10E1 CRE	0,19125529	0,582912004	0,225832707

Mother Mid1lox/Mid2lox nr. 10			
M11E1 CRE	0,112604167	0,597256944	0,290138889
Mother Mid1lox/Mid2lox nr. 11			
M13E3	0,0337	0,7594	0,2068
Mother Mid1lox/Mid2lox nr. 13			

Data Pax6+/GFP+

Animal	VZ	SVZ	CP
M6E2 Empty	0,777777778	0,222222222	0
Mother Mid1lox/Mid2lox nr. 6			
M6E3 Empty	0,84	0,16	0
Mother Mid1lox/Mid2lox nr. 6			
M8E1 Empty	0,944444444	0,055555556	0
Mother Mid1lox/Mid2lox nr. 8			
M6E1 Empty	0,75	0,25	0
Mother Mid1lox/Mid2lox nr. 6			
M9E1 CRE	0,5	0,5	0
Mother Mid1lox/Mid2lox nr.9			
M9E5 CRE	0,866666667	0,133333333	0
Mother Mid1lox/Mid2lox nr. 9			
M10E1 CRE	0,846153846	0,153846154	0
Mother Mid1lox/Mid2lox nr. 10			
M11E1 CRE	0,933333333	0,066666667	0
Mother Mid1lox/Mid2lox nr. 11			
M13E3	0,0337	0,7594	0
Mother Mid1lox/Mid2lox nr. 11			

Data Tbr2+/GFP+

Animal	VZ	SVZ	CP
M6E1 Empty	0,5	0,5	0
Mother Mid1lox/Mid2lox nr. 6			
M6E2 Empty	0,2	0,8	0
Mother Mid1lox/Mid2lox nr. 6			
M6E3 Empty	0,230769231	0,769230769	0
Mother Mid1lox/Mid2lox nr. 6			
M8E1 Empty	0,176470588	0,823529412	0
Mother Mid1lox/Mid2lox nr. 8			
M9E1 CRE	0,4	0,6	0
Mother Mid1lox/Mid2lox nr.9			
M9E5 CRE	0,375	0,625	0

Mother Mid1lox/Mid2lox nr. 9			
M9E6	0,25	0,75	0
Mother Mid1lox/Mid2lox nr. 9			
M10E1 CRE	0,2	0,8	0
Mother Mid1lox/Mid2lox nr. 10			
M11E1 CRE	0	1	0
Mother Mid1lox/Mid2lox nr. 11			

Data Satb2+/GFP+

Animal	VZ	SVZ	CP
M6E1 Empty	0	0,885714286	0,114285714
Mother Mid1lox/Mid2lox nr. 6			
M6E2 Empty	0,081081081	0,675675676	0,243243243
Mother Mid1lox/Mid2lox nr. 6			
M6E3 Empty	0	0,875	0,125
Mother Mid1lox/Mid2lox nr. 6			
M8E1 Empty	0	0,916666667	0,083333333
Mother Mid1lox/Mid2lox nr. 8			
M9E1 CRE	0	0,384615385	0,615384615
Mother Mid1lox/Mid2lox nr.9			
M9E5 CRE	0	0,833333333	0,166666667
Mother Mid1lox/Mid2lox nr. 9			
M9E6	0	0,5	0,5
Mother Mid1lox/Mid2lox nr. 9			
M10E1 CRE	0,208333333	0,708333333	0,083333333
Mother Mid1lox/Mid2lox nr. 10			
M12E4 CRE	0	0,5	0,5
Mother Mid1lox/Mid2lox nr. 12			

Data Ki67+ and GFP+/GFP+

Animal	VZ	SVZ	CP
M6E1 Empty	0,6666667	0,33333334	0
Mother Mid1lox/Mid2lox nr. 6			
M6E2 Empty	0,6	0,4	0
Mother Mid1lox/Mid2lox nr. 6			
M6E3 Empty	0,75	0,25	0
Mother Mid1lox/Mid2lox nr. 6			
M8E1 Empty	1	0	0
Mother Mid1lox/Mid2lox nr. 8			
M9E1 CRE	0	1	0
Mother Mid1lox/Mid2lox nr.9			
M9E5 CRE	0	1	0

Mother Mid1lox/Mid2lox nr. 9			
M9E6	0,25	0,25	0,5
Mother Mid1lox/Mid2lox nr. 9			
M12E4 CRE	0,4	0,4	0,2
Mother Mid1lox/Mid2lox nr. 12			

Data Casp3+ and GFP+/GFP+

Animal	VZ	SVZ	CP
M6E1 Empty	0	1	0
Mother Mid1lox/Mid2lox nr. 6			
M6E2 Empty	0	1	0
Mother Mid1lox/Mid2lox nr. 6			
M6E3 Empty	0	0	0
Mother Mid1lox/Mid2lox nr. 6			
M8E1 Empty	0	0	0
Mother Mid1lox/Mid2lox nr. 8			
M9E1 CRE	0	1	0
Mother Mid1lox/Mid2lox nr.9			
M9E5 CRE	0	0,666666667	0,333333333
Mother Mid1lox/Mid2lox nr. 9			
M11E1 CRE	0,166666667	0,666666667	0,166666667
Mother Mid1lox/Mid2lox nr. 11			

7.3 Acknowledgement

My heartfelt thanks go to the entire team at Human Genetics Department in Mainz. In particular to my supervisors, who supported me on every step. I would like to thank them for their advice and support during my work.
I would like to thank the whole team for their active support.
I thank my family and friends who always believed in me and stood by me.
Without all of you this work would never have been possible.

7.4 CV

Katharina Anna Ruppert
born 2nd Juli 1996 in Neustadt a. d. Aisch
Citizenship: German

Higher Education

10/2015 – 10/2017	Humanmedizin,Friedrich-Alexander-Universität, Erlangen-Nürnberg
09/2017	Erster Abschnitt der ärztlichen Prüfung
10/2017 – 06/2022	Humanmedizin an der Johannes-Gutenberg-Universität, Mainz
04/2021	Zweiter Abschnitt der ärztlichen Prüfung
05/2022	Dritter Abschnitt der Ärztlichen Prüfung
31.05.2023	Ärztliche Approbation

Scholarship

08/2018	FamuLAND-Förderung, KVB
10/2018 – 10/2019	Doktorandenstipendium, FTN Mainz

Career

08/2023 – today	Assistenzärztin Pädiatrie am Zentrum für Kinder- und Jugendmedizin Universitätmedizin Mainz
10/2022 – today	Mitglied der AG Nachhaltigkeit des Zentrums für Kinder- und Jugendmedizin